THE POTENTIAL OF NEAR INFRARED SPECTROSCOPY AND NIR HYPERSPECTRAL IMAGING FOR THE NONDESTRUCTIVE PREDICTION OF LIME QUALITY

HO THANH HUONG

A THESIS SUBMITTED IN PARTIAL FULFILLMENT
OF THE REQUIREMENT FOR DEGREE OF
MASTER OF SCIENCE IN FOOD SCIENCE
FACULTY OF AGRO-INDUSTRY
KING MONGKUT'S INSTITUTE OF TECHNOLOGY LADKRABANG
2016

KMITL-2016-AI-M-053-266

Thesis	The Potential of Near Infrared Spectroscopy and NIR Hyperspectral Imaging for The Nondestructive Prediction of Lime Quality
Student	Miss HO THANH HUONG
Student ID	57608038
Degree	Master of Science
Program	Food Science
Year	2016
Main Advisor	Assoc. Prof. Dr. SONTISUK TEERACHAICHAYUT
Co-Advisor	Dr. PANUWAT SUPPRUNG

ABSTRACT

The objective of this study was to evaluate the potential of conventional near infrared spectroscopy (NIRs) and NIR HSI to assess internal qualities of lime. The prospects for the use of visible to near infrared spectroscopy (Vis/NIRs) and hyperspectral imaging as non-destructive techniques to sort lime were reviewed. Initial study of physio-chemical characteristics of limes which were selected from four different locations, namely Vietnam, Cambodia, Bangkok and Khon Kaen province, Thailand were conducted to have an over view of lime's quality from different geography. Classification of "Paan" limes and "Other" limes _Kai, Cambodia and Vietnam limes_ from different growing locations, was conducted by using Fourier transform NIR (FT-NIR) and portable handheld NIR (NIR-Gun). The main objective is to compare the possibility of FT-NIR and NIR-Gun and to increase the range to ensure that it was sufficiently robust to accurately classify qualities of lime from any cultivar. It was found that the FT-NIR in diffuse reflectance mode could classify total soluble solid (TSS) with a slightly higher accuracy and robustness comparing with NIR-Gun. However, NIR-Gun was easy to practically use as portable handheld instrument that was suitable to apply in the market and on-field. In addition, the comparison is made about the accuracy of prediction of TSS of "Paan" lime using Vis/NIRs XDS Rapid Content TM Analyzer and NIR-Gun. The result showed that using NIR-Gun to predict TSS of "Paan" limes resulted in higher precision than using Vis/NIR XDS Rapid Content TM Analyzer. Finally, using of NIR HSI showed more clear illustration of internal qualities (TSS, Citric and Juice content) for "Paan" limes. The results demonstrated the prospect of hyperspectral imaging can be used as a non-destructive tool for sorting lime based on internal qualities explicitly.

Key words: conventional NIRs, HSI, lime, internal qualities

ACKNOWLEDGEMENT

I would like to express my profound gratitude and appreciation to the following people and institutions:

1. First of all, I would especially like to thank Faculty of Agro-Industry and King Mongkut's Institute of Technology Ladkrabang (Research fund: KREF125801) for financial support which providing research fund and living expense that is really meaningful to my study life in Thailand.

2. Secondly, I appreciated my advisor - Assoc. Prof. Dr. Sontisuk Teechaichayut, who unconditionally provided knowledge, patience, motivation, invaluable guidance and good advices to enhance my experiences during 2 years study abroad.

3. Thirdly, I would like to say thank to Dr. Panuwat Supprung, my co-advisor during research at Department of Postharvest and Processing Engineering, Rajamangala University of Technology Isan Khon Kaen, Khon Kaen province, Thailand, for giving me the opportunity and to welcome me in his laboratory. Your continuous support, guidance, advices and determination for the research helped me throughout this project.

4. Next, I would like to thank to committee members, namely Dr. Rachit Suwapanich and Dr. Kittichai Banjong and Assoc. Prof. Dr. Anupun Terdwongworakul for being committee members and revise my work with their brilliant comments and suggestions.

5. I would like to thank my best partner in Thailand, Sinenart Suktanarak for her friendship and support whenever I had problem. In addition, I am specially thank all the students of the Food Engineering at Agro-Industry Faculty, KMITL.

6. I am specially thankful to all lecturers, technical staffs, officers, laboratory staffs in the Faculty of Agro-industry at King Mongkut's Institute of Technology Ladkrabang and all technical staffs in Faculty of Engineering, Department of Postharvest and Processing Engineering, Rajamangala University of Technology Isan Khon Kaen, Khon Kaen, Thailand for their training, listening and assisting my study courses.

7. Last but not least, I would like to say thank to my parents and my sisters who always be my sides.

Ho Thanh Huong

December, 2016

TABLE OF CONTENTS

LIST OF FIGURES

LIST OF TABLES

LIST OF ABBREVIATIONS

A	Absorbance
CCD	Charge-Coupled Devices
c	The concentration of the solute
ε	Absorption coefficient
EMCCD	Electron-Multiplying Charge-Coupled-Device
FOV	Field Of View
F	Factor
HSI	Hyper-Spectral Imaging
InGaAs	Indium Gallium Arsenide
l	thickness of the sample
MSC	Multiplicative Scatter Correlation
N	Number Of Samples
NIRs	Near Infrared spectroscopy
nm	Nanometer
OD	Optical density
PC	Principle Component
PCR	Principle Component Regression
PCA	Principle Component Analysis
PLSR	Partial Least Square Regression
PLS-DA	Partial Least Square Discriminant Analysis
QE	Quantum Efficiency
R	Correlation Coefficient
R2	Coefficient Of Determination
RMSEC	Root Mean Square Error Of Calibration
RMSECV	Root Mean Square Error Of Cross Validation
RMSEP	Root Mean Square Error of Prediction
SD	Standard Deviation
SECV	Standard Error Of Cross Validation
Si	Silicon

SNR	Signal-To-Noise Ratio
SNV	Standard Normal Variate
T	Transmittance
TSS	Total Soluble Solids
Vis/NIR	Visible Near Infrared

CHAPTER 1 INTRODUCTION

1.1 OVERVIEW

Lime is an economically significant horticultural crop and its harvest season is from July to September (Pranmornkith *et al.*, 2005). Thousands tons of limes are consumed yearly, indicating its importance in Thai economy (Amolsiri and Intira, 2016). Limes have been used both for enhancing the taste of various Thai foods and for using in Thai traditional medicine (Amolsiri and Intira, 2016). The price of lime strongly depends on its availability and quality characteristics. Outside of the harvest period, the price rises gradually and reaches the highest price in the dry season (i.e. February to April) (Pranmornkith *et al.*, 2005). After harvesting and handling, lime should be sorted for meeting grades and quality standards. A quality classification systems of fresh fruit (both manually operation and mechanized system), are based on subject assessment of visible external characteristics of fruit such as surface color, size, shape and presence of defects (Kader, 2002; Liu *et al.*, 2009). Until recently the internal properties could be determined non-destructively at the typical speed of commercial grating lines, which may estimate about ten fruits per second (Nicolaï *et al.*, 2008). The non-destructive and high speed analysis techniques to determine the intact quality of fruit, such as moisture content, citric acid and TSS, etc., has been studied using some modern techniques, namely Visible and Near Infrared Spectroscopy (Vis/NIR) (Juan, 2015) and Hyper-spectral imaging (HSI) techniques (Wang *et al.*, 2015). These techniques are necessary to the success of the lime grading and on-line production, in order to satisfy an ever increasing consumer demand for detection the internal quality properties combined with agribusiness demand for chemical-free, rapid measuring methods with limited sample preparation and cost effective detection.

There are many researchers who apply NIRs on measuring the interior quality of fruit and vegetable such as mandarin (Gómez *et al.*, 2006). They found the fact that the wavelengths in the range of 750-2500 nm are readily transmitted through a fruit (Liu *et al.*, 2007), but it does not mean that other wavelengths could not extract useful information. Therefore, the addition of relevant visible range wavelengths to the spectra analysis could

add an improvement to detect internal qualities of lime. In addition, no information was found relating NIRs prediction or classification for internal quality of lime. Evaluation of the potential of NIRs on detection of limes' quality would be highly beneficial in view of its well-known nondestructive and efficient benefits.

In this research, Vis/NIR, NIRs and NIR HSI techniques were used to measure lime's quality parameters. Partial least squares regression (PLSR) and partial least squares discriminant analysis (PLS-DA) are used for the statistical analysis of the spectra data and the construction of the calibration models for each internal quality characteristic.

1.2 OBJECTIVE OF RESEARCH

The aims of this study were to research the possibility of nondestructive techniques, including NIRs and NIR HSI measurement for the classification of different fresh lime. Samples were collected from four different geographical origins (Can Tho city - Vietnam, Siem Reap city - Cambodia, Khon Kaen city - Thailand and Bangkok city - Thailand). More specifically, the present research has two main objectives:

1. To obtain the relationship between spectral information and quality parameters of lime by conventional NIRs measurement.
2. To obtain the relationship between spectral and spatial information and quality parameters of lime by NIR HIS measurement.

1.3 SCOPE OF RESEARCH

1.3.1 Physiochemical properties of lime

a. Physical properties: weight, width, height, thickness of lime, seediness, thickness of peel.

b. Chemical properties: TSS (°Brix), citric acid (%), moisture content (%) and juice content (%).

1.3.2 Nondestructive evaluation of lime

b. The potential of conventional NIR for nondestructive evaluation of lime's quality.

b. The potential of NIR HSI for nondestructive evaluation of lime's quality.

1.4 EXPECTED BENEFITS

Knowledge of the physiochemical characteristics of limes origin from different geographies (Thailand, Vietnam and Cambodia) has not mentioned in books and other publications. The gaining knowledge is the most important key in developing the new system for determining the quality of lime nondestructively in the market.

Knowledge of various nondestructive techniques provides the appropriate nondestructive methods in order to predict and classify lime's quality.

Gain more profound knowledge of the applicability of NIRs and NIR HSI on detection of internal quality of limes.

1.5 THESIS ORGANIZATION

Chapter 1 introduces about limes and nondestructive methods, objectives, scopes and expected benefits.

Chapter 2 provides literature review of limes, conventional NIR spectrometers, HSI and their application on detection quality of fruit.

Chapter 3 describes the materials, instruments and methods for destructive analysis (physiochemical parameters) and nondestructive analysis using XDS Rapid Content TM Analyzer, FQA-NIR Gun instrument, NIR Flex N-500 Solid instrument and HSI Instruments.

Chapter 4 Results and Discussions

Chapter 5 Conclusions and Suggestions

CHAPTER 2 LITERATURE REVIEW

2.1 LIME AND QUALITY PROPERTIES OF LIME

2.1.1 Botany review

Lime is a berry or hesperidium, which is non-climacteric thus lack the dramatic rise in ethylene and respiration (Young, 1977). Lime is one type of citrus (Figure 2.1). Therefore its characteristics are as similar as citrus in generally.

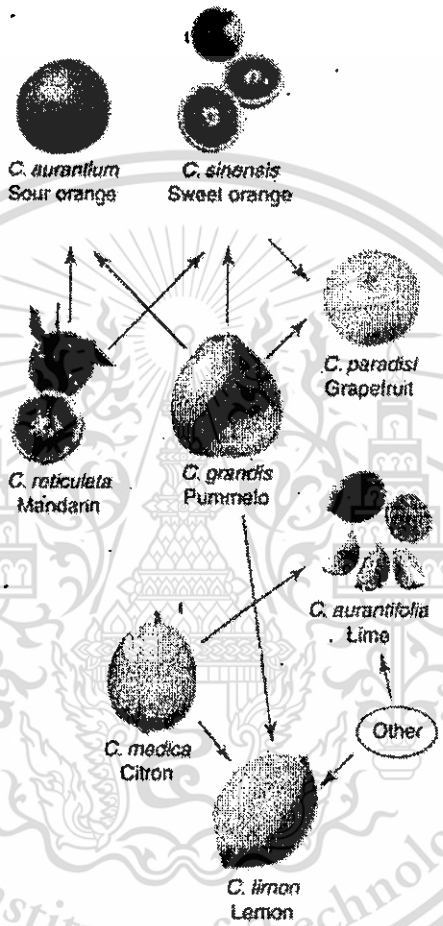

Figure 2.1 The most probable relationships among the different citrus types

Source: Gloria (2000)

Citrus fruits are low in starch reserves and thus undergo very slow change in internal quality during storage. Prolonged storage does decrease stored acids converting them to sugars and CO_2 used in respiration (Echeverria and Ismail, 1987), which undertake considerable increase in acid content during treatment. The fruit peel consists of an outer colored exocarp (flavedo) and an inner white spongy mesocarp (albedo). The edible

portion comprises the internal portion of the carpels which expand into segments containing juice vesicles and seeds.

Limes are thought to have originate in northeastern India (Young, 1977). Limes are grown in mild, subtropical and tropical areas, because trees are very cold sensitive. It was separated into three big groups:

- Group 1 - Small-Fruited Acid Limes: The West India lime, a small-fruited acid lime (*Citrus aurantifolia Swinge*) is grown in semitropical and tropical areas. Fruits are small, round, elliptical, greenish yellow at maturity, and moderately seedy. The rind is thin, smooth, and leathery. The flesh is juicy, acid and aromatic.
- Group 2 - Large-Fruited Acid Limes: Large-fruited acid limes are larger than West Indian limes, but other fruit characteristics are similar. A chief cultivar in this group (*Citrus latifolia Tan.*) is the Tahiti, or Persian lime, which was introduced into California from Tahiti and may have originated there, but definitely not in Persia. The Bears lime, whose description corresponds to that of Tahiti, originated from California from seed of a fruit of Tahiti origin.
- Group 3 - Sweet limes: The Palestine, or India, sweet lime (*Citrus limettioides Tan.)* originated in northeastern India and is well liked in India, the Near East, Egypt, and Latin American. Fruits are medium in size and round to oblong. The rind is smooth, thin, and greenish to orange-yellow at maturity. Rind oil has a distinctive aroma. Fruit flesh is straw-yellow in color, juicy, and tasteless due to no acid.

2.1.2 Harvesting

They are commonly harvested when fully grown, but still green. This is judged when the skin loses its irregular bumpy surface, becomes smooth and the peel may turn a lighter shade of green. There are no quality differences between this stage and when fruit turns fully yellow, it is just that make markets prefer limes to be green (Thompson *et al.*, 1974). As the fruit matures, their chlorophyll level is reduced and it is possible to separate limes into different classes on the basis of the chlorophyll levels of the peel. Therefore light transmission properties can be used to measure their maturity.

2.1.3 Lime composition

The composition of lime varies cultivar, climate, rootstock and cultural practices. Most of limes are primarily water, but also content over 400 other constituents including moderate level of carbohydrates, organic acids, ascorbic acid and minerals and small

quantity of flavonoids, volatiles and lipids. Citrus are low in protein and fats (Nagy and Attaway, 1980). Limes are a good source of pectin and roughage.

Total soluble solids (TSS), which include carbohydrates, organic acids, proteins, fats and various minerals, comprise from 10-20% of the fresh weight of citrus fruit (Erickson, 1968). Carbohydrates account for 70-80% of the TSS in the fruit. The major groups of carbohydrates in citrus fruit include mono-saccharides (glucose and fructose), oligosaccharides (sucrose) and polysaccharides (cellulose, starch, hemicellulose, pectin). Pectin is an important polysaccharide in the cell wall matrix. TSS increases as the fruit size increases.

2.1.3.1 Organic Acids

Total acidity (TA) of citrus juices is an important factor in overall juice quality which contributed significantly to overall juice acidity. Citric acid is a primary organic acid (70-90%). The rate of decrease in acidity is positively correlated with average temperatures during the season (Davies and Albrigo, 1994).

2.1.3.2 Ascorbic acid

Citrus fruits are a valuable source of ascorbic acid (vitamin C). Level of ascorbic acid is quite variable among citrus fruits and tends to decrease seasonally. Ascorbic acids level is generally higher in the peel than the extract juice (Erickson, 1968).

2.1.3.3 Limonin and other limonoids

Triterpene derivative which produces flavors in the juice are present in most citrus cultivars but affect palatability in a few cultivars. Limonin was firstly identified as an important bitter principle in navel oranges in the peel and is released into the juice at juicing.

2.1.3.4 Pectin

Pectin is high molecular weight carbohydrates composed of chains of hydro-galacturonic linkages. During maturation of citrus fruits, insoluble pectin is converted to water-soluble pectin and pectinate (Nagy and Attaway, 1980). Total pectin substance decreases in the peel and pulp over the season, and water-soluble pectin increases as percentage of the total pectin. This change in pectin composition signals fruit softening or over-maturity.

2.1.3.5 Essential oils

Volatile lime essential oil components are listed in the Table 2.1.

Table 2.1 Volatile lime essential oil components

tert-Amylalcohol	Citral	Camphene	Pentadecane
Decanol	Decanal	Caryophyllene	α-Pinene
Geraniol	Dodecanal	P-Cymene	β-Pinene
Linalool	Geranial	α-elemene	Sabinene
2-Methyl-3-buten-2-ol	Neral	β-elemene	γ-Terpiene
Nerol	Octanal	Δ-elemene	Terpinolene
1-Nonanol	Undecanal	Guaiene	Tetradecane
Octanol	Geranyl Acetate	α-Humulene	α-Thujene
Terpinen-4-ol	Methyl Anthranilate	β-Humulene	Nootkatone
α-Terpineol	Neryl acetate	Limonene	1,4-Cineole
β-Terpineol	α-Bergamotene	Myrcene	1,8-Cineole
Thymol	β-Bisabolene	Nonane	

Source: Davies and Albrigo (1994)

2.1.3.6 Flavonoid constituents

Three types of flavonoid occur in citrus: flavonones (including 3-hydroxyflavanones or flavanonols), flavones (including 3-hydroxyflavanones or flavanols) and anthocyanins. Flavones are the most abundant flavonoids in the fruit of most citrus species that are neither bitter nor sweet may sometimes exhibit interesting effects on taste.

2.1.4 Quality features to be inspected in citrus fruits

The flavor and palatability of lime are function of relative levels of TSS, TA and presence or absence of various aromatic or bitter principles. The juiciness and aroma of juice affect the palatability of the fresh limes (Erickson, 1968).

2.1.5 Physiological and physicochemical characteristics of citrus fruits that affects inspection as using NIR techniques

There are some characteristics that should be considered during using NIR spectroscopy. Firstly, excessive cold storage or chilling in the field or in storage room has an important effect on citrus, not only on the external appearance but also on the internal quality because citrus are very sensitive to chilling. Secondly, citrus fruits generally show round surface that make it difficult to inspect the boundary of each fruit in the images and to perform an accurate measurement of the commercial size of the fruit based on the

"equatorial diameter" which produce a particular light reflection pattern. Finally, almost citrus fruits have heterogeneous peel color. In addition citrus fruit can be waxed after passed the inspection chamber that is the reason why specular reflectance happened during measurement.

2.1.6 Packinghouse Procedures

Packinghouse layout and design varies from basic sorting of fruit by size or color using high speed ultramodern sorting connected with a computer. Nevertheless, most packinghouses in Florida contain the same basic operations which consist of a bin blencher, an initial wet or dry dumping operation, pre-grading, washing, grading, drying, fungicide treatment, waxing-drying, sizing, packing and shipping (Grierson *et al.*, 1978). Most grading worldwide is still done visually. Fruits pass along belts where they are visually evaluated for defects. A certain usually predetermined percentage of the fruit surface area must be free of blemishes. Alternatively, some packinghouses have high speed photo-grading systems that can detect off-color or physical defects.

2.1.7 Storage

Citrus fruits are non-climacteric and have low respiration rates and thus are quite unable to storage in long-term. Lemons, limes and grapefruit cannot be stored at temperatures less than 10°C because they develop chilling injury which is manifested as pitted necrotic spot in the peel. Consequently, lemon and limes are usually stored at 10-12°C (Davies and Albrigo, 1994). Refrigerated storage recommendation is 11.1-12.8°C and 85-90% R.H. for 7 weeks with 18% weight loss for green fruits (Pantastico, 1975).

Destructive assessment of quality parameters is one of the old techniques in fruit postharvest management. Most qualified citrus fruit classification systems are based on surface color, size, shape and presence of defects (Kader, 2002; Liu *et al.*, 2009). As we know the increasing consumer demand for internal quality attributes such as citric acid and juice content, coupled with industry demand for rapid and cost-effective detection and monitoring of physiochemical, have encouraged considerable interest among researchers on the application of NIRs for monitoring and evaluating quality of citrus fruit in specifically and for fruit industry in generally.

2.2 NEAR INFRARED SPECTROSCOPY

2.2.1 Principle of infrared spectroscopy

Spectroscopy can split into two large groups (Wilson, 1994): photonic spectroscopy and particle spectroscopy. The photonic spectroscopy group consists of spectroscopic methods displaying an analytical potential for rapid control. The particle spectroscopy group is represented by mass spectrometry and derived methods. All spectroscopic methods, except mass spectrometry, can be classified according to the energy involved during measurement (Da-Wen Sun, 2010). Electromagnetic radiation is the radiant energy released by electromagnetic processes, exists as waves that are produced from a source and move in the straight line if they are not reflected or refracted. Electromagnetic waves can be characterized by the frequency or wavelength. The frequency (ν) is in cycles per second (s^1, or Hertz (Hz)).

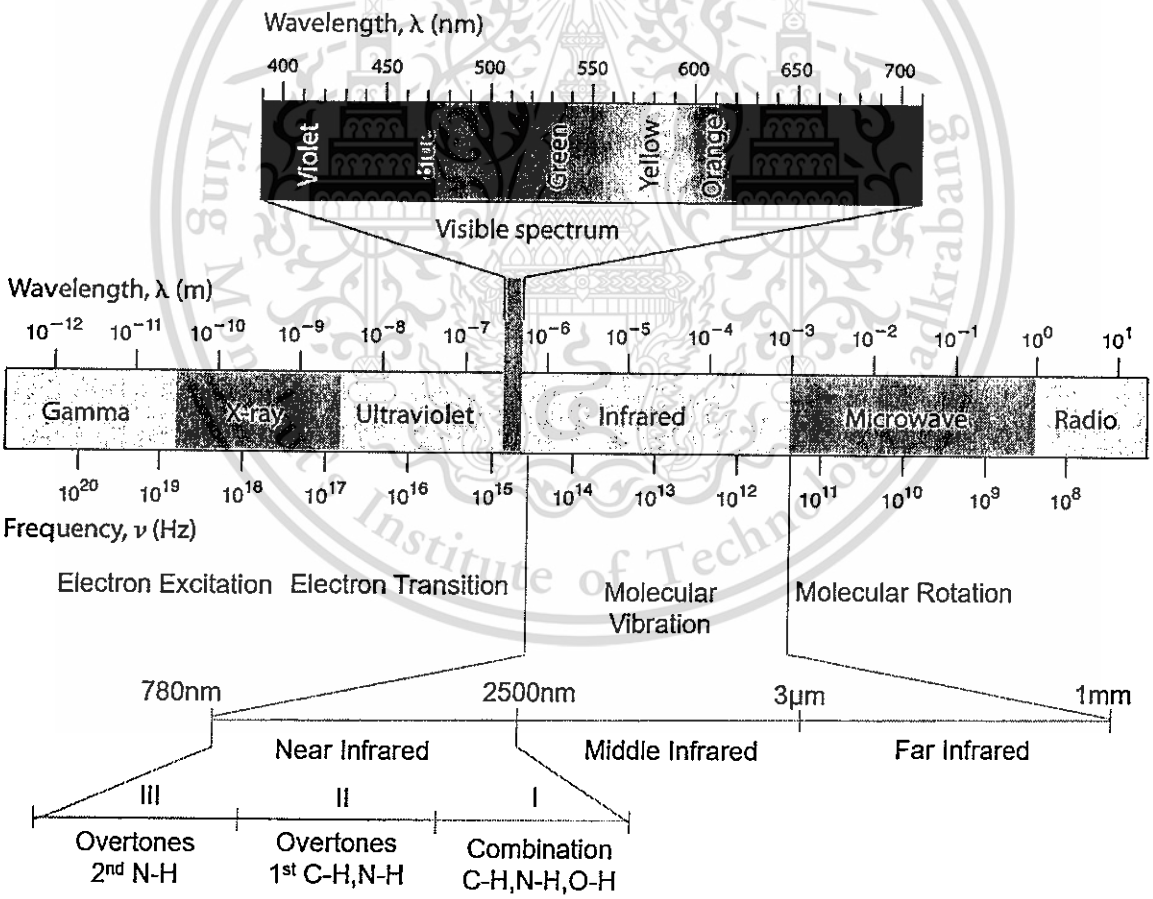

Figure 2.2 Electromagnetic spectrum

Source: Da-wen Sun (2010)

The wavelength (λ), which is the distance covered by light during the full cycle, can be represented by the formula: $\lambda = c/v$, where c is a universal constant, equal to 3×10^8m/s. In spectroscopy, the wavelength are expressed using different unit, namely centimeter (1 cm = 10^{-2}m), millimeter (1mm = 10^{-3}m), micrometer (1 μm = 10^{-6}m), nanometer (1nm = 10^{-9}m) and angstrom (1Å= 10^{-10}m). Spectral region (Figure 2.2) can be defined as a function of wavelength:

+ X-ray region (0.5 - 10nm),
+ Far-ultraviolet region (10-200 nm),
+ Near-UV region (200-350 nm),
+ The visible region (350-780 nm),
+ The NIR region (780-2500 nm) is characterized by a harmonics and combination bands that is widely used in food analysis,
+ The mid-infrared spectroscopy (MIR) region (2500-25 000 nm),
+ The microwave region (100μm -1cm),
+ The radiofrequency region (1cm-10m).

2.2.2 NIR spectroscopy

2.2.2.1 Basics (Reginald, 1994)

Classical absorption spectroscopy involves a cuvette containing a liquid positioned between a monochromatic source and a detector. The monochromatic energy (energy is used to distinguish NIR energy from visible light) falling on the input surface of the cuvette is given the symbol I_o; the energy passing through the cuvette is given the symbol I. Classical absorption spectroscopy requires the liquid to be homogeneous and non-scattering. That is, absorption of the energy passing through the liquid is diminished only by the solute. In addition, the area of the detector D must be large enough to capture all of the transmitted energy. If the solute is dissolved at concentration c in the liquid (solvent), then the Beer – Lambert law (Eq. 2.1) holds, which states that the absorption is proportional to the concentration of the substance dissolved in the liquid, or

$$I = I_o 10^{-\varepsilon c l} \qquad \text{(Eq. 2.1)}$$

where ε is called absorption coefficient, l is the thickness of the sample and c is the concentration of the solute. As the concentration c increases, or if the thickness l increases, I decreases.

It is not always to know ε, l, or c. However, we can manipulate equation (Eq. 2.1) in the following manner:

$$T = I/I_o = 10^{-\varepsilon cl} \quad \text{(Eq. 2.2)}$$

$$I_o/I = 10^{\varepsilon cl} \quad \text{(Eq. 2.3)}$$

$$A = \log_{10}(1/T) = \log_{10}(I_o/I) \quad \text{(Eq. 2.4)}$$

where T is transmittance and A is absorbance. In equation 2.4, A increases to infinity when I becomes zero, or when the sample has absorbed all the energy entering to the sample.

2.2.2.2 Importance of light in NIRs

Light is a nonmaterial wave composed of oscillating electric and magnetic field which travel through a vacuum without the aid of the material substance or medium (Da-wen Sun, 2010). Light consists of a stream of particles, called photons that travel at the speed of light and carry an amount of energy proportional to the light frequency (Da-wen Sun, 2010). When light is considered as particles, each particle has an energy related to the frequency of the wave, given by the following *Plank's relation* (Eq.2.5):

$$E = h\nu \quad \text{(Eq. 2.5)}$$

where E is the energy of the photon, h is *Plank's* constant (6.626×10^{-34} J.s) and ν is the frequency (Hertz). When light interacts with a single atom and molecule, its behavior depends on the amount of energy per quantum it carries. Wave interference and polarization were discovered, and the speed of light was measured in different media. Instruments using prism and diffraction grating gave rise to analysis of light spectra from various sources.

2.2.2.3 Interaction of light with the sample

The interaction of light with food samples is importance in identifying molecules based on their intrinsic properties in order to monitor interactions between different molecules, to detect morphological changes within biological materials, and to correlate changes that occur in the samples with the relevant physiological disorders (Da-Wen Sun, 2010). In fact, all materials, including food samples, continuously emit and absorb energy by lowering or raising their molecular energy levels (Da-Wen Sun, 2010). The strength and wavelengths of emission and absorption depend on the nature of material. Basically, when an electromagnetic wave (from light source) strikes the surface of a sample, the wave may

be partly or totally reflected, and any non-reflected part will penetrate into the material. If an electromagnetic wave passes through a material without any reduction or with partial attenuation, the materials are called transparent or semitransparent. Most raw food or fruit samples in solid tend to be strong absorbers for most wavelengths, making them opaque over a distance of a few nanometers to a few micrometers.

When a continuous wave light-beam impinges on an opaque object such as a fruit, several form of light interaction with the fruit will take place (Da-Wen Sun, 2010). Some light will be reflected at the surface of the fruit, giving observers a sensation of glossiness or shininess, which is called surface or specular reflectance that should be avoided in most imaging and specular applications. The majority of the light, however, will penetrate the fruit. Light will attenuate in the fruit as a result of scattering and absorption, which is wavelength-dependent. Some light will be absorbed in the fruit tissue, and is subsequently converted into other form of energy (such as heat and fluorescence). Some light will reflect back or re-emerge (after multiple scattering) from the same side of the fruit around the beam incident point; this is often called diffuse reflectance. Some light may go through the whole fruit and emerge from the opposite side; this is term transmittance, and it is essential another form of diffuse reflectance. Visible light reflected, emitted or transmitted from a product carries information used by inspectors and consumers to judge several aspects of its quality. However, human vision is limited to a small region of the spectrum. When a sample is exposed to light, some of the incident light is reflected at the outer surface, causing specular reflectance, and the remaining incident energy is transmitted through the surface into the cellular structure of the sample where it is scattered by the small interfaces within the tissue or absorbed by cellular constituents (Birth, 1976). This is called refused reflection, where incoming light is reflected in a broad range of direction. Some of the light may be absorbed by the materials. For opaque objects such as most food products, there is no transmission. The detected energy is converted by the spectrometer into spectra. These spectra are sensitive to the physical and chemical states of individual constituents. The high spectral signal-to-noise ratio (SNR) obtained from modern instruments means that even constituents present in quite low concentrations can be detected (Gao *et al.* 2003).

2.2.2.4 Diffuse reflectance spectroscopy

There are basically two types of reflectance from the solid samples:

+ Diffuse reflectance,

2.2.2.4 Diffuse reflectance spectroscopy

There are basically two types of reflectance from the solid samples:

+ Diffuse reflectance,

+ Specular reflectance

Figure 2.3 Technology of reflectance spectroscopy (a) Diffuse reflectance and (b) Specular reflectance

Source: McClure and Hamid (1994)

Diffuse reflectance is of primary concern in NIR reflectance spectroscopy. If the energy I_o impinging on the solid sample is reflected equally in all directions, diffuse reflectance is said to exist. Some of reflected energy may have travelled through the sample before being returned to the detector. Equation 2.4 may be rewritten as:

$$OD = log_{10}(1/R) = log_{10}(I_o/I) \quad \text{(Eq. 2.6)}$$

Equation 2.6 is noted about optical density (OD), has been substituted or absorbance (*A*). The term optical density was invented to distinguish the scattering case from the classical non-scattering case. Practically, OD varies between 0 and 4 for single monochromator instruments and between 0 and 6 for double monochromator instruments where stray light within the monochromator becomes the limiting factor. There are several deviations from the classical requirements of absorption spectroscopy. If the sample is nonhomogeneous, scattering is present, and only a portion of the reflected energy is collected by the detectors. Actually, NIR reflectance instruments make use of integrating spheres or more than one detector in order to collect more of the energy reflected from the sample (McClure and Hamid, 1994).

2.2.2.5 Wavelength versus wavenumber (McClure and Hamid, 1994)

The formula to converting from wavelength to frequency is:

$$\nu = \frac{c}{\lambda} \quad \text{(Eq. 2.7)}$$

where c is the speed of light (cm/sec), ν is frequency in Hertz (sec^{-1}), λ is wavelength in cm. The relations between frequency, wavelength and wave number (cm^{-1}) that is defined by Eq. 2.8:

$$\tilde{\nu} = \frac{1}{\lambda} = \frac{\nu}{c} \qquad \text{(Eq. 2.8)}$$

The transfer from the wavelength domain to the wavenumber domain is a nonlinear transformation. For example, spectra recorded on a FT-NIR instrument have poorer wavelength resolution at the long wavelength end of the spectra than at the short wavelength end.

2.2.2.6 Overtone

The term overtone is a way of understanding the relationship between the major absorption of a substance and its minor absorptions. For example, the first, second, and third overtone of the fundamental absorption of water, which occurs at approximately 3.84μm in the infrared region, will be found at approximately one-haft, one third, and one fourth of the fundamental, or 1.92μm, 1.28μm, and 0.96μm, respectively. The fourth overtone has a very weak absorption coefficient and therefore can be seen only for very high concentrations of water.

2.2.2.7 Sensor types for NIRs (McClure and Hamid, 1994)

Silicon diode arrays for conventional NIRs are essentially Si–CCD that is limited to the region 400 to 1100 nm. A typical diode array spectrometer is usually made up of a fixed holographic grating and a linear CCD array. The system is more suitable for transmittance determination than for reflectance. With the use of fiber optics, reflectance measurements are easily obtained (McClure and Hamid, 1994). The advantage of FT-NIR could enhance the use of fiber optics. It has less energy output for fiber optics than a mono chromator-based system. Peirs *et al.* (2002) compared Fourier transform (FT-NIR) spectroscopy with dispersive NIRS, and the instrument stability, the light penetration depth and the predictive capacity of some quality characteristics when both instruments were compared. Based on the results, they concluded that FT-NIR reflectance spectroscopy is an interesting alternative for standard dispersive instruments for non-destructive quality evaluation. Some researchers (Belton *et al.*, 1995; Rodriguez-Saona *et al.*, 2001) used FT-NIR transmission to measure the main components of fruit juices.

2.2.3 Application of NIRs on fruit and vegetable industries

2.2.3.1 Application of NIRs on fruit and vegetable industries

in the NIR and the MIR region have been taken into consideration for fruit and vegetables by Schulz and Baranska (2009). Fruit and vegetables have been mainly analyzed with regard to their major components such as sugar and acidity, and defects like internal browning. Another general overview of on-line measurements by means of NIR spectroscopy in food engineering can be found in the review of Lee (2007). The authors concluded that all the reviewed applications of NIRs, often in combination with chemometric analyses, may play a valuable role in food industry.

The Vis/NIRs, NIR HSI spectroscopy and microwave absorption have been employed for nondestructive determination of water of samples which contain other volatile substances or decomposition reactions than water. A calibration on the basic of a drying technique may be possible. This calibration can then however only predict a mass loss, but not the water content of the product (Joseph and Christoph, 2008). In NIR region, the first harmonic of stretching vibration, νOH, is located between 1400 and 1500 nm. The combination band νOH + δOHis observed at 2086 nm. Water is that strongly absorbs in the NIR and MIR regions. In the NIR region, the spectrum of water exhibits two strong bands at 1442 and 1932 nm. The frequency at 1442 nm is of the first harmonic of νOH, the one at 1932 nm originates from the combination of νOH + δOH. Some nondestructive techniques are presented below, which are applied affectively on agriculture and food industry.

2.2.3.2 Application of NIRs in citrus fruit quality analysis

The application of NIRs for analyzing the quality of citrus fruits was reviewed (Magwaza et al., 2012). Most of the NIRs researches on citrus have focused on assessing internal quality attributes (Liu et al., 2010a, b; Fraser et al., 2003). Citrus quality properties such as TSS and total acidity (TA) are related to organic molecular that contain C-H, C-O, O-H and C-C bonds; thus, it is possible to use NIR methods to determine their concentration. Table 2.2 summarizes the applications of NIRs to assess internal quality parameters of citrus fruit. As the previous results, the NIR technique has significantly greater accuracy for finding out TSS in citrus than any other quality parameters such TA, and the low success could be attributed to the fact that total acids concentration on intact fruit is relatively low; therefore, calibration of this parameter is likely to represent secondary correlations to attributes related to fruit maturity (Guthrie *et al.*, 2005a).

Table 2.2 Overview of applications of NIRs to measure fruit quality of Mandarin fruit

Cultivar	Parameter	Mode	Wavelength (nm)	Preprocess	Validation	Analysis	R/R^2	Prediction error	Ref
Imperial	SSC DM TA % Juice	Interactance	306–1,130	SNV Detrending 1st Derivative 2nd Derivative	Cross validation	MLR MPLS	R^2=0.75 R^2=0.90 R^2=0.30 R^2=0.20	RMSEC=0.4 RMSEC=0.6 RMSEC=0.2 RMSEC=5.0	Guthrie *et al.* (2005a; b)
Nanfeng	SSC TA Vit. C Colour	Transmittance	400–1,040	Smoothing MSC 1st der. 2nd der.	Cross-validation	BPNN PLS	R=0.93 R=0.66 R=0.81 R=0.57	RMSEP=0.65 RMSEP=0.09 RMSEP=2.7 RMSEP=0.81	Liu *et al.* (2009)
Nafeng	SSC TA	Transmittance	350–1,040		Cross and external	PLS	R=0.92 R=0.64	RMSEP=0.65 RMSEP=0.09	Liu *et al.* (2010b)
Page tangelo	SSC TA	Transmittance	400–1,000		Full cross-validation	PLS	R=0.85 R=0.88	RMSECV=0.45 RMSECV=0.09	Antonucci *et al.* (2010)
Sastuma	SSC TA	Reflectance	400–1,000	SavitzkyGolay	Full cross-validation	PLS	R=0.84 R=0.81	RMSECV=0.59 RMSECV=0.07	Antonucci *et al.* (2010)
Sastuma	SSC TA	Reflectance, interactance and transmittance	500–1,100	2nd derivative SNV	Cross and external	PLS	R^2=0.93 R^2=0.65	RMSEP=0.32 RMSEP=0.15	McGlone *et al.* (2003b)
Satsuma	SSC pH Firm	Reflectance	350–2,500	Smoothing, MSC	Cross and external	PLS	R=0.94 R=0.80 R=0.83	RMSEP=0.33 RMSEP=0.18 RMSEP=8.53	Gómez *et al.* (2006)
Gannan	SSC	Reflectance	800–2,500	SNV, MSC	-	PLS, PCR	R=0.995	RMSEP=0.75	Lu *et al.* (2006)
Navel	SSC	Reflectance	350–1,800	MSC, SNV	Cross- and external validation	PLS and PCA-BPNN	R=0.90	RMSEP=0.68	Liu *et al.* (2010a)
Navel	Vitamin C	Reflectance	800–2,500	COE, SLS, SVN, M MN, MSC, 1st der and 2nd der	Cross-validation	PLS	R=0.96	RMSECV=3.9	Xing *et al.* (2007)

Source: Guthrie *et al.* (2005a)

The band assignments of the major water and sugar (O-H and C-H) vibrations are summarized in Table 2.3. Hydrated objects are characterized by complex hydrogen bonding interactions between water, sugar, protein, etc. In NIR spectra of hydrated samples with large molecules such as fruit and vegetables, the effective absorption bands are relatively wide and complex, even at the fundamental or infrared (IR) frequency, due to different chemical environment of each O-H and C-H bonds in water and sugar molecules (Guthrie *et al.*, 2005a). The wavelength drift or shift in informative peaks may be observed

due to color differences, mechanical changes of the monolithic spectrophotometer and temperature changes resulting in the physicochemical properties of fruit tissue (Gaffney, 1973; Zude *et al.*, 2008).

Table 2.3 The band assignments of the major vibration bonds

Tentative assignment	Unit	Fundamental	Vibrational frequency overtones		
			1st	2nd	3rd
OH stretching	nm	2860-3120	1410-1440	970	738
	cm^{-1}	3200-3500	6950-7100	10300	13550
OH combinations	nm	1920-2068	1100	840	
	cm^{-1}	14800-5200	9090	11900	
CH stretching	nm	3300-3470	1600-1800	1100-1230	910
	cm^{-1}	2880-3000	5550-6250	8100-9100	11000
CH combination	nm	2100-2352			
	cm^{-1}	4250-4750			
CH_2 stretching	nm	3460-3500	1720-1765	1215	930
	cm^{-1}	2880-2910	5670-5820	8230	10750
CH_2 combination	nm	2310-2325			
	cm^{-1}	4300-4330			
OH, CH, and CH_2 deformations	nm	6900-8330	2250-2320	2400-2600	1850-2120
		11111-25000			
	cm^{-1}	1200-1450	4310-4440	3840-4170	4720-5400
		400-900			

Source: Da-Wen Sun (2010)

2.2.4 Influence of external factors on NIR spectra

The influence of external factors such as fruit temperature, spectrometer temperature and ambient tray light was studied (Guthrie *et al.*, 1998). In the research of Liu and Ying (2004) about concerning the influence of external parameters, the NIR based model for sugar content prediction in apples is affected by fruit and spectrometer temperature variations whereas ambient light was not influential. It is therefore necessary to measure the fruit temperature when data are being taken to correct for the bias. The influence of the spectrometer temperature is twice as great as that of fruit temperature.

In the visible region, an absorption band is observed at round 670 nm when the plant parts have chlorophyll. In the NIR region, there are many absorption bands due to water at 970, 1170, 1450, and 1950 nm, and part of the plant have higher reflectance in the region of 700-900 nm are not due to flower petals and leaves but due to fruits and stems. These wavelengths can be used on images for discriminating them from the other parts of the plant in the NIR region. Many fruits have smooth and glossy surface because of cuticle layers which is a transparent layer and is made from cutin and wax, which makes it glossy. This may sometimes become a difficulty to acquire high-quality images of fruit product.

The effects of citrus peel should not be ignored. The peel can affect the spectroscopy results especially in thick-skinned fruit. There are some researchers studying on effect of fruits' peel on non-destructive determination of fruit composition by NIRs. Fraser *et al.* (2003) studied light distribution inside mandarin fruit during internal quality assessment by NIRs. It was found that the skin of mandarin created a significant internal reflection leading to elevated light level in the fleshy part, thus influencing the scatter and absorption of light. In addition, sound peel and different types of blemishes display distinct spectral responses (Gaffney, 1973). In contrast, Jamashidi *et al.* (2011) concluded that the effect of chemical composition of the peel can be ignored in non-destructive spectroscopy of intact citrus. Moreover, Fujita and Tono (1985) demonstrated that some external damage to citrus fruits could be detected within the range of 265-325 nm using ultraviolet spectrometry. Therefore, commercial citrus inspection system are recently often equipped with two different types of camera–one sensitive to visible light and the other to capable of detecting infrared radiation.

2.3 NIR HYPERSPECTRAL IMAGING

2.3.1 Differences between HSI, conventional NIRs and conventional Imaging

Image processing and image analysis are the core of computer vision which became an integral of the industry's move forwards automation. However, the computer vision system has some drawbacks that are inefficient in the case of objects of similar color and unable to quality attributes. Because, the product's quality index can be identified based on the correlation between the spectral response and the specific quality attributes of the products, usually a chemical parameters (Park *et al.*, 2002). Recently, optical techniques using NIRs is able to obtain information about the sample components based on the light absorption

of the sample, but it is not easy to know the location or position information. The combination of the strong and weak points of conventional spectroscopy and conventional imaging techniques are the HSI techniques which has been regarded as a promising analytical tool for analyses conducted in research and industries. While a gray scale image typically reflects the light intensity over the electromagnetic spectrum in a single band, a color image reflects the intensity over the red, blue and green bands of the spectrum. Increasing the number of bands can greatly increase the amount of information with different resolution values. HIS has been invented to integrate spectroscopic and spatial (image) (Chen *et al.*, 2002) which be impossibly achieved with either vision system or NIRs techniques. HIS can be carried out in reflectance, transmission or fluorescence modes while the majority of published research on HSI has been performed in reflectance mode. The main differences and advantages of HSI over conventional imaging and spectroscopic techniques are shown in Table 2.4.

Table 2.4. Main differences among imaging, spectroscopy, and HSI techniques

Attribute	Imaging	NIRs	HSI
Spatial information	√	X	√
Spectral information	X	√	√
Multiconstituent information	X	√	√
Building chemical images	X	X	√
Flexibility of spectral information extraction	X	X	√

Source: Da-Wen Sun (2010)

For better understanding the differences between HSI and conventional imaging and conventional spectroscopy, general system configurations for conventional imaging, conventional spectroscopy, and HSI are illustrated in Figure 2.4.

Different imaging spectroscopy makes use of the following equation (Eq.2.9)

$$\Delta I = I_{\lambda i} - I_{\lambda j} \qquad \text{(Eq. 2.9)}$$

where $I_{\lambda i}$ is an image at the wavelength i and $I_{\lambda j}$ is the same image at wavelength j. The image at wavelength i is the measuring wavelength and the image at wavelength j is the reference wavelength. The resulting different image ΔI is due solely to the absorption band of interest. The essence of this approach is that the camera is turned into a spectrometer

with multiple sensors. This system enhances the ability to measure concentration distributions with high resolution. In addition, light plays a crucial role in the HSI system in order to see clearer, farther, and deeper and to gain detailed information about different targets. The HSI system can capture light from frequencies beyond the visible light range. This can allow extraction information that the human eyes failed to capture.

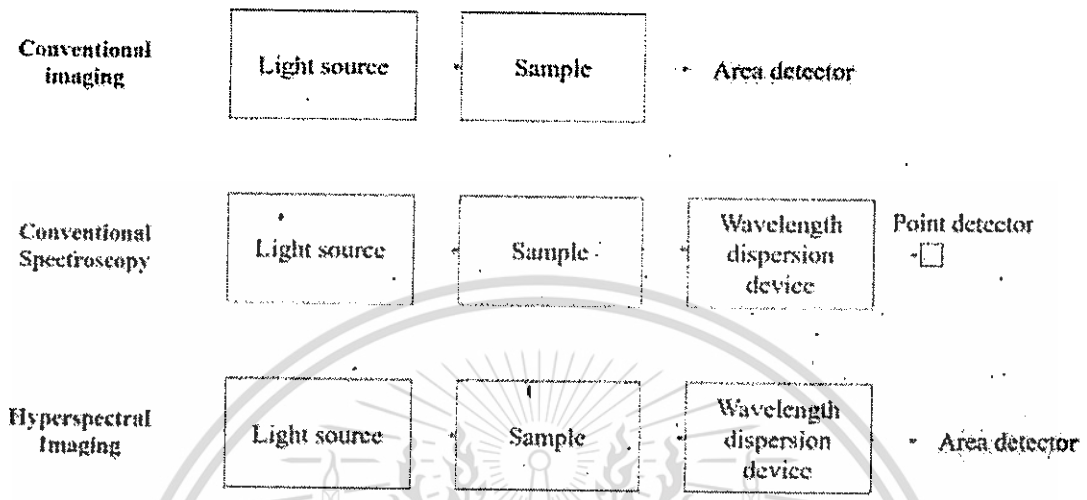

Figure 2.4 General system configurations for conventional imaging, conventional spectroscopy, and HSI

Source: Da-Wen Sun (2010)

2.3.2 Terminology

2.3.2.1 Spectral resolution

The spectral resolution of the HSI system is related to its spectrograph as a measure of its power to resolve feature in the electromagnetic spectrum. Spectral resolution is defined as the absolute limit of the ability of the HSI system to separate two adjacent monochromatic spectral features emitted by a point in the image.

2.3.2.2 Spatial resolution

The spatial resolution of the HSI system determines the size of the smallest object that can be seen on the surface of the specimen by the sensor as a distinct object separate from its surroundings. Spatial resolution also determines the ability of a system to record detail explained. The parameter most commonly used to describe spatial resolution is the field of view (FOV). Spatial resolution is determined by the pixel size of the two dimensional camera and the objective lens as the spectrograph is designed with a unity magnification.

2.3.2.3 Band number

The number of bands is one of the main parameters that characterize HSI system. The number of bands in the HSI system could be about 100-250 spectral bands in the electromagnetic spectrum.

2.3.2.4 Signal-to-noise ratio (SNR)

The SNR is the ratio of radiance measured to the noise created by the detector and instrument electronics (Da-Wen Sun, 2010). In HSI system, the SNR is always wavelength-dependent because of overall decreasing radiance towards longer wavelengths. The higher the ratio, the less obtrusive the background noise is.

2.3.2.5 Spectral signature

Hyperspectral imaging exploits the fact that all materials, due to the difference of their chemical composition and inherent physical structure, reflect, scatter, absorb, and/or emit electromagnetic energy in distinctive pattern at specific wavelengths. This characteristic is called spectral signature or spectral fingerprint, or simply spectrum. Every image element (pixel) in the hyperspectral image contains its own spectral signature. In principle, the spectrum can be used to uniquely characterize, identify, and discriminate by class/type any given object (s) in an image over a sufficiently broad wavelength band (Shaw and Manolkis,. 2002).

2.3.3 Configuration of HSI system

In this section the main components of a HSI system employing the push-room design, also called line scanning, is going to be explained. The push-broom HSI system consists of these main components: a light source to provide illumination; a light irradiation of samples, a camera containing a cooled two-dimensional (2D) light detector, a hyper-spectrograph to disperse the wavelengths of the reflected, transmitted, or scattered light and deliver signals to the photosensitive surface of the detector, translation stage, illumination units, and a computer.

The basic elements of a HSI spectrograph are shown in Figure 2.5. The light source such as halogen lamp, illuminates the object to be measured, and the entranced optics, e.g. camera lens, collects the radiation from the object and forms an image on the image plane 1, where the entrance slit of the imaging spectrograph is located. The slit acts as a field-stop to determine the instantaneous FOV in spatial directions to a length of Δx and a width of Δy, marked as the measured area in Figure 2.5. Each point A in the spatial x-direction of the measured area has its image A' on the entrance slit. The radiation from the slit is

collimated by either a lens or a mirror and then dispersed by a dispersing element, which is typically a prism or grating, so that the direction of propagation of the radiation depends on its wavelength. It is then focused on image plane 2 by the focusing optics, i.e. a lens or mirror. Every point A is represented on image plane 2 by a series of monochromatic images forming a continuous spectrum in the direction of the spectral axis, marker with different sizes of "A". The focused radiation is detected by the 2D detector array such as CCD detector. In addition to define spectral resolution, slit width controls the amount of light entering the spectrograph. Also, the collimator makes this light parallel so that the disperser (a grating or prism) disperses it. The dispersed light is then mapped onto the detector array, resulting in a 2D image, one dimension representing the spectral axis and the other containing the spatial information for the scanning line. By scanning the entire surface of the specimen, a complete 3D hyper-spectral image cube is created, where two dimensions represent the spatial information and the third represents the spectral information (Lu, 2003).

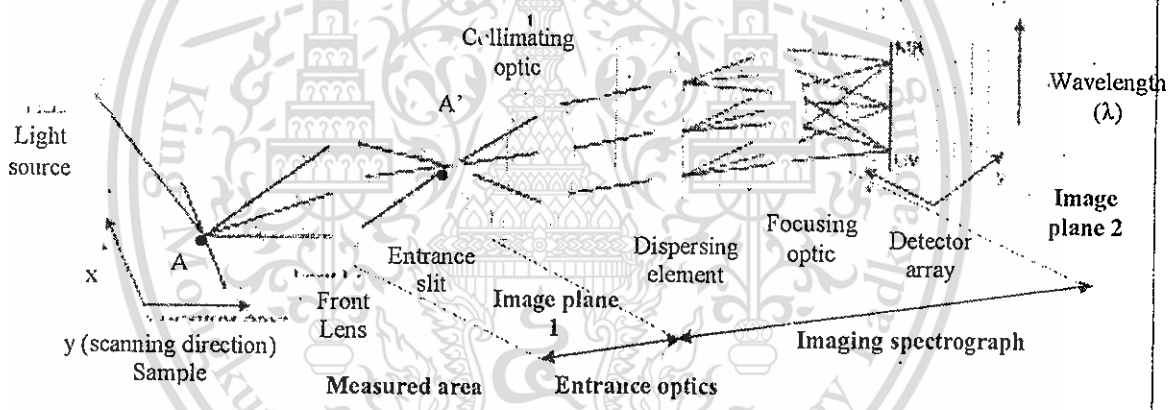

Figure 2.5. The basic elements of a HSI spectrograph, with the entrain optics and generation of the 3D data-cube: spatial (x,y) and spectral (λ) dimensions

Source: http://www.specim.fi/

Utilization of diffusers between lamps and object gives higher illumination, but it often causes halation on glossy surface objects. To improve these problems in dome and diffuser, polarizing (PL) filters are used in front of camera lens and lighting devices. A key technique for using the PL filters is how to protect the PL filter which is so weak for heat and starts melting at 60°C. When an uncertain –shaped object is radiated by lighting device, it is important to uniformly illuminate the object. For 10cm diameter fruits such as apples, pears, peaches, and other round-shaped objects, three or four lighting devices with about

20 cm distance are appropriate. When recently developed color CCD cameras are used, 5000 to 7000 lux illumination is enough for 1/1000 seconds shuttle speed, even if PL filters, which reduce luminous flux into 1/3, are used in front of the lighting devices and camera lens. For example, two 12V and 50W halogen lamps, with 38° radiation angle, 3200 K color temperature, and 4000 hours life, are used in an actual fruit grading system. There are many other types of lamps such as incandescent lamp, fluorescent lamp, LED (light – emitting diode) and HID (high-intensity discharge) lamp. It is important to select an appropriate lamp based on the optical properties of the object and on its own purpose because the properties of luminance, lumen maintenance, color rendering, color temperature, life, and cost vary depending on the lamp. Kondo *et al.* (2006) studied about PL filtering image with halogen lamp, which shows irregular fruit shapes often make unexpected halation occur at local places or unevenness of illumination may be found on the fruit surfaces, even when illumination conditions are perfectly adjust for the fruit variety. The number of halation sometimes exceeds the number of light sources due to the irregular shape. To eliminate the halation and the surrounding reflection is the most important subject for a construction of machine vision system as well as to uniform the illumination condition for the fruit variety.

Detector of HSI system

The main part of this system is the spectrograph which is a system for delivering multiple images of an illuminated entrance slit onto a photosensitive surface, called detector. For the HSI system detector, there are three basic choices of cameras for this application, including silicon (Si)-based CCD, indium gallium arsenide (InGaAs), and mercury cadmium telluride (HgCdTe). The choice of the camera in a particular HSI system depends on the required wavelength, the quantum efficiency (QE) representing the sensitivity (the higher QE indicates higher sensitivity), and the cost. At present, the CCD camera (300 – 1,100 nm) is the most widely used Vis/NIR detector in food quality and safety analysis, with the advantage of lower cost and potential wider availability (compared to InGaAs and HgCdTe). Three types of InGaAs detectors were studied, including InGaAs1700 (900–1,700 nm), InGaAs2200 (1,000–2,200 nm), InGaAs2500 (1,200–2,500 nm). An intersection point of the QE curves of InGaAs and Si based cameras was observed around 900 nm. The QE of InGaAs1700 falls to under 40% below 900 nm, while the QE of Si based camera falls to 40% above 900 nm. If the required wave band is

around 900 nm, the choice of camera may depend on whether it tends to Vis or NIR. In contrast of three types of InGaAs detectors, a better choice would be the InGaAs1700, whose QE is higher than 50% above 950 nm and keep higher than 80% between 1,000–1,600nm, with an average QE of 60%. The InGaAs2200 and InGaAs2500 have average QE around 50% and 55% separately at the desired wavelength ranges, but not good as same as InGaAs1700. All types of InGaAs cameras have better sensitivity than Si-based cameras in the NIR region especially above 900 nm. HSI systems based on InGaAs camera may provide increased accuracy for assessment and analysis of food quality and safety (Ariana and Lu, 2010; Ariana *et al.*, 2006; Williams *et al.*, 2009) but the cost of NIR cameras is higher than for Vis/NIR cameras, which may affect the application of NIR HSI. To increase detector efficiency especially in the infrared regions, the detector should be cooled. Cooling reduces the array's dark current, thus improving the sensitivity of the detector to low light intensities and hence reducing the thermal noise to a negligible level.

2.3.4 Calibration of HSI

The goals of calibration process in HSI are:

- standardize the spectral axis of the hyperspectral image,
- determine whether a HSI system is operating properly,
- provide information about the accuracy of the extracted spectral data and thus validate their acceptability and credibility,
- diagnose instrumental errors, measurement accuracy, and
- reproducing under different operating conditions.

The most significant step in the calibration process is the spectral wavelength calibration that identifies each spectral channel with a specific wavelength. To determine the relation between distance (in pixels) on the spectral axis and wavelength, the spectral axis, must be calibrated by using a standard emission lamp as a light source.

In the practice, the calibration lamp is first scanned by the HSI system under controlled operating conditions. Once the calibration lamp is scanned, its peaks are then assigned to standardize the spectral axis. Then a polynomial regression of first or second order can be established to convert spectral axis (in pixels) to its corresponding wavelength using the reference wavelength of calibration lamp.

Finally, after acquiring hyperspectral images of real samples, another calibration step. Called reflectance calibration, should be performed to account for the background spectral

response of the instrument and the "dark" current of the camera. The background is obtained by acquiring a spectral image from a uniform, high reflectance standard or white ceramic (~100% reflectance), and dark response (~0% reflectance) is acquired by recording an image when the light source is turned off and the camera lens is completely covered with its non-reflective opaque black cap. These two reference images are then used to calculate the pixel-based relative reflectance for the raw line-scan images using the following formula (Eq. 2.10):

$$I = \frac{I_0 - D}{W - D} \qquad \text{(Eq. 2.10)}$$

Where I is the relative reflectance image, I_o is the raw reflectance image, D is the dark reflectance image, and W is the white reference image.

The corrected hyperspectral image can also be expressed in absorbance (A) by taking logarithms of the above equation 2.11 as:

$$A = log_{10}\left(\frac{I_0 - D}{W - D}\right) \qquad \text{(Eq. 2.11)}$$

2.3.5 Acquisition modes of HSI

There are three conventional ways to build one spectral image: area scanning, point scanning, and line scanning. In this research, we concentrated on the line scanning which is also called push-broom. It involves acquisition of spectral measurements from a line of sample which are simultaneously recorded by an array detector, and the resultant is stored in the Band Interleaved by Line (BIL) format. This method is particularly well suited to conveyor belt systems, and may therefore be more practicable than the former ones for food industry applications.

Line scanning devices record a whole line of an image rather than a single pixel at a time using a two –dimensional dispersing element (grating) and the two – dimensional array. A narrow line of the specimen is imaged onto a row of pixels on the sensor chip and the spectrograph generates a spectrum for each point on the line, spread across the second dimension of the chip. Therefore, hyperspectral images are acquired by a wavelength dispersive system that incorporates a diffraction grating or prism. These instruments typically require an entrance aperture, usually a slit, which is imaged onto the focal plane of the spectrograph at each wavelength simultaneously. Therefore, an object imaged on the slit will be recorded as a function of its entire spectrum and its location in the sample. This configuration is normally used when either the specimen or the imaging unit is

moving one in respect to the industrial applications. The sensor detectors in a push-broom scanner are lined up in the row called a linear array. HSI systems can be conducted either in reflectance or transmittance modes. To acquire images in transmittance mode, thin sample sizes are usually used to allow light to travel through the sample. Thicker samples can be used in reflectance HSI measurements. Thus, food materials can be inspected as a whole in reflectance mode without the need to make slices. For instance, Peng & Lu (2008) studied about firmness and TSS of apples using HSI in reflectance mode. In this research, we employed Sisu CHEMA that is a complete chemical imaging system, characterized by speed, simplicity and superior performance. SiSu CHEMA employs a push-broom imaging technology providing several advantages for the users, such as high speed, low heat load from illumination and flexibility to most sample shapes and sizes. Push-broom approaches these characteristics: (1) It is a line-scan device; (2) Full spectra of the all spatial positions along the imaged line is recorder in one single snapshot; and (3) Target must be imaged line-by-line form the 2D image.

The penetration depth could have effects on the HSI detection. By providing references for thickness determination, which could be valuable for designing an appropriate and accurate sensing configuration, penetration depth would prove beneficial. Light penetration depth is defined as the depth at which the incident light was reduced by 99%. It can vary according to the status, type of sample, and the detection waveband. Optical features of the light penetration depth are mainly determined by strong absorbing constituents in the sample. Lammertyn *et al.* (2000) proved that light penetration depth in apples was dependent on the detection wavelength by putting forward a non-linear model describing the correlation between the reflectance and thickness of apple slices. The penetration of apple is up to 4 mm in the 700–900 nm range and between 2 and 3 mm in the 900–1,900 nm range. In the research of Qin and Lu (2008), the light penetration depth in tissues of apple, peach, pear, kiwifruit, tomatoes, zucchini, cucumber, and plum was calculated according to the absorption and reduced scattering spectra of the test samples at different wavelengths. The minimum light penetration depths ranged from 7.1 mm at 535 nm for the plum to 13.8 mm at 720 nm for the zucchini. The wavelengths were correlated to the absorption peaks of the major pigments in the fruits and vegetables. The maximum penetration depths ranged from 18.3 mm for the apple to 65.2 mm for the zucchini. This study highlighted that penetration depth varies a great deal depending on the type of object

being studied and the applied depth, and on surface and texture of sample. Long wavelength and short wavelength has different energy so penetration depth is different. Short wavelength has high energy so penetration depth is longer than long wavelength.

Image Acquisition – Plant Materials (Naoshi, 2011)

Plant materials have unique characteristics in their color, shape, size, spectral reflectance, and biological structure that are different from industrial materials. In this entry, cuticle layers on fruit surfaces are in focus and how to acquire non-halation images of glossy surface fruits is described. Especially lighting devices, one of the most important components in machine vision systems and acquired images by three different methods using dome, diffuser, and polarizing filter, should be explained clearly.

2.3.6 Hyperspectral image data

Hyperspectral image data consist of several congruent images representing intensities at different wavelength bands composed of vector pixels containing three–dimensional hyperspectral cube, or hyper cube or data cube which can provide physiochemical information of the material under test (Cogdill *et al.*, 2004).

Intensity values of a spatial image in the hypercube at one wavelength may have 8-bit gray values meaning that 0 is the black and 255 is the white. In more precise system, the intensity values of each pixel having 12-bit (2^{12} gradations, i.e., 0-4095), 14-bit (2^{14} gradations, i.e., 0-16383), or 16-bit (2^{16} gradations, i.e., 0-65535) gray levels are used. For more demanding scientific applications such as cell, fluorescence or Raman imaging, a higher performance 16-bit cooled camera may be advantageous. Hyperspectral data volumes are very large and suffer from collinearity problems. This has implications for storage, management, and further image processing and analysis.

2.3.7 Spectral data analysis and chemometric

HSI system cannot stand alone without the help of some software for gaining high performance in acquisition, controlling, and analyzing. It is essential to support the system with software for image acquisition, software for controlling the motor to move the sample line by line, software for extracting spectral data and pre-processing steps, software for multivariate analysis, and software for final image processing. Typical steps, required to obtain the key information about the process or about the samples, usually undertaken in HSI experiments are outlined in the flowchart describes in Figure 2.6.

The first step is the collection of a HSI by utilizing ideal acquisition conditions in terms of illumination, spatial and spectral resolution, motor speed, frame rate, and exposure/ integration time. After acquiring a HSI for the tested sample, this image should be calibrated with the help of white and dark HSI as mentioned above. Extracted data should be preprocessed to reduce noise, improve the resolution of overlapping data, and to minimize contributions from imaging instruments responses that are not related to variations in the composition of the imaged sample itself. Pre-processing of spectral data is often of vital importance if reasonable results are to be obtained from the spectral analysis step. Pre-processing includes spectral and spatial operations. Spectral pre-processing includes some operations such as spectral filters, standard normal variate (SNV), multiplicative scatters correction (MSC), and smoothing. On the other hand, spatial operations include low-pass filters, high pass filters, and a number of other spatial filters.

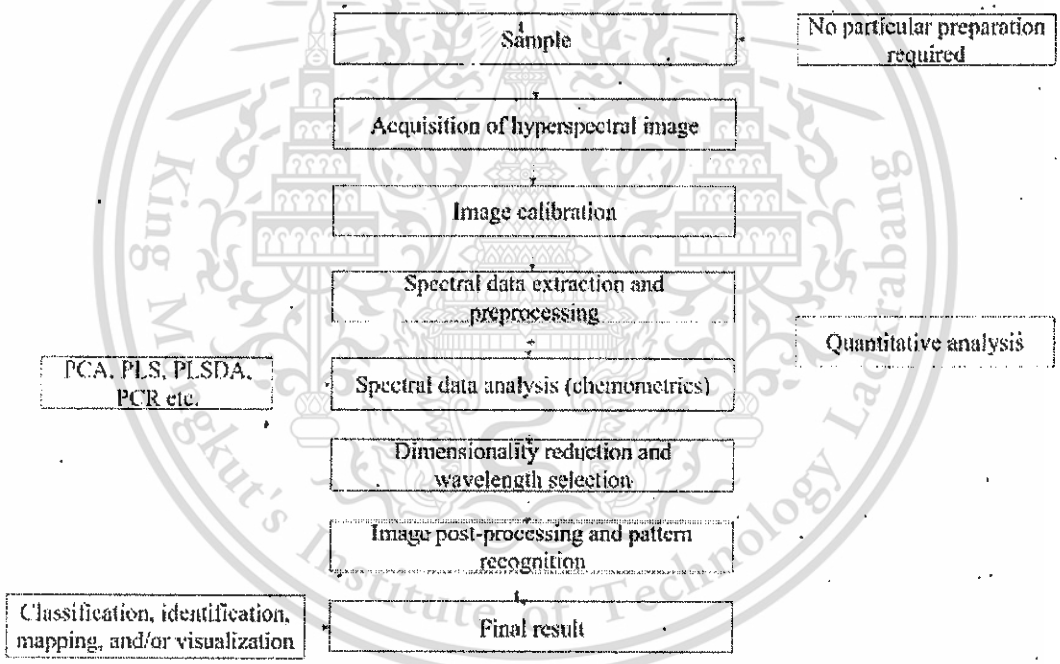

Figure 2.6 Flowchart of the key steps involved in HSI analyses

Results obtained from pre-processing, qualitative and quantitative analysis must be visualized either by scaling, surface mapping or pseudo-color representation. Once the final digital concentration images have been generated, traditional post-processing of these images, such as segmentation, enhancement, and morphological feature extraction can be applied as a final step of the workflow. The final image processing step is carried out to

convert the contrast developed by the classification step into a picture depicting component distribution. Grayscale or color mapping with intensity scaling is commonly used to display compositional contrast between pixels in an image. Final results of these calculations are used to develop key quantitative image parameters to characterize various traits in the tested samples in different categories by performing classification, identification, mapping and/or visualization.

2.3.8 Advantages and disadvantages of HSI

The foremost advantages of using HSI technology in food analysis can be summarized in the following points:

- No sample preparation;
- A chemical-free assessment method;
- It is noninvasive and nondestructive method, so that the same sample could be used for other purposes and analyses;
- It is eventually economic because it save in labor, time and reagent cost in addition to the large saving in the cost of waste treatments;
- Rather than collecting a single spectrum at one spot on a sample, as in spectroscopy, HSI records a spectral volume that contains a complete spectrum for every spot (pixels) in the sample;
- It has the flexibility in choosing any region of interest (ROI) in the image even after image acquisition;
- It is able to determine several constituents simultaneously in the same sample; and
- It allows for the visualization of different biochemical constituents presented in a sample based on their spectral signatures because regions of similar spectral properties should have similar chemical composition. This process is called building chemical images, or chemical mapping, for constructing detailed maps of the surface composition of foods which traditionally requires use of intense laboratory methods.

In spite of the abovementioned advantages, HSI does have some disadvantages, which can be summarized as follows:

- HSI contains substantial amount of data, including much redundant information, and present considerable computational challenges;

- It takes a long time for image acquisition and analysis, therefore HSI technology has to a very limited extent been directly implemented in on-line systems for automated quality evaluation purposes;
- One of the main analytical drawbacks of HSI technique is that it is an indirect method, which means that it is needs standardized calibration and model transfer procedures;
- One major factor that limits its industrial applications for food inspection is the hardware speed needed for rapid image acquisition and analysis of the huge amount of data collected; and
- Depending on the spatial resolution and the structure of the sample investigated, spectra from individual image pixels may not represent a pure spectrum of one singular material, but a mixed spectrum consisting of spectral responses of the various materials that cover the region of interest (ROI) selected from the sample.

2.3.9 Application of NIR HSI in fruit quality analysis

Imaging techniques have been developed and successfully applied as inspection tools for quality assessment of a variety of fruits (Xing *et al.*, 2005; Mehl *et al.*, 2004). One quality attribute of fruit that has been assessed using HSI is TSS. Peng and Lu (2008) designed a reflectance system to detect apple firmness and TSS using stable object stage. Optic fiber and focusing lenses were used to illuminate samples as a spot light source and 2D hyper-spectral images were collected. The light source used in this study was delivered by a circular beam of 1.5 mm, which scanned the fruit 1.6 mm off the incident center. Ten MLD functions were proposed to fit the spectral scattering profiles and the best one was chosen as the ideal method for predicting fruit firmness and SSC using MLR. The best prediction results with two attributes of apple were got with correlation coefficient of 0.85. In the study, over 20 wavelengths were used for prediction. This may influence the data processing speed. Later, Mendoza *et al.* (2011) employed integrated spectral scattering and image characteristics to predict the firmness and TSS of apples. The results indicated an increase of 6% of standard errors of prediction (SEP) for firmness and 3% of SEP for TSS. Kondo and other researchers (Kondo, 1995; Kondo *et al.*, 1995, 2000) introduced morphological features of oranges, such as shape, texture and size, which was calculated using image analysis, as input in a neural network to predict moisture content and pH of fruit. They concluded that it was possible to obtain these internal features from the

appearance of the citrus. Table 2.5 presents a summary of typical papers published in hyperspectral detection of fruits quality and safety since 2008.

Table 2.5 Summary of product type, analysis type, wavelength region, and modeling algorithm in representative papers published on HSI (in reflectance mode) of fruits

Camera	Product	Spectral coverage (nm)	Analysis type	Image processing	Modeling	Reference
CCD	Apple	600-1000	Quantitative	Thresholding (TH)	PLS, PLSDA	Huang and Lu (2010)
CCD	Apple	400-1000	Qualitative	TH	Artificial neural networks (ANN)	Elmasry *et al.* (2009)
CCD	Apple, peach, kiwi fruit, plum	500-1000	Quantitative	TH	Manual analysis	Qin and Lu (2008)
CCD	Citrus	400-1100	Qualitative	Geometric factor correction (GFC)	Digital elevation model (DEM)	Gómez-Sanchis *et al.* (2008a)
EMCCD	Citrus	450-930	Qualitative	TH	Spectral information divergence (SID) mapping	Qinet *et al.* (2009)
CCD	Mandarin	320-1100	Qualitative	GFC	Linear discriminant analysis (LDA)	Gómez-Sanchis *et al.* (2008b)
CCD	Oranges	400-1100	Qualitative	PCA	PCA, Band ratio (BR), TH	Li *et al.* (2011)

Source: Gomez *et al.* (2006)

Some works also have been done for defect detection of fruits. Qin *et al.* (2009) examined the relationship between hyperspectral area images and citrus canker, using an EMCCD imaging device which is a type of CCD with high photosensitivity. EMCCD is a quantitative digital camera technology that is capable of detecting single photon events whilst maintaining high QE, achievable by way of a unique electron multiplying structure built into the sensor. Later, the hyperspectral area images were processed and classified to different citrus canker lesion from normal and other peel diseased conditions including greasy spot, insect damage, scab, and wind scar. The overall classification accuracy was 96%. It was noted that canker lesions at different developmental stages affected the classification results. Indeed, canker lesions influenced the reflectance characteristics of a given object. In another agricultural work, Gomez *et al.* (2006) selected the most suitable wavelength for detecting infection penicillium digitatum in mandarins. The vast amount of information generated from images was reduced by using statistical techniques such as PCA and PLSR.

Further work should be targeted at the changing patterns of the citrus canker reflectance properties and incorporate canker spectra at different growth stages. Meanwhile, since this research used full spectral information which was not good for online citrus canker detection, more work could be done at exploring better method to optimize waveband combination and raise image processing speed.

2.4 STATISTICAL ANALYSIS

Qualitative and quantitative NIR spectroscopic methods required multivariate calibration algorithms referred to chemometric methods to model spectra response to quality properties of calibration set. The unique wavelength regions, where changes in the concentration of chemical properties or physical properties are correlated to the changes in the respond of the near-infrared spectrometer, are identified using chemometric methods (Workman and Weyer, 2008). Chemometric is the use of mathematical and statistical methods to improve the understanding of chemical information and the correlation between the quality properties and the analytical instrument data. It can be used to enhance method development and make use of statistical models for data analysis. The spectroscopists' chemometric include these following below requirements:

- Proper application of spectroscopic data pre-processing to reduce and correct interferences such as overlapped bands, baseline drifts, scattering, and path-length variation;
- A strong calibration and diagnostic means of sample selection and variable selection, statistic result calculation to build reliable models; and
- Model validation and integration means to supply rigorous prediction.

The detail description of NIRs calibration process is listed following parts.

2.4.1 Selecting the calibration set

Samples are firstly measured by the second methods (non-destructive methods). Then, the real property or analytical concentration of a sample must be measured with a reference method, such as HPLC, which may require sophisticated and expensive instrument experienced staffs and they may complicated, and time-consuming. The values were found by reference methods are called actual values (or laboratory value). The reference methods must be correct and its values must be true. If the reference method used not accurate, a good calibration may be built, however, on erroneous values. These erroneous reference values will then create the predicted values with the same errors as the reference method. Therefore, the vital condition for accurate predicted results is the reference values that must be correct.

A sample with unknown properties can now be measured by the indirect methods (nondestructive methods) the indirect methods (nondestructive methods) may work with simpler equipment and may easy to carry out, such as FQA-NIR Gun. These values of samples were recorded by nondestructive methods that are plotted versus the actual values, and a regression curve is erected. When chemometric methods are applied, the analytical data points are calculated from many measurements that are called predicted values. The calibration line is the graph of the predicted values obtained by the reference method. The scattering of data point around the calibration line, presented as the regression coefficient, is an assessment of the precision of the indirect methods (nondestructive methods).

The selection of a set of calibration standards included following important considerations:

- The analyst must prepare samples which include the complete range of component concentration as distributed as possible (Jerome and Workman, 1992). Random sample selection will cause the mathematical model to most closely fit to the middle

concentrated samples while the few samples at extremely high or low concentration level will influence the slope and intercept inordinately (Jerome and Workman, 1992). If the mathematical model is developed on standards but a small range in moisture, the calibration model will only to useful for samples with a narrow moisture range such as was represented by the standards (Jerome and Workman, 1992).

- The variance of the sample set used to produce NIRs calibration equations indicated both robustness and accuracy for a particular application. A calibration set includes a wide variation of sample types and a large constituent range will allow a calibration model where a wider range of materials may be analyzed, but with a resultant loss in accuracy. If the calibration set has a small variance in sample type and a narrow constituent range, the accuracy for analyzed samples within the range is increased (Jerome and Workman, 1992).
- Some common errors must be included are technician error in sample preparation, temperature differences in standards or instrument while taking data, calibration standard instability, instrument noise and drift, changes in instrument wavelength setting, stray light effects, color differences with concentration, solvent interaction differences with change in concentration, and the reference method does not measure the same component as a spectroscopic method (Jerome and Workman, 1992).
- Calibration must not only uniformly cover an entire constituent range; they must be composed of a uniformly distributed set of sample types. Ideal calibration sets are composed of equal or greater than 10-15 samples per analytical term. These samples ideally have widely varying composition evenly distributed across the calibration range.

The quality of the calibration equation may strongly depend on the number of calibration samples used for quantitative and qualitative analyses. The predictive value of the equation obtained is generally increased with the number of samples used for calibration. Moreover, sample selection proves to be a crucial step of the calibration procedure. In order to obtain a calibration model satisfyingly predicting desired target parameters in unknown samples by means of NIRs, calibration samples and samples to be predicted need to be part of the same population. Calibration samples should be

representative for the population to be predicted with a variation as large as possible, but limited to the region of interest. The entire natural range of spectral and reference value variability should be covered: Moreover, the samples should be evenly distributed within the range. For agricultural commodities the sample set should be sufficiently variable with respect to variety, production area, production year, and maturity stage to meet the aforementioned requirements (Kawano, 2002; Næs *et al.*, 2002; Williams, 2008). Several chemometric algorithms are available for the efficient selection of calibration samples fulfilling these criteria. Among them, the Kennarde Stone algorithm is the most widely used (Blanco and Alcala, 2009).

2.4.2 Outlier detection

An outlier is characterized by abnormal spectral data or a high residual between the predicted value and reference value. Removal of outliers may improve the model performance; however, useful variance from the model may be removed, leading to poorer predictions of new sample sets. Therefore, outliers should only be removed for good reasons, when their origin and the causes for their unreasonable behavior is clear. To be exact, for practical purposes in routine commercial analysis, there can be no outliers since every sample must be tested. Hence, the removal of outliers may lead to the loss of a valuable source of information for the prediction of unusual samples or under unexpected measurement conditions (Herold *et al.*, 2009; Williams, 2007). Spectra with a Mahalanobis distance, which is a measure how many standard deviation away is from the mean, greater than 3.0 was deemed as outliers and were mostly because of poor spectral quality (Blakey and van Rooyen, 2011).

2.4.3 Data pre-processing of NIRs data

Pre-processing of NIRs spectral data is a vital part of chemometric modeling. The main goal of pre-processing is to transform data in such a way that the (multivariate) signals will be better adhere to Beer's law, which states that absorbance (A) and concentration are linearly correlated follow Eq. 2.12:

$$A = \varepsilon \times l \times c \qquad \text{(Eq. 2.12)}$$

where ε is the molar absorptivity, l is the path length, and c is the concentration of the constituent of the interest. The collective term $\varepsilon \times l$ is constant, thus making the relationship between A and c linear.

2.4.2 Outlier detection

An outlier is characterized by abnormal spectral data or a high residual between the predicted value and reference value. Removal of outliers may improve the model performance; however, useful variance from the model may be removed, leading to poorer predictions of new sample sets. Therefore, outliers should only be removed for good reasons, when their origin and the causes for their unreasonable behavior is clear. To be exact, for practical purposes in routine commercial analysis, there can be no outliers since every sample must be tested. Hence, the removal of outliers may lead to the loss of a valuable source of information for the prediction of unusual samples or under unexpected measurement conditions (Herold *et al.*, 2009; Williams, 2007). Spectra with a Mahalanobis distance, which is a measure how many standard deviation away is from the mean, greater than 3.0 was deemed as outliers and were mostly because of poor spectral quality (Blakey and van Rooyen, 2011).

2.4.3 Data pre-processing of NIRs data

Pre-processing of NIRs spectral data is a vital part of chemometric modeling. The main goal of pre-processing is to transform data in such a way that the (multivariate) signals will be better adhere to Beer's law, which states that absorbance (A) and concentration are linearly correlated follow Eq. 2.12:

$$A = \varepsilon \times l \times c \qquad \text{(Eq. 2.12)}$$

where ε is the molar absorptivity, l is the path length, and c is the concentration of the constituent of the interest. The collective term $\varepsilon \times l$ is constant, thus making the relationship between A and c linear.

Many physical and chemical phenomena can cause a deviation from this linear relationship, including scatter from particulates, interferents, molecular interactions, changes in refractive index at high concentrations, shifts in chemical equilibrium as a function of concentration, stray light, changes in sample size path length, etc. Pre-processing techniques are aimed to make up for these deviations from linear relationships and to improve the linear relationship between the spectral signals and analyzed concentrations.

Spectral pre-treatments, included MSC, SNV, smoothing, first-order derivative and second-order derivatives (using SavizkyGolay method) and the combination of smoothing and the mentioned pre-processing methods (MSC, SCV, 1st and 2nd

derivative), were carried out in order to improve the subsequent multivariate regression and predictability.

- The MSC reduces the effect of scattering of light due to variation in sample's particle size and brings the spectra of different samples closer as compared to original spectra (De Noord, 1994).
- The SNV was developed by Barnes *et al.* (1989) to remove multiplicative interferences of scatter and particle size and to account for the variation in baseline shift and curvilinearity in diffuse reflectance spectra.
- Smoothing operation is beneficial in presence of noise in spectra (Chalmers and Griffiths, 2002).
- The derivative computation is usually more beneficial for consideration when spectra are having overlapping peaks (Goodson, 2011).

2.4.4 Mathematical model

Particularly NIRs is characterized by the lack of selective wavelengths directly correlated with distinct sample properties. A wide range of different chemical and physical attributes of complex samples has an impact on NIR spectra resulting in overlapped bands. Thus, the univariate calibration based on least square regressions (LSR) is inappropriate, since a direct relationship of the property to be predicted and the measured signal is required. To overcome this problem, multiple or all spectral predictor variables (e.g. wavelengths) are used for establishing multivariate calibrations.

Principal component regression (PCR) and partial least squares (PLS) regression are most frequently applied data compression techniques that construct new variables (Blanco and Alcala, 2009; Martens and Næs, 1989; Næs *et al.*, 2002). The PLS regression algorithm using the information of both the spectroscopic variables and the respective parameter variables of the analyzed samples is the main difference between PLSR and PCR. PCR comprises PCA of the spectral variables for data compression and subsequent least squares regression between selected principal components (PC) and the corresponding reference values (Blanco and Alcala, 2009; Mark, 2008). Data are compressed by directly relating spectral and parameter variances instead of using selected, most dominant PCs. The resulting linear combinations of the variables used for calibration are referred to as latent variables, factors or components. These contain the entire spectral information and are more directly related to spectral variability than the

PC. Balancing of the spectral and parameter information reduces the impact of large but irrelevant spectral variance to the calibration model. Hence, the objective is to ensure that the first few latent variables contain as much information of predictive value as possible (Blanco and Alcala, 2009; Martens and Næs, 1989). The optimal number of factors, latent variables or components should be selected to minimize the error of the prediction model. An insufficient number of factors do not cover all relevant information, leading to under-fitted, suboptimal calibration models. Using too many factors goes along with redundancies and noise of the spectral variability within the calibration equation. Therefore, the model becomes over-fitting and being strongly data dependent with poor prediction results for new samples. Smaller numbers of factors together with approximately the same prediction error are therefore preferable. The optimum number of factors is commonly determined by prediction testing, using a test set or cross-validation (Blanco and Alcal, 2009; Næs *et al.*, 2002). The aforementioned linear calibration techniques frequently perform well. However, in some cases, non-linear methods are required in order to obtain satisfactory calibration models. Important methods for solving extrinsic non-linearity problems are based on mathematical pre-treatment by applying transformation techniques. For leave-one-out full-cross-validation, samples are successively deleted from the calibration set. Alternatively, segments of the sample set may be selected for prediction group. Subsequently, the calibration equation is developed by using the remaining samples. Calibration performance is tested by predicting the remaining samples and comparing the predicted values with the reference values. The selected samples are reintroduced into the calibration set, and the next sample is deleted. The procedure is continued until all samples have been deleted once.

2.4.5 Validation of the mathematical model

Following the computation of calibration equations, its prediction performance for unknown samples needs to be evaluated. This is of particular importance for the selection between alternative calibration methods and for the decision how many factors are to be used in the calibration. The root mean square error (RMSE) is an important criterion, which is indicated in the same units as the original measurements. RMSE values should be as low as possible to obtain acceptable calibration equations (Næs *et al.*, 2002).

Root mean square error of prediction (RMSEP) is an estimate of the variation of the referenced and predicted values of an independent validation set not contained in the calibration set. Prediction testing is based on splitting the total data set into two subsets, one of which is used for calibration and the other for validation only. RMSEP is calculated as the square root of the mean square for residuals for a number of n_{val} samples in the validation set, where the residual equals predicted ($\hat{y}_i$) minus reference (y_i) values for samples outside the calibration set (Eq. 2.15).

$$RMSEP = \sqrt{\frac{\sum_{i=1}^{nval}(\hat{y}_i - y_i)^2}{nval}} \qquad \text{(Eq. 2.15)}$$

The removal of samples for validation at the expense of the calibration set poses a major disadvantage of this approach. Therefore, these samples cannot contribute to obtain enhanced regression coefficients allowing better prediction. Moreover, it is of particular importance to cover the relevant range of test samples best possible since calibration equations will exhibit varying properties for different test sets. Hence, validation meeting this prerequisite may yield a much more reliable estimate of the prediction error than internal validations (Blanco and Alcala, 2009; Næs *et al.*, 2002; Workman and Weyer, 2008). If samples for the test set are part of the entire sample set also used for calibration, they are not independent in a strict sense. Therefore, real independent validation requires a truly independent test set, e.g. originating from a different season or field, to be predicted (Herold *et al.*, 2009).

d. Correlation coefficient (R)

Linear correlation coefficient, measures the strength and the direction of a linear relationship between two variables. The linear correlation coefficient is sometimes referred to as the Pearson product moment correlation coefficient in honor of its developer Karl Pearson. The mathematical Eq. 2.16 for computing R is:

$$R = \frac{n(\sum xy) - (\sum xy)(\sum y)}{\sqrt{[n\sum x^2 - (\sum x)^2][n\sum y^2 - (\sum y)^2]}} \qquad \text{(Eq. 2.16)}$$

where n is the number of pairs of data. The value of R is such that $1 < R < +1$. The + and – signs are used for positive linear correlations and negative linear correlations, respectively.

- Positive correlation: If x and y have a strong positive linear correlation, R is close to +1. An R value of exactly +1 indicates a perfect positive fit. Positive values

indicate a relationship between x and y variables, such that as values for x increases, values for y also increase.

- Negative correlation: If x and y have a strong negative linear correlation, R is close to -1. An R value of exactly -1 indicates a perfect negative fit. Negative values indicate a relationship between x and y such that as values for x increase, values for y decrease.
- No correlation: If there is no linear correlation or a weak linear correlation, R is close to 0. A value near 0 means that there is a random, nonlinear relationship between the two variables.

A correlation greater than 0.8 is generally described as strong, whereas a correlation less than 0.5 is generally described as weak. These values can vary based upon the "type" of data being examined. A study utilizing scientific data may require a stronger correlation than a study using social science data. Moreover, the obtained plot can be used for the identification of regions exhibiting different levels of prediction accuracy (Næs *et al.*, 2002).

The quality of the calibration models was quantified by the root mean square error of calibration (RMSEC), the root mean square error of prediction (RMSEP) and the correlation coefficient (R) between the predicted and the measured parameters. Acceptable models should have low RMSEC and RMSEP, high R and small difference between RMSEC and RMSEP (Shao *et al.*, 2007).

e. Selection of the number of factors

The selection of the optimal number of factors, latent variables or components to be used in the calibration model is another crucial topic with regard to all data compression techniques. Too few factors do not comprise all relevant information of the spectral data for establishing a reliable model. Therefore, this under fitting effect yields suboptimal calibration models. On the other hand, using too many factors goes along with redundancies and noise of the spectral variability within the calibration equation. Hence, the model becomes over fitting and will be very data dependent, and prediction results will be poor. The over-fitting effect is of lower relevance with higher numbers of samples. Parameter estimates, and thus, the predictions are getting more precise the more samples are involved (Blanco and Alcala, 2009; Næs *et al.*, 2002).

CHAPTER 3 MATERIALS AND METHODS

3.1 MATERIALS

Limes (Fig 3.1a) were purchased from four wholesale markets including Khon Kaen Province (Thailand), Bangkok (Thailand), Can Tho City (Vietnam) and Siem Reap city (Cambodia) in order to increase the range and validate the models to ensure that it is sufficiently robust to accurately measure the internal quality of lime from many regions. The season period is from July to August, 2015.

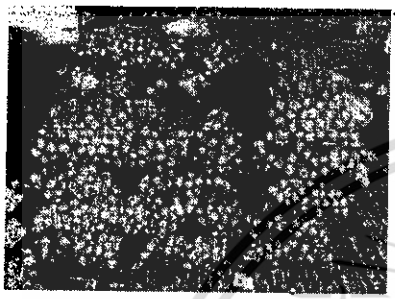

Figure 3.1a Limes at the wholesale market

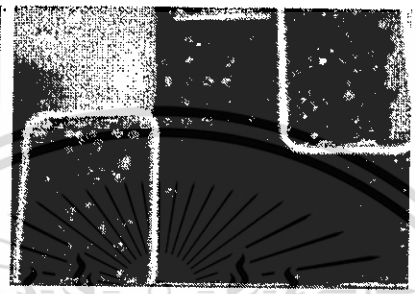

Figure 3.1b Limes were sorted in laboratory

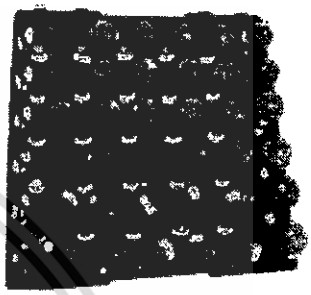

Figure 3.1c Numbered limes

The shape of limes from four different geographies were displayed in Figure 3.2. Their shape are similar in generally.

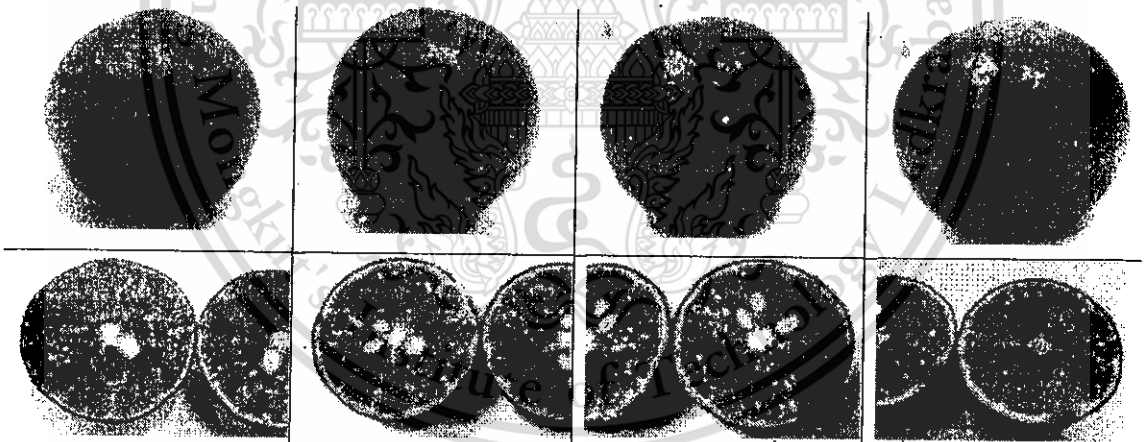

Paan lime from Khon Kaen, Thailand | Kai lime from Bangkok, Thailand | Lime from Can Tho - Vietnam | Lime from Siem Reap - Cambodia

Figure 3.2 Shape of Limes selected from four different geographies, including Khon Kaen Province (Thailand), Bangkok (Thailand), Can Tho City (Vietnam) and Siem Reap city (Cambodia)

"Paan" lime (*C. aurantifolia* (Cristm.) Swinge) is the main object in this research. Anatomy of lime was shown in Figure 3.3. Lime is a hesperidium or a berry with an

exocarp (leathery rind) which contains volatile oil glands in pits. The fleshy interior is composed of carpel filled with fluid-filled sacs called juicy vesicle.

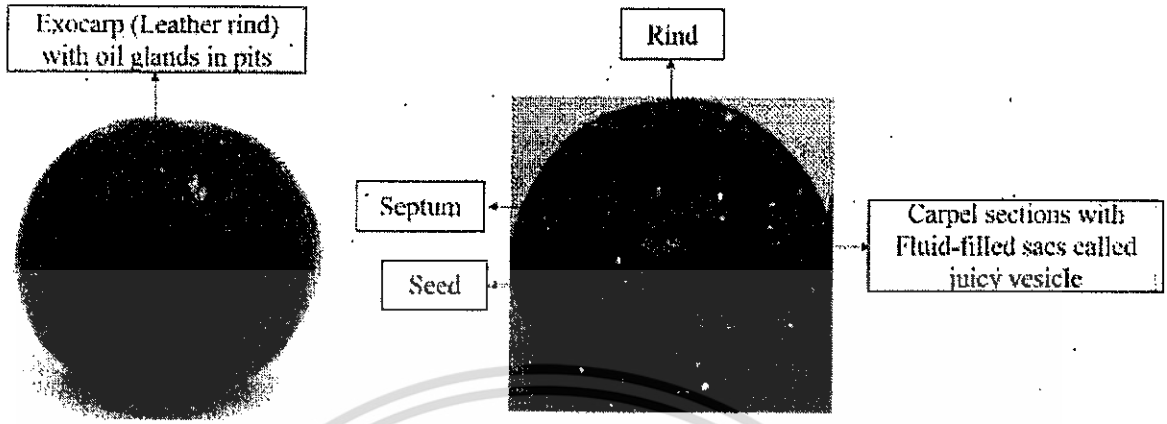

Figure 3.3 Hesperidium anatomy of "Paan" lime (*C. aurantifolia* Cristm. Swinge)

The overall experiment was conducted in laboratory after carrying limes from the markets. Limes were stored at 11 – 13°C and 85-90% R.H. in the refrigerator (Pantastico, 1975). Before measurement, limes were put under room temperature (25°C) for 24 hours in order to obtain the constant temperature (25-26 °C) of each sample during measurement. For the whole experiment, fruit temperature, ambient temperature and ambient light were maintained constant and near the conditions involved in the model development. Good appearance and similar size of samples were used in this research then these samples were individually numbered (Fig 3.1b). Each sample was measured for non-destructive variables: weight, diameter (including width, height and thickness of fruit) , spectral data by XDS Rapid Content ™ Analyzer, FQA-NIR Gun instrument, NIR Flex N-500 Solid instrument, and Hyperspectral imaging Sisu CHEMA instrument as well as for destructive variables: peel's thickness, seediness, citric acid, TSS, juice and moisture content of each sample.

3.2 PLACE OF STUDY

Faculty of Engineering, Department of Postharvest and Processing Engineering, Rajamangala University of Technology Isan Khon Kaen, Khon Kaen, Thailand.

Faculty of Agro-Industry, Department of Food Science, King Mongkut's Institute of Technology Ladkrabang, Bangkok, Thailand.

3.3 METHODS

The overall procedure of experiment was displayed in Figure 3.4. Samples were selected with a similar size and shape then each sample was numbered. Limes were scanned at three positions (the top, bottom and the equator positions) by using individual equipment (XDS Rapid Content ™ Analyzer, FQA-NIR Gun instrument, NIR Flex N-500 Solid instrument, and Hyperspectral imaging Sisu CHEMA) which will be described in detail in the following sections of instrument in this chapter. After scanning, samples were analyzed for physicochemical parameters, such as weight, height, width, thickness of fruit, thickness of peel, seediness, TSS, citric acid, juice content and moisture content individually.

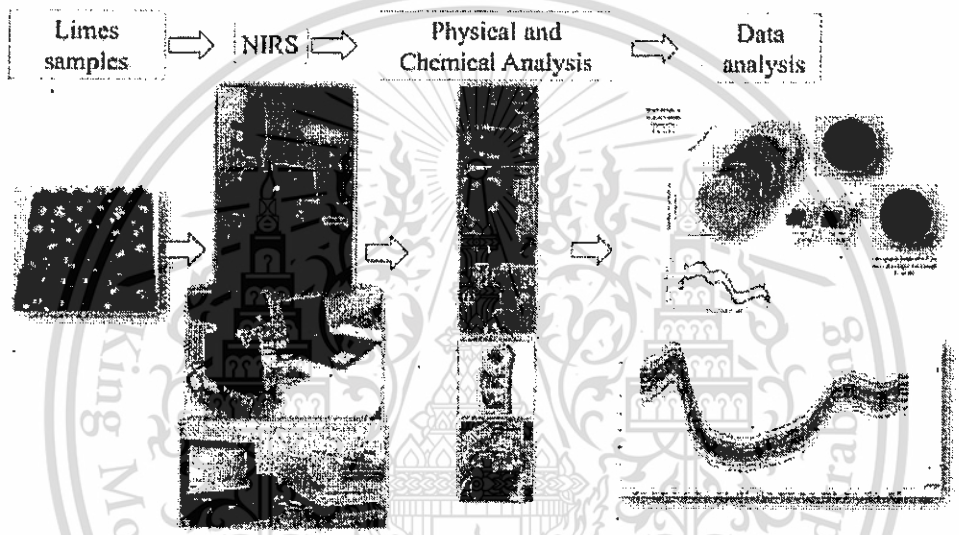

Figure 3.4 Measurement procedure

3.3.1 Physical properties determination

Height, width and thickness of fruit of each sample were measured by a vernier caliper (Auto-lock vernier caliper, Long Jer, Taiwan) with resolution of 0.01mm (Figure 3.5).

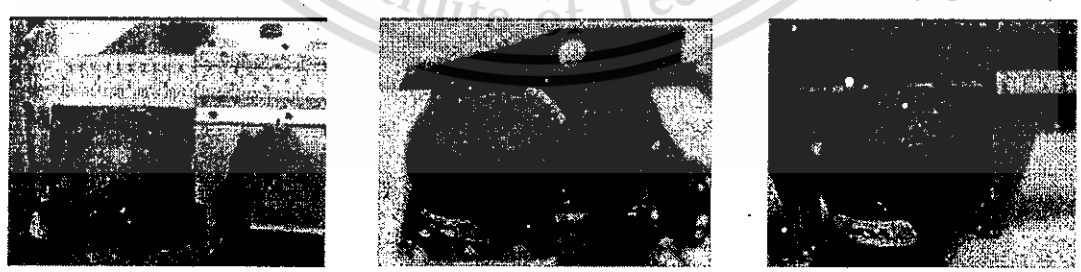

Width **Height** **Thickness of lime**

Figure 3.5 Measure diameter of limes (width, height and thickness of lime fruit)

Weight of lime was measured by an electronic digital weighing scale (WANT, Jiangsu, China) with resolution of 0.001g.

3.3.2 Thickness of peel and weight of seed

Each sample was cut into half then using a vernier caliper (Auto-lock vernier caliper, Long Jer, Taiwan with resolution of 0.01mm) to measure the thickness of peel. Seeds of fruit were carefully separated from the central core of fruit. Weight of seeds was scaled by an electronic digital weighing scale (WANT, Jiangsu, China) with resolution of 0.001g.

3.3.3 Total soluble solids determination

Samples were cut and extracted by using a manual fruit squeezer after nondestructive measurements had been taken. Juice was used to measure TSS using a digital refractometer (PAL-RI Digital Hand-held "Pocket" Refractometer by Atago U.S.A). Be careful avoiding pulp or air bubble in the refractometer prism during measuring.

3.3.4 Citric acid determination

Titratable acidity (AOAC Official Method 942.15 Acidity) can be expressed conventionally in g acid per 100g or per 100mL product. Distill test sample of known weight with neutralized H_2O and titrate to just before end point with 0.1 M alkali, using 0.3 mL phenolphthalein for each 100mL solution being titrated, to pink persisting 30s report as mL 0.1M alkali/100g or 100mL original material. The citric acid content (%) of the sample was calculated by the following formula (Eq. 3.1):

$$Citric\ acid\ content\ (\%) = \frac{VNaOH \times 0.0064 \times 100}{V\ of\ sample} \quad \text{(Eq. 3.1)}$$

3.3.5 Moisture content analysis (ASAE standard, 1994)

Each quarter of whole fruit was scanned in duplicate at the equator and sampled immediately for moisture content analysis. After NIR measurement, each sample was dried to a constant weight in a hot air oven at 103°C for 24 hours according to the ASAE standard (1994). The moisture content of the sample was calculated by this formula (Eq. 3.2):

$$MC = [(A-B)/A] \times 100 \quad \text{(Eq. 3.2)}$$

where A is the original weight of the sample and B is the dried weight.

3.3.6 Yield percentage analysis (or juice content) (ASAE standard, 1994)

After NIR measurement, fruit juice was extracted using a manual juice squeezer (Figure 3.6). Juice content of the sample was calculated by below formula (Eq. 3.3):

$$Yield\ (\%) = [a/b] \times 100 \quad \text{(Eq. 3.3)}$$

where a is the weight of extracted juice and b is the original weight of the sample.


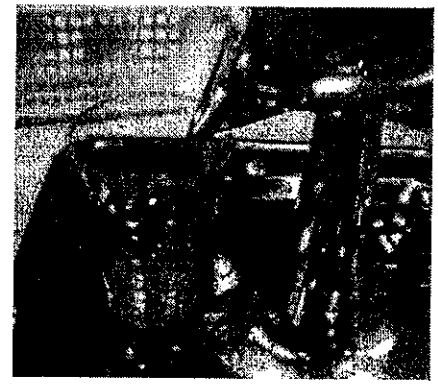

Figure 3.6 Squeezing lime juice

3.4 INSTRUMENTS

3.4.1 Vis/NIR Spectroscopy measurement by XDS Rapid Content TM Analyzer

The angle between incident light (light source) and the detectors (Si: 400-1100 nm and lead sulfide: 1100-2500 nm) was 45°. The fiber cable delivered the collected optical energy into the spectrometer, where it was projected onto a holographic diffraction grading. The grating separated and reflected the wavelength components for independent measurement by the detectors. For each fruit, three spectral were measured on the circumference of the equator positions in every 120° rotating. Then the averaged spectrum of each lime was obtained.

Some specifications for XDS Rapid Content TM Analyzer (Figure 3.7) are shown in Table 3.1

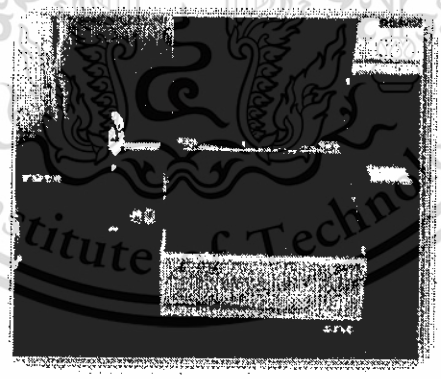

Figure 3.7 XDS Rapid Content ™ Analyzer

Source: Technical Specification for XDS Rapid Content TM Analyzer

Table 3.1 Technical Specification for XDS Rapid Content TM Analyzer

Technical specifications	XDS Rapid Content TM Analyzer
Sample type	Solid, liquids/semi-liquids & viscous
Example parameters	Multi parameter incl. protein, fat, moisture, fibre, starch, amino acids, & more
Sample presentation	XDS sample cups, disposable bags, glass vials or beakers
Swappable modules	Yes
Sample temperature control	No
NIST traceable performance test	Yes
Transferable calibrations	Yes
Auto Sampler	Yes
NIR technology	Reflectance
Wavelength range	400- 2500 nm
Operating temperature	5 – 35°C (40 – 95°F)
Operating humidity	10 – 90% relative
Dual detector system	Silicon (400-1100nm), Lead sulphide (1100-2500nm)
Data acquisition rate	2 scan/sec
Spectral resolution	0.5 nm
Wavelength accuracy	<0.05 nm
ISI scan software	Yes
Dimensions (w x d x h)	380 x 574 x 347 mm
Weight	38 kg

Source: Technical Specification for XDS Rapid Content TM Analyzer

3.4.2 NIRs measurement by FQA-NIR Gun instrument

Some specifications for FQA–NIR Gun Instrument (Figure 3.8) are shown in Table 3.2. FQA-NIR Gun is one of hand-held instruments available commercially that is convenient for use for food and agricultural researchers. At the beginning of spectral acquisition that was illustrated in Figure 3.9, a white reference sample made of 99% reflectance standard polymer disc, thickness of 60 mm, was measured before each measurement. For each fruit, three spectra were measured on the circumference of the equator positions in every 120° rotating. Then the averaged spectrum of each lime was obtained.

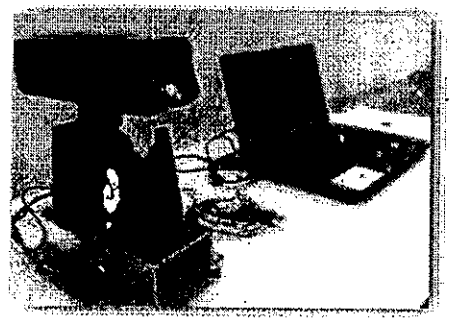

Figure 3.8 Fruit Quality Analyzer (FQA - NIR Gun)

Table 3.2 Technical Specification for FQA-NIR Gun

Technical Specifications	**FQA-NIR Gun**
Measurement method	Reflectance mode
Detector	Silicon diode array
Wavelength region	600-1100nm
Interval	2 nm
Lamp	Small size halogen lamp
Integral time	6-100 ms
Measurement time	Approximately 1 second (depending on integral time
Operating range	Temperature: 10-35°C, Relative humidity: 25-80%
Software	Software for controlling the hardware and to perform calibration
Material to be measured	Fruit, Fish, Vegetable
Material that could not be use	Liquid

Source: Specification for FQA-NIR Gun

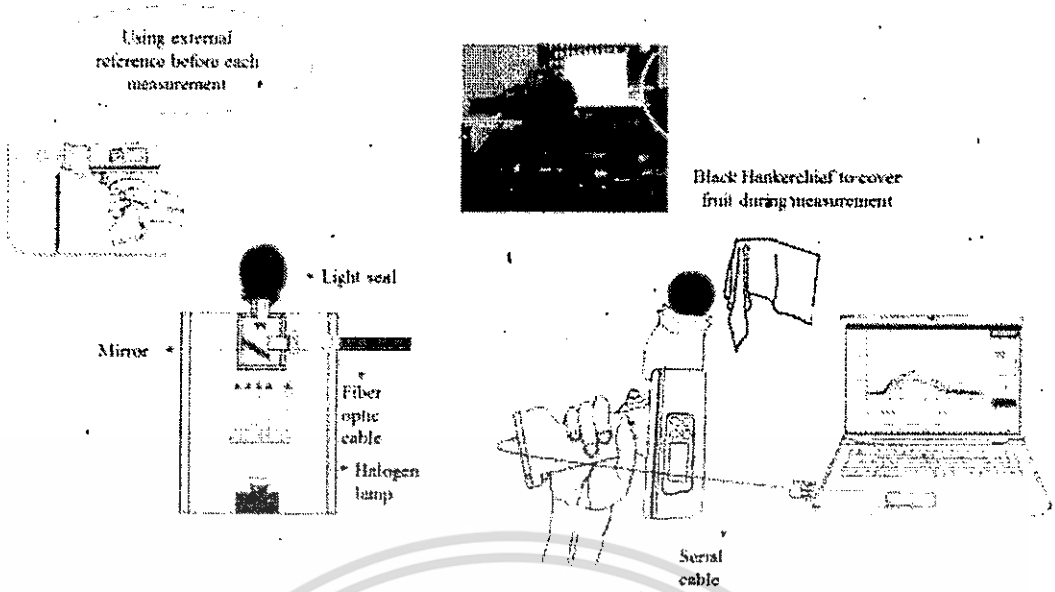

Figure 3.9 A schematic diagram of the NIR reflectance mode of FQA-NIR Gun instrument

3.4.3 NIRs measurement by NIR Flex Solid

A commercial spectrometer (NIR Flex solid, BUCHI, Switzerland) was used for this research (Figure 3.10). This device was equipped with an interferometer, an InGaAs detector, and a wide band light source (50 W) quartz halogen to provide reflectance measurements. A bifurcated optical fiber and a fruit holder (Figure 3.11) as the main accessories were used for the experiment.

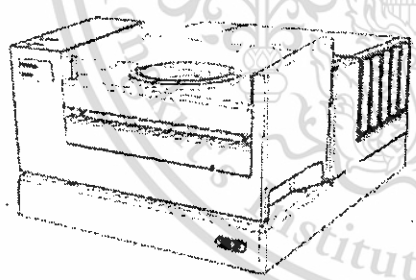

Figure 3.10 NIR-Flex Solid
Source: NIRFlex N-500 Solid Technical data sheet

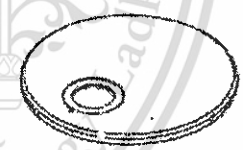

Figure 3.11 Sample holder
Source: NIRFlex N-500 Solid Technical data sheet

XL holder is used for solid samples in diffuse reflectance. Its illumination spot diameter is 9mm. Description and technical specification of NIR Flex instrument were shown in Table 3.3 and Table 3.4.

Table 3.3 Description of NIR Flex specification

Sampling option	Substance	Reference	Comment
NIR Flex Solids	Solid, Powder	Spectral in a reference holder	Make sure that there is as much sample in the dish that the light beam is not visible

Source: NIRFlex N-500 Technical data sheet

Table 3.4 Technical Specification for NIR Flex N-500 Solids

Name	NIR Flex N-500 Solids
Spectral range	1000-2500 nm
Resolution	8 cm^{-1} with boxcar apodization
Type of interferometer	Polarization interferometer with TeO_2 Wedges
Wavenumber accuracy	± 0.2 cm^{-1} measured with HF gas cell at an ambient temperature of 25 ± 5°C
SNR	10000/peak – to –peak noise of a linear corrected baseline
Number of scan/sec	2 -4 (depends on resolution)
Types of lamp	Tungsten halogen lamp
Detector	Extended range InGaAs (Temperature controlled)
Operating temperature	5 – 35°C
Background reference applied	External reference (White reference)

Source: NIRFlex N-500 Technical data sheet

NIR Flex is a single-beam polarization interferometer (Figure 3.12), generating its interferogram in four steps:

- **Step 1**: Polarization of the light source output. The polarizer ❷ generates a well-defined polarization output of the undefined polarized light, emitted by the light source ❶ . Thus, only diagonally polarized light is transmitted.
- **Step 2**: Beam splitting and orthogonal polarization. The polarized light enters a double refracting block (comparator)❸ . Here, the light is broken down into two, orthogonally polarized components with a small, static phase shift.
- **Step 3**: Generating the ongoing phase shift. An assembly of two double refracting wedges is arranged after the comparator. Wedge ❹ is stationary, while wedge ❺ is constantly shifted back and forwards by a fast linear-drive. The movement and the geometric arrangement provide a change of thickness in the light path. This leads to an ongoing phase shift between the light beams.

• **Step 4**: Beam recombination and interferogram output. A second polarizer ❻ converts the phase shifted beams into a single light output with intensity variation – the interferogram.

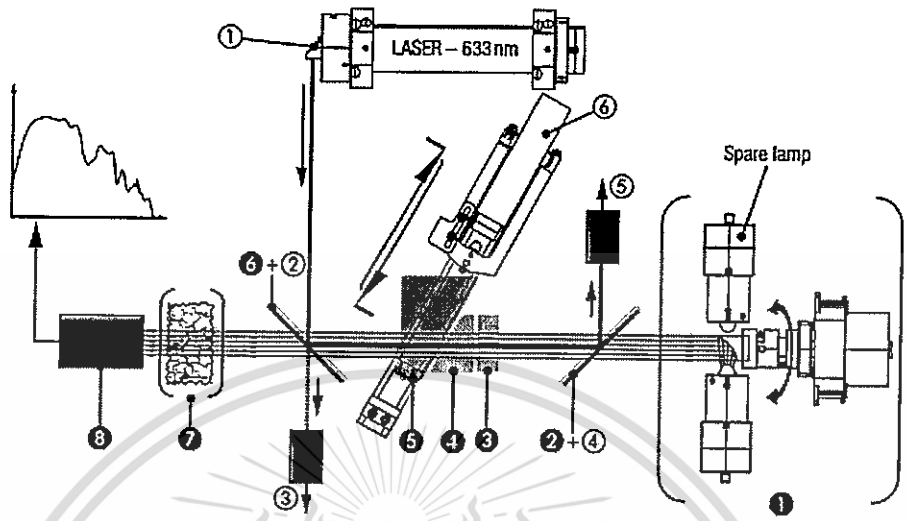

Figure 3.12 A schematic illustration of the NIR-Flex system

Source: NIR Flex N-500 Solid Technical data sheet

Figure 3.13 illustrated the measurement description of lime by using FT-NIR Flex instrument.

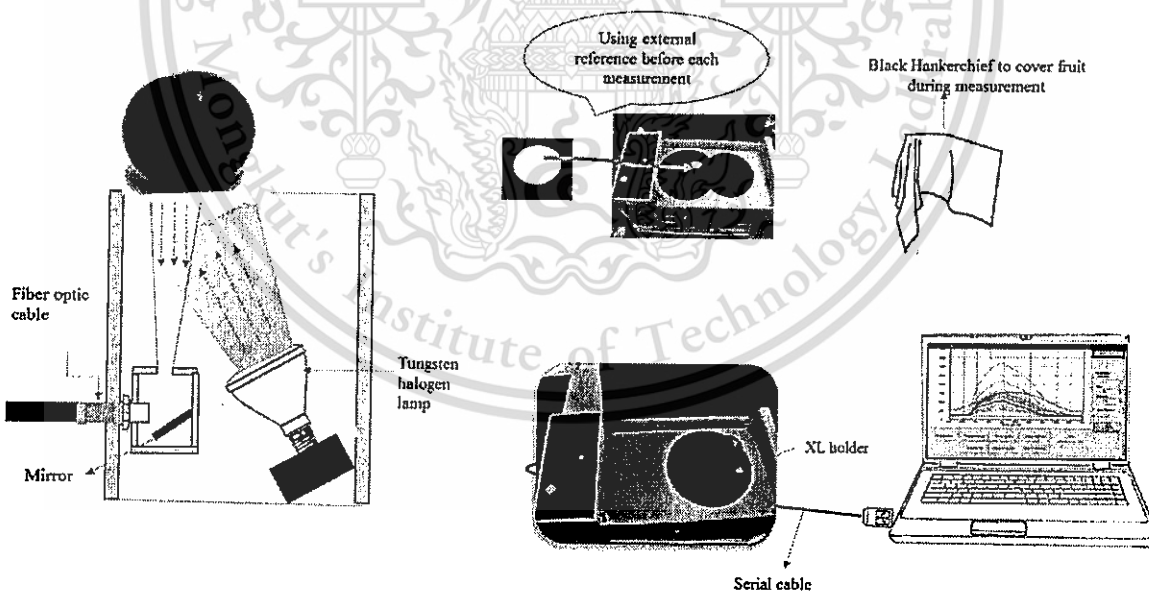

Figure 3.13 A schematic diagram of the NIR reflectance mode of FT–NIR Flex instrument

Limes were placed steadily on the fruit holder, with the stem-calyx axis horizontal. For each lime, three diffuse reflectance spectra were taken at three equidistant positions along the equator. The light was directed to the sample by source fiber and from the sample with

the detector fibers to Nexus FT-NIR spectrometer, with spectral range of 1000–2500 nm and the interferograms were co-added followed by strong Beer-Norton apodization. The interferogram is an interference pattern of phase-shifted beams which interacts with the molecules of a sample, generating a characteristic feedback. The feedback is picked up via a measurement cell by a detector and mathematically processed via Fourier transformation into a spectrum. This spectrum is characteristic for a given sample and allows identification as well as quantification of its components. Each spectrum was recorded as absorbance, log (1/*R*), where *R* is reflectance, by averaging three scans for each lime. A mean spectrum was calculated by averaging the spectra collected at the three positions around the lime. The mirror velocity was 0.9494 cm/s and the resolution was 16 cm^{-1}. In order to avoid surface reflectance and ensure subsurface penetration of the light into the lime flesh, the bifurcated optical probe was placed at a 75° angle to the level (Liu et al., 2010). For each fruit, three spectra were measured on the circumference of the equator positions in every 120° rotating manually. Then the averaged spectrum of each lime was obtained.

3.4.4 NIR Hyperspectral imaging by Sisu CHEMA

Each lime was imaged individually in the line-scan push-broom Sisu chemical imaging workstation system that is shown in Figure 3.14. The HSI system consists of an imaging spectrograph (Imspector N17E, Specim, Spectral Imaging Ltd, Oulu, Finland), an EMCCD camera (Xeva 992, Xenics Infrared Solutions, Belgium), an adjustable slit, two reflectors, an illumination unit including two halogen lamps (Lowel Light Inc., NY, USA), an OLES 22.5 fore objectives lenses, fiber optic, a sample stage, an internal white reference, a linear positioning stage, a power supply unit combined with a PC acquisition supported with Spectral Cube data acquisition software from spectral Imaging Ltd. (Oulu, Finland).

The camera was attached to the image spectrograph SPECIM Inspector N17E of the spectral range of 896-1731 nm. The image spectrograph has a pixel-size internal slit to define the FOV for the special line for the separation of the spectra along the spatial line. To improve the spatial resolution of the hyper-spectral images, an external adjustable slit is placed between the sample and the camera optical set.

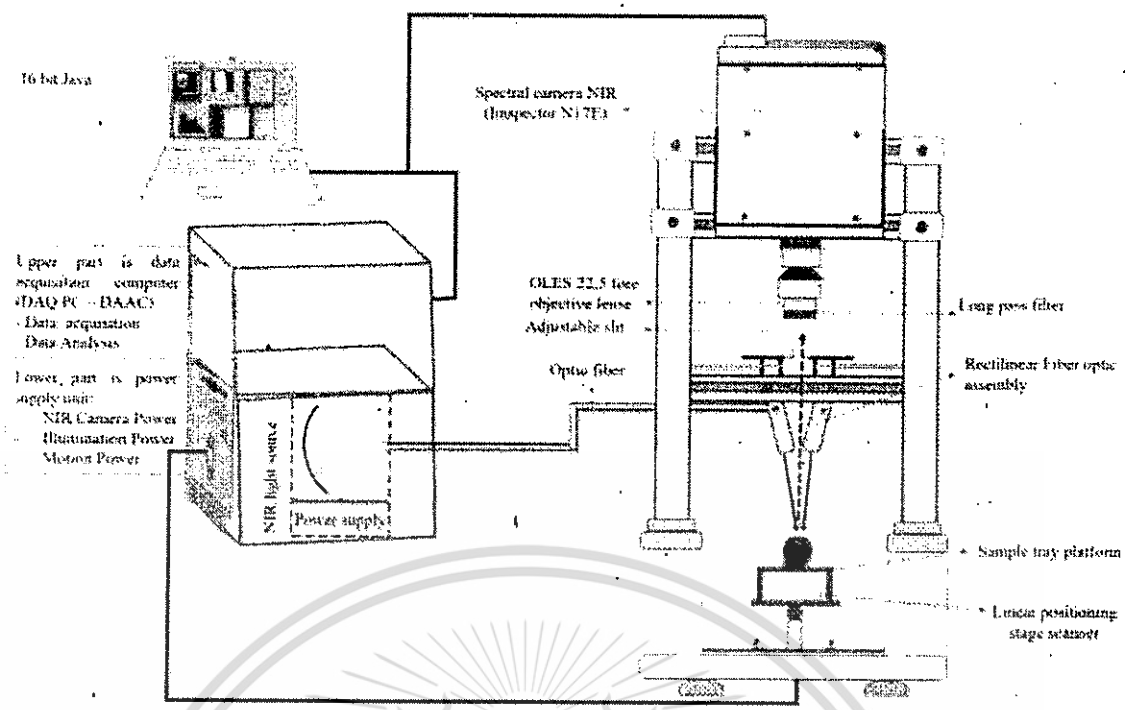

Figure 3.14 Schematic representation of the HSI system

The performance specifications of Sisu CHEMA are shown in Table 3.5. The lens optimized for NIR range was also attached to the front of the spectrograph to control the resolution and the FOV in the first spatial axis (x). The spectrograph consists of a prism-grating-prism arrangement that disperses the reflected light coming through 5 nm (30μm slit). To get efficient light intensity for reflection measurement in the NIR region, the sample was illuminated with two halogen lamps so that the high rate of radiation is reflected by the sample and captured by the camera. The light that passes the objective lens (30mm) and the entrance slit of spectrograph was dispersed into its NIR spectrum. This thin aperture slit limits the instantaneous field of view (IFOV) of the imaging system resulting in the line scanning the lime samples. The reflected light from the IFOV passes through the slit and is dispersed by a prism device and projected into the EMCCD sensor. The system acquired an image of the line across the sample, scanning the 320 pixels width of the sensor and the spectrograph spreads the spectra for each single pixel of that line across the other dimension of the sensor, spanning the 256 pixels this direction (λ). By moving the sample via the linear positioning stage the second spatial axis (y) was obtained. The particular speed was precisely calculated to fit the predetermined camera exposure time or integration time (1.5 ms) and scanning frequency (50 frames per second) to provide the same vertical and horizontal spatial resolution. In addition, the whole image acquisition

process was controlled and recorded by a computer (64-bit Java) supported with the ChemaDAQ data acquisition software.

Table 3.5 Sisu CHEMA's performance specifications

Optical and technical characteristics	High speed push-broom NIR SISU chemical imaging workstation system
Spectral range	896-1731 nm
Spectral sampling/pixel	4 nm
Spectral resolution	6 nm
Spatial pixel/line	320
Pixel size on sample	Scalable from 30 to 300 microns
FOV on sample	Scalable from 10 to 100 mm
Maximum sample size	100 x 100 x 40 mm
Scanning rate	10 hyperspectral line images/s (max), correspond to: (1) 3 mm/s with 30 micron pixel; (2) 30 mm/s with 300 micron pixel; (3) 6 mm/s with 600 micron pixel
Typical scanning time	< 7 s for single 320x320 pixel image capture with 256 spectral bands
Illumination	SPECIM's diffuse line illumination unit
Instrument calibration	Instrument is delivered with spectral calibration. Image data is automatically calibrated to reflectance by measuring an internal standard reference target before each sample scan.

Source: Sisu CHEMA Chemical Imaging Analyzer

For measurement, two positions on each lime were scanned in two times per each side on the circumference of the equator positions in every 180° rotating by using the commercial push-broom HSI system shown in Figure 3.11. At the end of scanning, a hypercube or data cube was shaped and saved in the computer in a band interleaved by lines (EVI) format.

3.5 STATISTICAL ANALYSIS

3.5.1 NIRs data analysis

The Vis/NIR spectra were analyzed by the Unscrambler® Software Version 9.7 (CAMO, Oslo, Norway) and Microsoft Office Excel 2003. Using the Unscrambler® for spectroscopic data analysis, modeling, classification and prediction are common in spectroscopy. The PLSR was used to establish the calibration models for citric acid content, moisture content, juice content and TSS determination of lime.

The procedure of data analyzing process (Figure 3.15) in ordered as outlier detection, data pre-processing, calibration and application of the calibration model to predict the other samples in order to validate the model's accuracy. Detailed calibration process of NIRs was described in Literature review (Chapter 2).

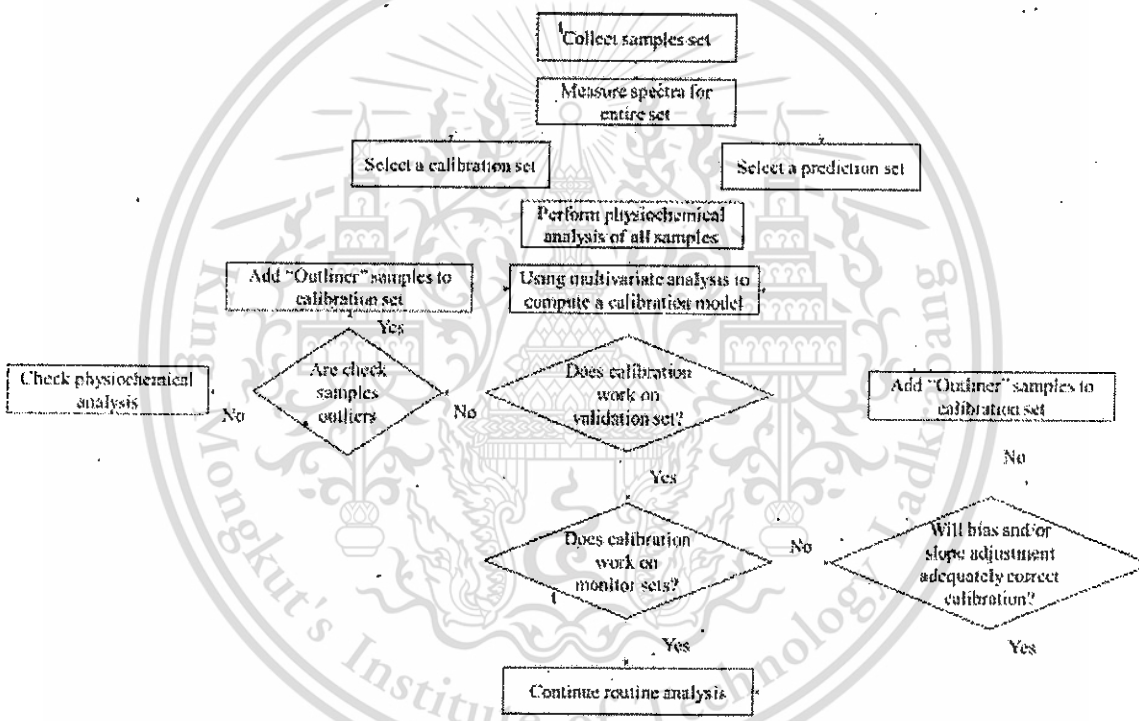

Figure 3.15 Procedure of data analyzing process of NIRs

Source: Jerome and Workman (1992)

Partial least squares discriminant analysis (PLS-DA) in the Unscrambler® was applied to classify "Paan" and "Others" limes (Kai, Vietnam and Cambodia limes) by rotating PCA components in order to understand which variables carry the class separating lime types. Data were divided into two sets: calibration set and prediction. Classification models were developed and cross-validated using PLS with a value of 0 for "Paan" limes and a value of 1 for "Other" limes. However, the chemical of fruit is variable, the value cannot

be "0" or "1" as hypothesis. Therefore it need to be used a cut off value of 0.5 for discrimination. Sample has a predicted value of up to 0.5 were classified as "Paan" while sample with a predicted value of more than 0.5 is classified as "Other" limes. Pre-processing procedures such as smoothing, 1st derivative, 2nd derivative, MSC and SNV were applied to acquired spectra in order to obtain optimal conditions for the models.

3.5.2 Hyperspectral image data analysis

Flow chart of the key steps involved in HSI analyses was showed in Figure 3.16.

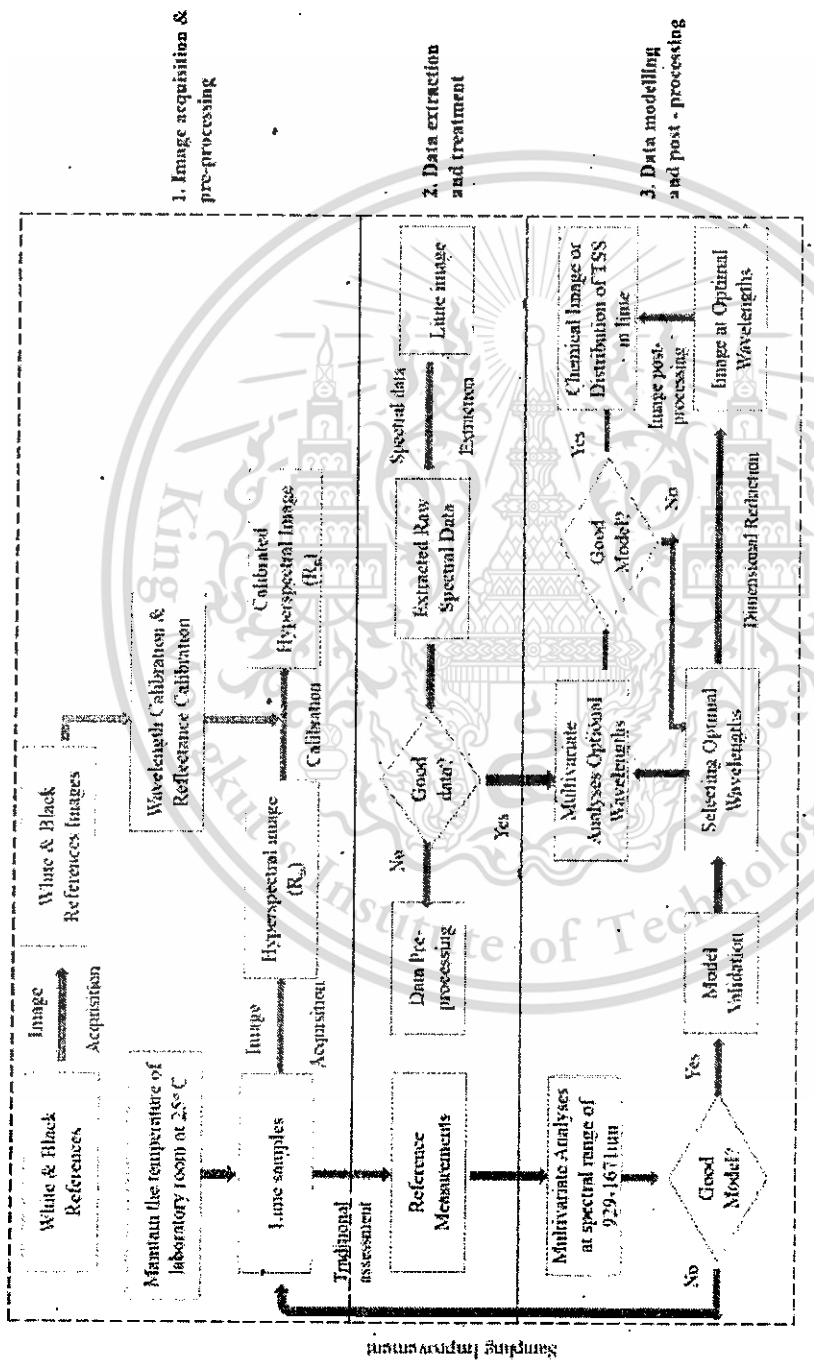

Figure 3.16 Experiments and image processing flow including three main steps: (1) Image acquisition and pre-processing; (2) Data extraction and treatment; and (3) Data modelling and post-processing
Source: Gamal and Shigeki (2016)

Generally, there are three different sections that are usually applied on hyperspectral images process, namely: (1) image acquisition and image pre-processing, (2) data extraction and data treatment and (3) data modelling and image post-processing in order to deal with a 3-dimensional hyperspectral image, to acquire hyperspectral image, to extract spectral data, to build the calibration multivariate models and then to process the final visual images (Gamal and Shigeki, 2016).

3.4.2.1 Image acquisition and image pre-processing

The camera was attached to the image spectrograph SPECIM Imspector N17E of the spectral range of 896-1731 nm with 256 spectral bands. But the visual inspection of the acquired hyperspectral images revealed that the quality of the images at both ends of the spectrum was rather noisy due to the low SNR in these two regions. Therefore, the two spectral regions of 896–926 nm and 1675–1731 nm were entirely excluded. The first step in the experiment and image processing flow is acquisition of a high-quality hyperspectral image in a 929-1671nm spectral range by utilizing an ideal acquisition conditions in term of acquisition mode, scanning speed, frame rate, exposure/integration time, and illumination arrangement. In this study, lime was placed on the linear positioning stage to be scanned one by one. To get efficient light intensity for reflection measurement in the NIR region, the sample was illuminated with two halogen lamps were placed 0.23 m away from the imaging area at 45° angle which were capable of emitting light in a wavelength range of 929-1671nm so that the high rate of radiation is reflected by the sample and captured by the camera. As the result, a hyperspectral image with a dimension of (x, y, λ) or hypercube consist of two spatial dimensions (x, y) and one spectral dimension (λ) was shaped (Figure 3.17) and were saved in the computer in a band interleaved by environment for visualizing Images (ENVI) format.

The three dimensional array data were reshaped into a two dimensional array by means of pixel intensities (reflectance) rearrangement of the lime sample into a column at all the 226 wavelengths. Final images with a dimension of 320 pixels x 430 pixels x 226 bands were obtained and used to extract the spectral information. At each wavelength at the same pixel, every point obtains the full spectral response of the object imaged at the correlated pixel. This is different from traditional spectroscopy that the spectra are recorded at every single point throughout the entire image, instead of just one spectrum at one position. In the same manner, if two pixels of two different positions in

they can show different fingerprints of different spectral signatures. Therefore, the different in spectral signatures between high brix and low brix pixels of the tested lime sample are distinctly categorized at various locations in the spectral bands.

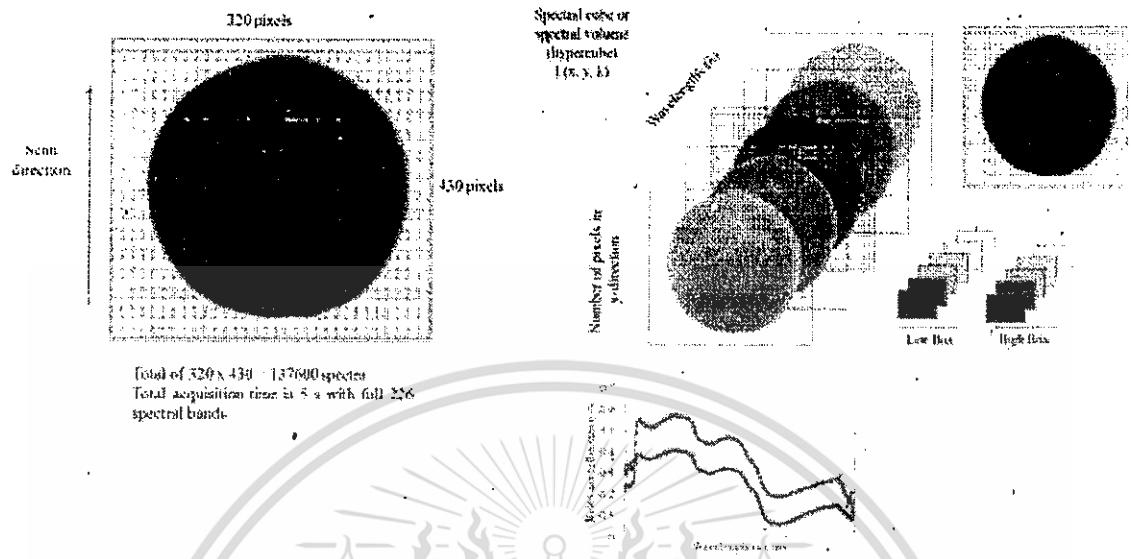

Figure 3.17 Hypercube is displayed either as different spatial 2-D images (x; y) at any wavelength (λ) at different spatial locations

Image pre-processing

The raw obtained images were corrected using two extra images acquired for standard dark and white reference in order to diminish the effects of illumination and detector sensitivity and geometry, which may cause the noise in the samples images. This condition is called radiometric calibration because it converts the digital intensity values registered by the sensor to the real or relative reflectance values. The white image (W) (with a~99% reflectance) was obtained automatically and the dark image was acquired by recording a spectral image when the light source is turned off and the camera lens was completely covered with its non-reflective opaque black cap to exclude the thermal activities of the detector with a~0% reflectance.

3.4.2.2 Data extraction and data pre-treatment

Before going further in extracting data from hyperspectral images, "dead pixels" that usually caused by anomalies in the detectors leading to distortions in the multivariate models should be located and handled. Dead pixels are missing or zero values in the images and they may be a single pixel, a group pixel or a total pixel line. Similarly, "spike" pixels have a sudden and sharp rise in the spectrum because of abnormal behavior of the detector,

imperfections of electronic circuits or environment conditions. To handle "dead" and "spike" pixels, the good way is to substitute their value with an interpolated value from neighboring pixels by using the average of neighboring values (Vidal and Amigo, 2012).

The reflectance spectra of lime sample were collected by using the ENVI software. The extracted spectral data may include some noise and variability. The raw hyperspectral data obtained from the HSI contained scattering noise generated from the camera (Kandpal *et al.*, 2013). Therefore, we need to apply mathematical pre-treatments, including smoothing, 1st derivative, 2nd derivative, multiple scatter correction (MSC) and standard normal variate (SNV) which were implemented into acquired spectral in order to reduce noise, to improve the resolution of overlapping data and to diminish impact from the hyperspectral image system (Vidal and Amigo, 2012).

All processes of image correction and spectral data extraction were programed in Unscrambler software (CAMO, Osla, Norway), Excel Microsoft 2003 and the UmBio Evince hyperspectral image analysis software (Prediktera Evince, version 2.7.5, Sweden). Because ENVI can be used to analyze high spectral resolution images from many different sensors.

3.4.2.3 Data modelling and image post-processing

The numerous spectral data acquired from the NIR-HSI system were processed using multivariate data analysis in order to develop calibration models for prediction of the actual values of TSS, citric acid, and juice content in limes. The average extracted spectral data from all limes were then put in a matrix (X) where the rows of this matrix represent the number of samples and the columns correspond to the number of variations (226 wavelengths). The whole data was split into two groups: a training group and a testing group. Chemometric multivariate calibration model was then aimed to exploit the spectra in the spectral data matrix (X) to predict TSS, citric acid and juice content in column vector (Y). The calibration model of the regression model will allow the prediction of chemical composition based on the spectral data (Berzaghi and Riovanto, 2009). Firstly, principal component data analysis (PCA) was applied to the spectral data (X) to acquire an overview of systematic spectral variations in order to cut background data that was included in obtained spectral data. Then calibration and prediction of TSS, citric acid and juice content in lime samples based on spectral information were presented with PLSR. In this research, full cross-validation (leave-one-out) was employed for prediction and for estimating the

correct number of latent factors in order to avoid over-fitting of the models (Varmuza *et al.*, 2009).

The calibration models developed by PLSR were exploited in predicting TSS, citric acid and juice content in unknown samples in the prediction set, the same model could be applied on predicting TSS, citric acid and juice content in each single pixel of the spectral image. This was obtained by multiplying the model regression coefficients by the spectrum of each pixel in the image at selected wavelengths. It is very helpful and simple to visualize the degree of heterogeneity of the sample where different colors represent different concentration of TSS within the lime sample (Wold *et al.*, 2006).

CHAPTER 4 RESULTS AND DISCUSSION

4.1 PHYSICO-CHEMICAL CHARACTERISTIC OF LIMES

Table 4.1 showed some physiochemical properties of limes which were collected at four different locations, namely Khon Kaen-Thailand, Bangkok-Thailand, Can Tho city-Vietnam and Siem Reap city-Cambodia.

Table 4.1 Physiochemical characteristics of limes collected at four different locations

Name and Location	Amount of Fruit	Weight of fruit (g)[ns]	Fruit length (mm)[ns]	Fruit thickness (mm)	Fruit width (mm)	Peel thickness (mm)	Weight of seeds (g)	Juice content (%)	Moisture content (%)	Citric acid (%)	TSS (°Brix)
Paan – Bangkok	100	34.79±1.19	3.711±0.72	3.86±0.34	3.82±0.25	0.06±0.017	0.28±0.03	58.37±4.58	90.37±0.94	8.37±0.28	8.30±0.34
Kai – Khon Kaen	100	35.06±0.75	3.74±0.41	3.84±0.83	3.78±0.31	0.12±0.031	0.34±0.02	56.35±3.76	89.78±1.03	6.75±0.32	7.37±0.15
Vietnam	100	35.14±0.94	4.091±0.53	3.91±0.42	3.82±0.28	0.15±0.028	0.81±0.07	43.34±2.84	88.72±0.82	7.36±0.21	7.44±0.23
Cambodia	100	35.03±0.83	4.052±0.62	3.77±0.35	3.66±0.42	0.20±0.054	0.62±0.05	42.27±4.19	87.11±0.73	7.88±0.17	7.91±0.20

ns= No significant different ($p>0.005$).

There were statistical differences among cultivars at different locations in most of characteristics due to different climate, rootstock and cultural practices. In addition, the distribution and level of attributes, such as TSS, within the fruit may differ with maturation and cultivar, growing conditions and size of the fruit (Guthrie *et al.*, 2005a, b). Average fruit weight was about 34.79 (Paan limes) to 35.14 (Vietnam limes) that is not significantly different. A statistical distinction was observed in citric acid and weight of seeds.

Major component of limes is primarily water. The results showed that "Paan" limes contain the highest moisture percentage (%) and no significant difference with limes from Cambodia. Average range of Brix values was about 7.37 to 8.3°Brix that was dissimilar with the reference information of Erickson (1968) who stated TSS comprise from 10-20% of the fresh weight of the fruit. TSS (8.3°Brix), juice content (58.37%) and moisture content (90.37%) values of "Paan" limes were significantly higher than "Others" limes.

Citric acid of citrus juice is an important factor in overall juice quality which contributed significantly to overall juice acidity. Citric acid is a primary organic acid (70-90%). In this research, "Paan" had the highest value (8.37%) while "Kai lime" had the lowest value (6.75%). The rate of decrease in acidity was positively correlated with average temperatures during the season. Higher temperatures increase respiration rates causing less storage of acids in the vacuoles and their more rapid utilization in metabolism (Milind, 2008).

"Paan" limes contained the lowest amount of total seeds weight (0.28g) while "Vietnam lime" had the highest values. In contract, Vietnam limes and Cambodia limes' peel were thicker than "Paan" and "Kai" limes' peel. Thickness of peel and seediness are also considered as one of quality indicator. The thin peel and seedless limes shall be preferred than the thick and seedy limes.

In conclusion, limes grown at different locations showed significantly difference in the chemical quality that can be explained by many factors, such as cultivar, growth region, growing year and mature level of the fruit. In addition, "Paan limes" collected at Khon Kaen, Thailand had the best quality among other limes selected at other locations.

4.2 NONDESTRUCTIVE EVALUATION OF LIME'S QUALITY USING CONVENTIONAL NIRs

4.2.1 Spectra of "Paan" limes

Water constitutes about 80–90% of fruit and vegetables (Goméz *et al.*, 2006) and because of the high water content, water absorption bands take over the NIR spectrum of fruit and vegetables (Palmer and Williams, 1974). Typical Vis/NIR spectra of lime in the region of 606-1070nm measured by FQA-NIR Gun is shown in Figure 4.1. In the visible region 606-780 nm, high absorbance observed at 647 nm is indicative of chlorophyll b absorbing pigments that gives the fruit its characteristically green color (Gómez *et al.*, 2006). After this peak, there is a very sharp drop in absorbance as the spectrum enters the NIR region (>780nm). The absorbance spectrum reached a prominent peak at 958 nm. Based on the research results of Williams and Norris (1987), this peak is result from water absorption.

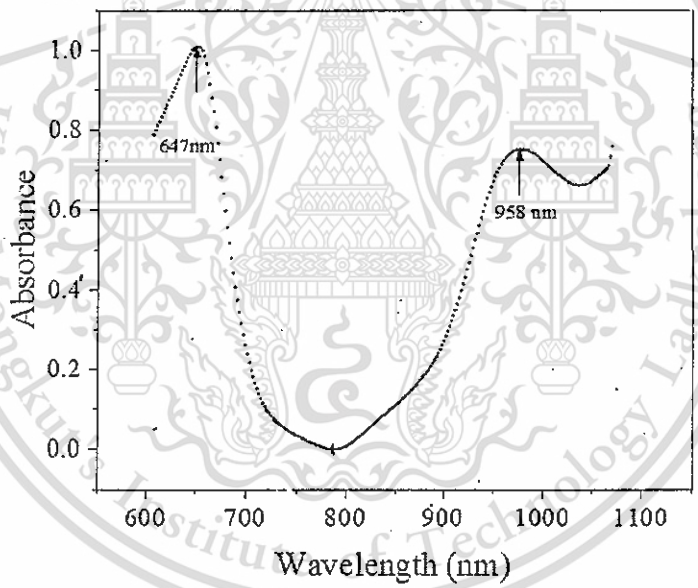

Figure 4.1 Average absorbance spectra of intact limes measured by FQA-NIR Gun in the region of 606-1070 nm

The average reflectance spectra of limes measured by FT–NIR in the region of 1000-2500nm are shown in Figure 4.2. In lime, these water peaks occur at 1068, 1184, 1450, 1942 and 2218 nm which are similar to the reference of Williams and Norris (2001).

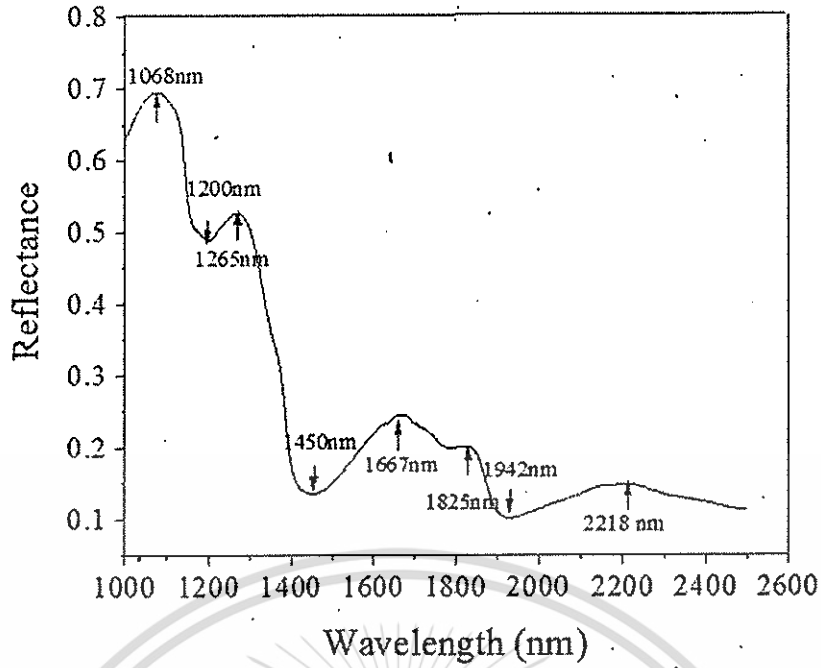

Figure 4.2 Average reflectance spectra of intact limes measured by FT-NIR in the region of 1000-2500 nm

4.2.2 Qualitative analysis using FQA-NIR Gun and FT-NIR instruments

The averaged absorbance spectra of "Paan" samples (N=188) and "Others" varieties samples (N=188), including "Kai", "Vietnam" and "Cambodia" limes, which are obtained from the FQA-NIR Gun spectrometer and the FT-NIR spectrometer, are shown in Figure 4.3 (a) and (b), respectively. Overall, "Paan" variety samples appeared to absorb more light than others.

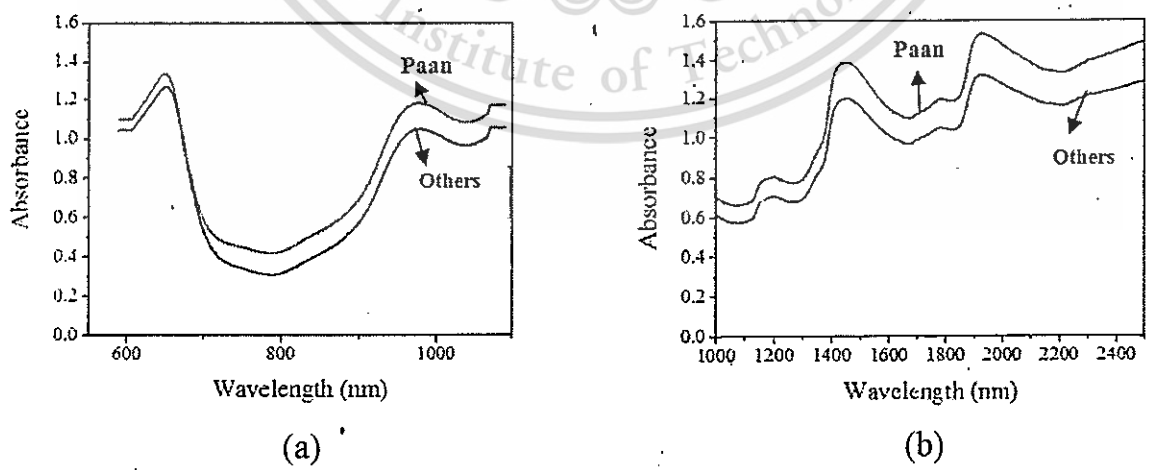

Figure 4.3 Averaged absorbance NIR spectra from "Paan" variety group (N=188) and "Others" variety group (N=188) using (a) the FQA-NIR Gun spectrometer and (b) the FT-NIR spectrometer

The effect of spectral pre-treatments, including smoothing, the 1st derivative, the 2nd derivative (SavitzkyGolay method), MSC and SNV on original spectra, was presented in Table 4.2.

Table 4.2 The results of classification and spectral pre-treatments in the calibration set

Spectral Pre-treatment	The FQA-NIR Gun spectrometer						The FT-NIR spectrometer					
	F	Paan limes		Other limes		Average accuracy (%)	F	Paan limes		Other limes		Average accuracy (%)
		C (%)	IC (%)	C (%)	IC (%)			C (%)	IC (%)	C (%)	IC (%)	
Original	9	95.23	4.77	95.23	4.77	95.24	14	97.62	2.38	93.65	6.35	95.63
Smoothing	7	98.41	1.59	96.83	3.17	97.62	14	98.41	1.59	94.44	5.56	96.43
1st derivative	6	98.41	1.59	96.03	3.97	97.22	8	99.21	0.79	96.03	3.97	97.62
2nd derivative	13	97.62	2.38	95.23	4.77	96.43	4	98.41	1.59	96.03	3.97	97.22
MSC	7	97.62	2.38	96.83	3.17	97.22	6	99.21	0.79	98.41	1.59	98.01
SNV	8	96.83	3.17	97.62	2.38	97.22	5	95.23	4.77	98.41	1.59	95.24

C: Correct; IC= Incorrect

As the results of validation, the smoothing and the MSC pre-treatment methods obtained the highest accuracy (97.62% and 98.01%) and low number of factors (7 and 6) in the calibration set for classification lime's variety using the FQA-NIR Gun spectrometer and the FT-NIR spectrometer, respectively.

Table 4.3 showed that the correctness of discrimination during calibration step were 97.62 % and 98.81 % which indicates that overall samples were successfully classified into the correct class based on the acceptance criteria. The models were validated to prove the predictive ability in the prediction set. Using the FQA-NIR Gun spectrometer, the accuracy of prediction was 98.39% (61 samples from a total of 62 samples) for the "Paan" kind of limes group and 95.16 % (59 samples from a total of 62 samples) for the "Others" kind of lime group. The overall accuracy was 96.00% (120 samples from a total of 124 samples). On the other hand, using the FT-NIR spectrometer showed that the accuracy of prediction was 100% (62 samples from a total of 62 samples) for the "Paan" variety group and 96.77 % (60 samples from a total of 62 samples) for the "Others" kind of lime group. The overall accuracy was 98.39 % (122 samples from a total of 124 samples).

Table 4.3 Percentage of correct values for classification of lime varieties ("Paan" and "Others" limes)

Items		The FQA-NIR Gun spectrometer		The FT-NIR spectrometer	
		The calibration set	**The prediction set**	**The calibration set**	**The prediction set**
N		252	124	252	124
Wavelength(nm)		588-1091	588-1091	1000-2500	1000-2500
Spectral pre-treatment		Smoothing	Smoothing	MSC	MSC
Factor		7	7	6	6
"Paan" limes	Correct (%)	98.41	98.39	99.21	100
	Incorrect (%)	1.59	1.61	0.79	0
"Others" limes	Correct (%)	96.83	95.16	98.41	96.77
	Incorrect (%)	3.17	4.84	1.59	3.23
Average accuracy (%)		97.62	96.00	98.81	98.39

Hypothetically, there were only two values, 0 ("Paan" variety) and 1 ("Others" variety). The value of 0 that object was recognized as the class of "Paan" variety and was rejected from the class if the value was 1. However, as the chemical component of each sample was diverse, the value wasn't 1 or 0 exactly (Broadhurst and Kell, 2006). The calculation used a cut off value of 0.5 for discrimination. Samples which had a predicted class value of up to 0.5 were classified as "Paan" variety, while samples with a predicted class value of more than 0.5 were classified as "Others" variety. The results showed in Figure 4.4a and 4.4b that the accuracy of prediction using the FT-NIR spectrometer was slightly higher than those of prediction using the FQA-NIR Gun spectrometer. Hence, using FT-NIR has slightly more potential to classify varieties of limes than using FQA-NIR Gun due to FT-NIR enhance the use of fiber optics, so that reflectance measurements are easily obtained (McClure and Hamid, 1994)..

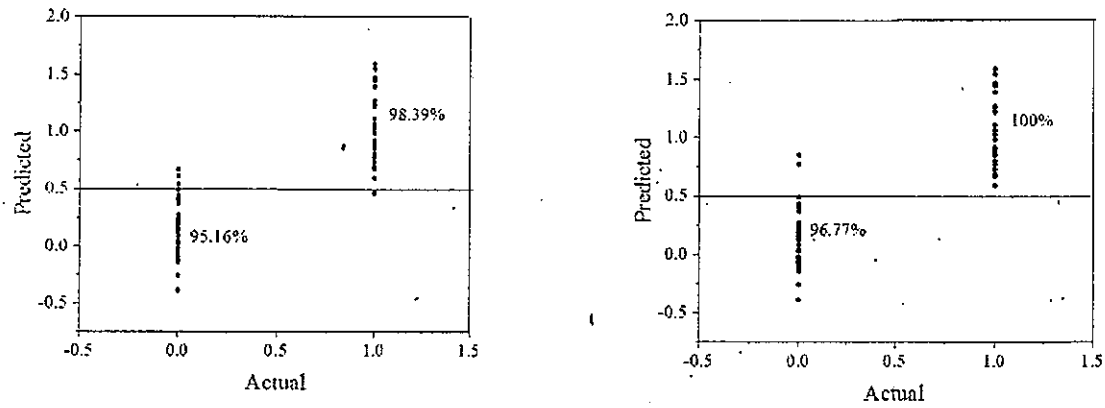

(a) (b)

Figure 4.4 Classification results of "Paan" and "Others" types of limes in the prediction set by (a) the FQA-NIR Gun spectrometer and (b) the FT-NIR spectrometer

4.2.3 Nondestructive prediction TSS of "Paan" limes by Vis/NIR using XDS rapid content TM analyzer and FQA-NIR Gun

Table 4.4 showed the summary statistics for all selected samples in each data set. When developing the calibration model for each parameter, some samples (outliers) were taken out, which might be caused by the instrument error or by the man-made error, due to their potential bad influences over the model.

Table 4.4 Statistical analysis of the calibration and prediction sets for TSS determination

Type of instrument	Item	Calibration	Prediction
XDS rapid content TM analyzer	N	78	39
	Range (°Brix)	6.2-8.7	6.9-8.7
	Mean (°Brix)	7.68	7.71
	SD	0.43	0.42
FQA-NIR Gun	N	128	64
	Range (°Brix)	6.57-9.95	6.77-9.70
	Mean (°Brix)	7.95	7.98
	SD	0.67	0.65

The effect of pre-processing of spectra (MSC, SNV, smoothing, the 1st derivative and the 2nd derivative (all using SavitzkyGolay method) on original spectra were presented in Table 4.5.As the results, the Multiple scatter correlation (MSC) spectral pre-treatment obtained the best results (R_{CV}=0.75, RMSECV=0.28°Brix) and smoothing spectral pre-treatment gained the best result (R_{CV}=0.82, RMSECV=0.19°Brix) in the calibration model

of using XDS rapid content TM analyzer and FQA-NIR Gun, respectively. Therefore, the MSC spectra pre-treatment were used for establishment the calibration models in this study.

Table 4.5 Effect of pre-processing techniques on selected models in the wavelength range of 400-2500 nm and PLS technique for prediction of TSS of lime

No.	Pre-processing techniques	XDS rapid content TM analyzer			FQA-NIR Gun		
		F	R_{CV}	RMSECV (°Brix)	F	R_{CV}	RMSECV (°Brix)
1	Original	12	0.74	0.29	10	0.80	0.25
2	Smoothing	12	0.74	0.29	10	0.82	0.19
3	1st Derivative	12	0.74	0.29	15	0.80	0.25
4	2nd Derivative	7	0.70	0.30	13	0.75	0.28
5	MSC	12	0.75	0.28	9	0.80	0.25
6	SNV	12	0.74	0.29	11	0.81	0.23

The calibration model for TSS obtained R_C = 0.87 and RMSEC = 0.20°Brix when the model was used to predict the other 39 samples, the prediction results obtained Rp = 0.81 and RMSEP = 0.24°Brix by using XDS rapid content TM analyzer (Table 4.6 and Figure 4.5). On the one hand, using FQA-NIR Gun gave a slight better accuracy of calibration model with R_C = 0.89 and RMSEC = 0.17°Brix then the model was used to predict the other 64 samples, the prediction results obtained R_p = 0.82 and RMSEP = 0.37°Brix (Table 4.6 and Figure 4.5).

Table 4.6 Results of the PLSR model for TSS determination in the calibration set and prediction set

Equipment	Pre-treatment	F	Calibration			Prediction		
			N	R_c	RMSEC (°Brix)	N	R_p	RMSEP (°Brix)
XDS rapid content TM analyzer	MSC	8	78	0.87	0.20	39	0.81	0.24
FQA-NIR Gun	Smoothing	10	128	0.89	0.17	64	0.82	0.37

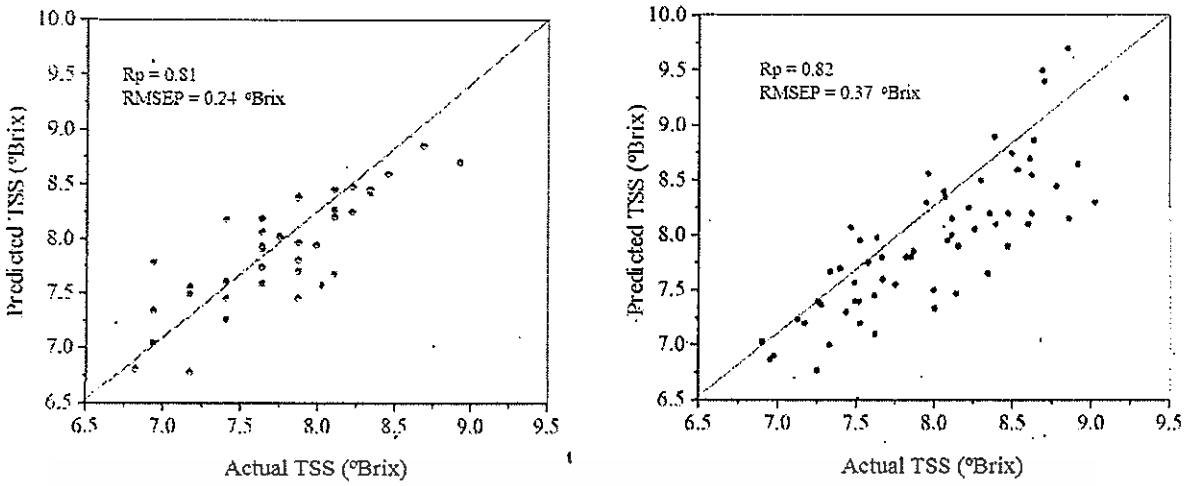

(a) (b)

Figure 4.5 Vis/NIR prediction results of the established the PLSR model for TSS of lime using XDS rapid content (a) TM analyzer and (b) FQA-NIR Gun

In conclusion, the results showed that using XDS rapid content TM analyzer is not significantly different with using FQA-NIR Gun. However, FQA-NIR Gun was portable and easy to use in sorting and handling lime in the market.

4.3. NONDESTRUCTIVE EVALUATION OF LIME FRUIT USING NIR HYPERSPECTRAL IMAGING SPECTROSCOPY

4.3.1 Spectra features of "Paan" limes in the range of 929-1671nm measured by HSI spectrometer

The original spectra of one fruit, obtained 51 spectra per one fruit, in the full range of 896-1731nm was shown in Figure 4.6.The camera was attached to the image spectrograph SPECIM Imspector N17E of the spectral range of 896-1731 nm with 256 spectral bands. But the visual inspection of the acquired hyperspectral images revealed that the quality of the images at both ends of the spectrum was rather noisy due to the low SNR in these two regions. Therefore, the two spectral regions of 896–926 nm and 1675–1731 nm were entirely excluded, resulting in hyperspectral images of only 226 bands in the spectral range of 929–1671 nm that was used for image acquisition and for developing the calibration models.

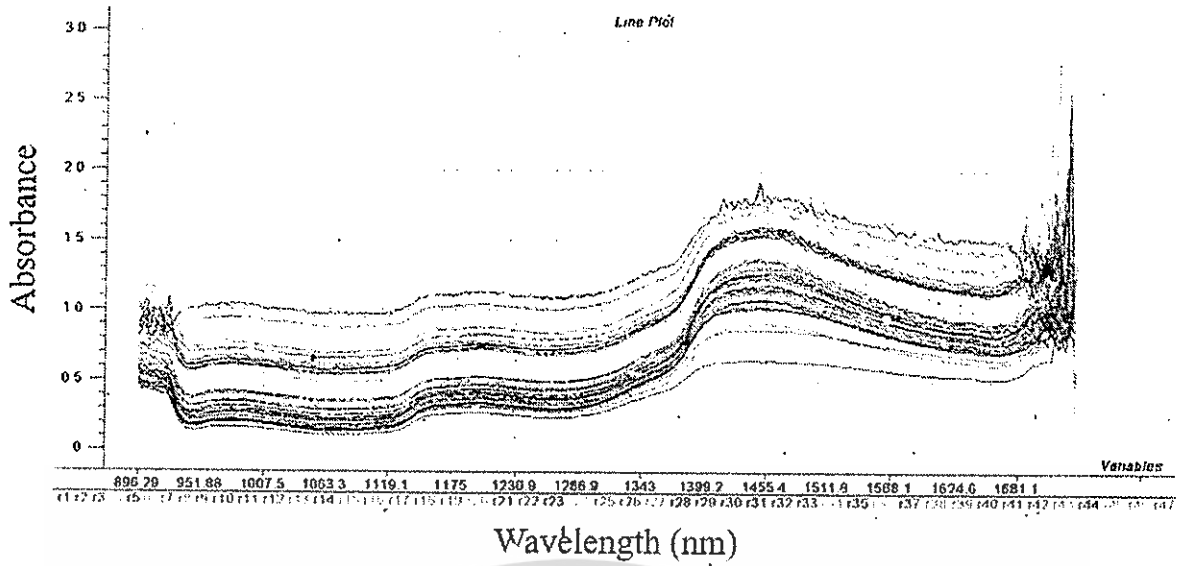

Figure 4.6 The original absorbance spectra of one lime sample at the range of 896-1731 nm

Figure 4.7 shows the average spectra of the 350 lime samples acquired from the NIR hyperspectral image system in the spectra range of 929– 1671 nm that was second derivative to show peaks clearly. For the spectrum ranging from 929 to 1671 nm, there were nine absorption peaks (935, 958, 1044, 1184, 1344, 1410, 1631, 1641 and 1657 nm). In NIR spectra of fruit, the effective absorption bands are relatively wide and complex, due to different chemical environment of every O–H or C– H bond in water and sugar molecules (Guthrie *et al.*, 2005).

Lime consist of about 80–95% of water and about 10-20% of TSS, which include carbohydrate, organic acids, proteins, fats and various minerals (Erickson, 1968). Due to the high water content, water absorption bands take over the NIR spectrum of fruit (Palmer and Williams 1974). Since a strong water and carbohydrate absorption band exists at 958 nm (Williams and Norris, 1987; McGlone and Kawano, 1998) and 935 nm (Kawano *et al.*, 1993) respectively, this peak is believed to result from water and carbohydrate absorption. According to the literature, wavelengths at 971 and 1410 nm are related to the absorbance of O–H bonds and could be associated to water content (Da-Wen Sun, 2010). Other two peaks related to the strong water absorbance bands exist in citrus fruit these water absorption peaks occur at 1,184 and 1,458 nm (Umezuruike *et al.*, 2011). Wavelengths around 1645 -1682 nm could be related to C–H stretching first overtones (Osborne, 2000).

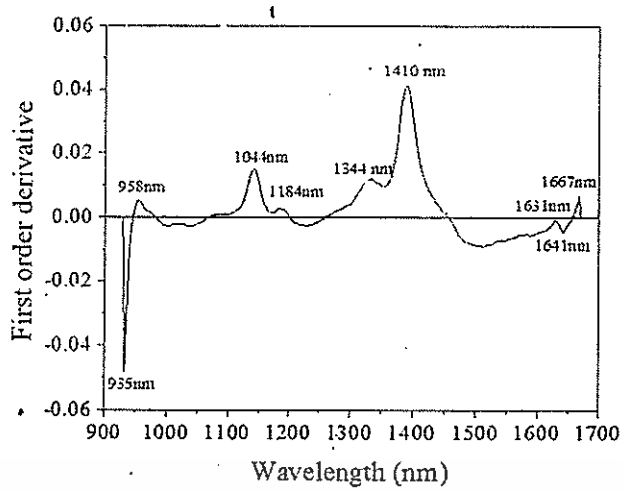

Figure 4.7 The first order derivative of mean absorbance spectra of lime samples at the range of 929-1671 nm

4.3.2 Nondestructive prediction of TSS of "Paan" limes in the range of 929-1671nm measured by HSI spectrometer

Table 4.7 showed the summary statistics for all samples selected in calibration set and prediction set. TSS values in both data sets were 6.01-9.30 and 6.85–8.40 (°Brix), respectively. It was observed that TSS showed a wide spread which would simplify building successful prediction models.

Table 4.7 Statistical analysis of the calibration and prediction sets for TSS (°Brix) determination

Item	Calibration	Prediction
N	70	30
Range (°Brix)	6.01-9.30	6.85-8.40
Mean (°Brix)	8.04	7.87
SD	0.69	0.67

The effect of pre-processing of spectra (MSC, SNV, smoothing, 1st derivative, 2nd derivative (using SavitzkyGolay method) and combination of MSC and SNV on original spectra were presented in Table 4.8 which shows RMSECV, R_{cv}, and F for TSS in lime samples by using the spectral region of 929-1671nm.

Partial least square regression (PLSR) was employed with full cross-validation that was used to find the most accurate PLSR model for the prediction of TSS. The obtained model was used for the prediction of TSS in the sample. As the results, the smoothing pre-processing obtained the best results (R_{CV} =0.92, RMSECV=0.22) in the calibration model

for TSS. The results indicated that PLSR models for TSS exhibited low values of RMSECV and high values of R_{CV}, determine good performance of the models for predicting TSS.

Table 4.8 Effect of pre-processing techniques on selected models in the wavelength range of 929 -1671 nm and PLSR technique for prediction of TSS of limes

No.	Pre-processing techniques	F	R_{cv}	RMSECV (°Brix)
1	Original	7	0.92	0.22
2	Smoothing	6	0.91	0.22
3	1st Derivative – 3 points (p)	4	0.81	0.32
4	1st Derivative – 5 p	6	0.81	0.35
5	1st Derivative – 7 p	6	0.84	0.32
6	2nd Derivative – 3 p	3	0.72	0.56
7	2nd Derivative – 5 p	2	0.63	0.46
8	2nd Derivative – 7 p	4	0.70	0.42
9	MSC	5	0.89	0.33
10	SNV	5	0.89	0.33
11	SNV+MSC	5	0.89	0.33

Figure 4.8a shows the TSS actual values and the values predicted by the PLSR calibrated model for lime samples. The predicted values for TSS (°Brix) range from 6.01 to 9.30°Brix, and there is a significant correlation between the measured and predicted values. The calibration model for TSS obtained $R_C = 0.946$ and RMSEC= 0.174°Brix then the model was used to predict the other 30 samples (Figure 4.8b) in order to get distribution map of TSS in lime samples (Figure 4.9). For a better illustration of the model's performance, a scatter plot between the measured TSS and the predicted TSS in the prediction set is shown in Figure 4.8b. The plot shows that the model was able to predict the TSS in lime samples with high accuracy ($R_P = 0.921$, RMSEP = 0.217°Brix). Therefore, the model which was established from obtained spectral in the range of 929-1671nm using HSI can be used to predict TSS in limes.

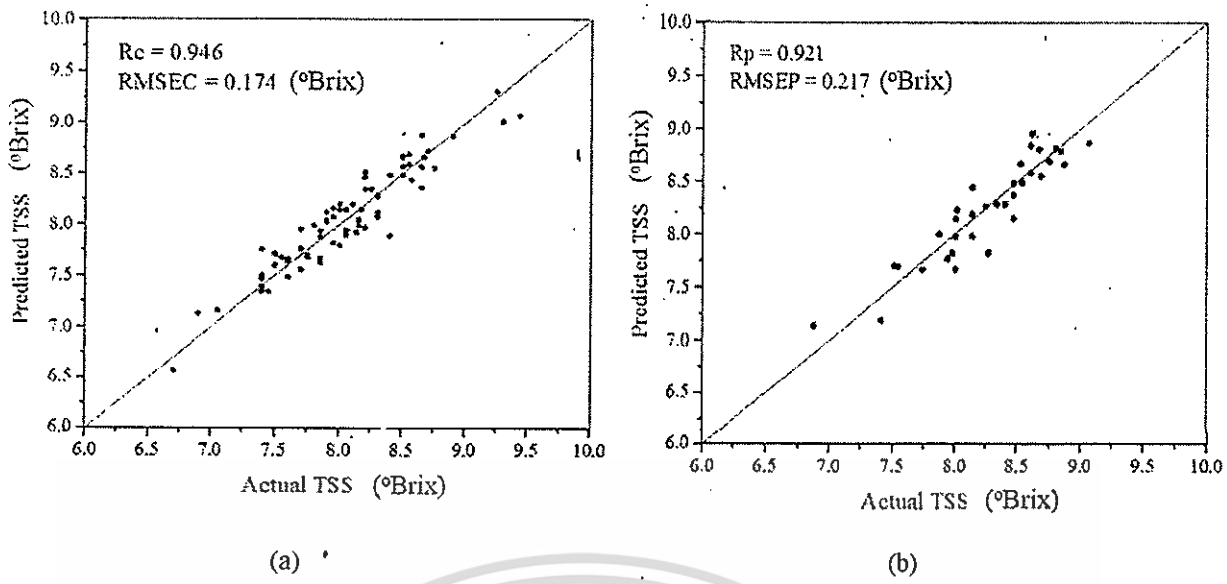

Figure 4.8 Scatter plot of cross-validation result of the established PLSR model (a) in calibration set and (b) in prediction set for TSS (°Brix) of limes

Distribution map (called "chemical images") of TSS were achieved by applying the resulting PLSR model in a pixel-wise manner that process pixels in one location at a time by a simple interpolation to constructing new data points within the range of an isolated set of known data points. It showed the distribution of TSS and its gradients from point to point in the sample. In the resulting chemical images, pixels having similar spectral features gave the same predicted value of TSS and were visualized in a similar color. On the other hand, pixels having different spectral patterns displayed different values of TSS and were visualized in different colors.

Figure 4.9 shows the final PLSR images of TSS of lime samples. The images were constructed by multiplying the obtained regression coefficient from the PLSR model with the spectra of each pixel in the image. Color scale ranges from 5 (green) to 10 (red) that meant fruit had high intensity of red color indicated that fruit had high TSS value. The changes in TSS were assigned to a linear color scale and the numbers below each sample were the average TSS predicted in the whole fruit. The highest TSS (8.40°Brix) and the lowest TSS (6.85°Brix) were found in prediction set. Therefore, red color increases steadily. Differences in TSS distribution observed among limes were mainly due to differences amount of organic acids, ascorbic acid and minerals and small quantity of flavonoids, volatiles and lipids of limes in difference of maturation, cultivar, growing condition (Burns and Ciurczak, 1990). The TSS varied among different parts of lime. That could be explained by the difference of chemical composition from stem end to blossom

end, and from sun to shade sides of the fruit based on the study of Guthrie and Walsh (1997). In study of Smith (1984) the SSC content of the bottom of the pineapple fruit was about 3°Brix higher than the top of the fruit that was similar to the trend was reported by Guthrie and Walsh (1997). These researchers further reported that SSC of the sun-exposed side, where light intensity and photosynthetic activity would be greatest, of the fruit was generally 1°Brix higher than SSC of the shaded side.

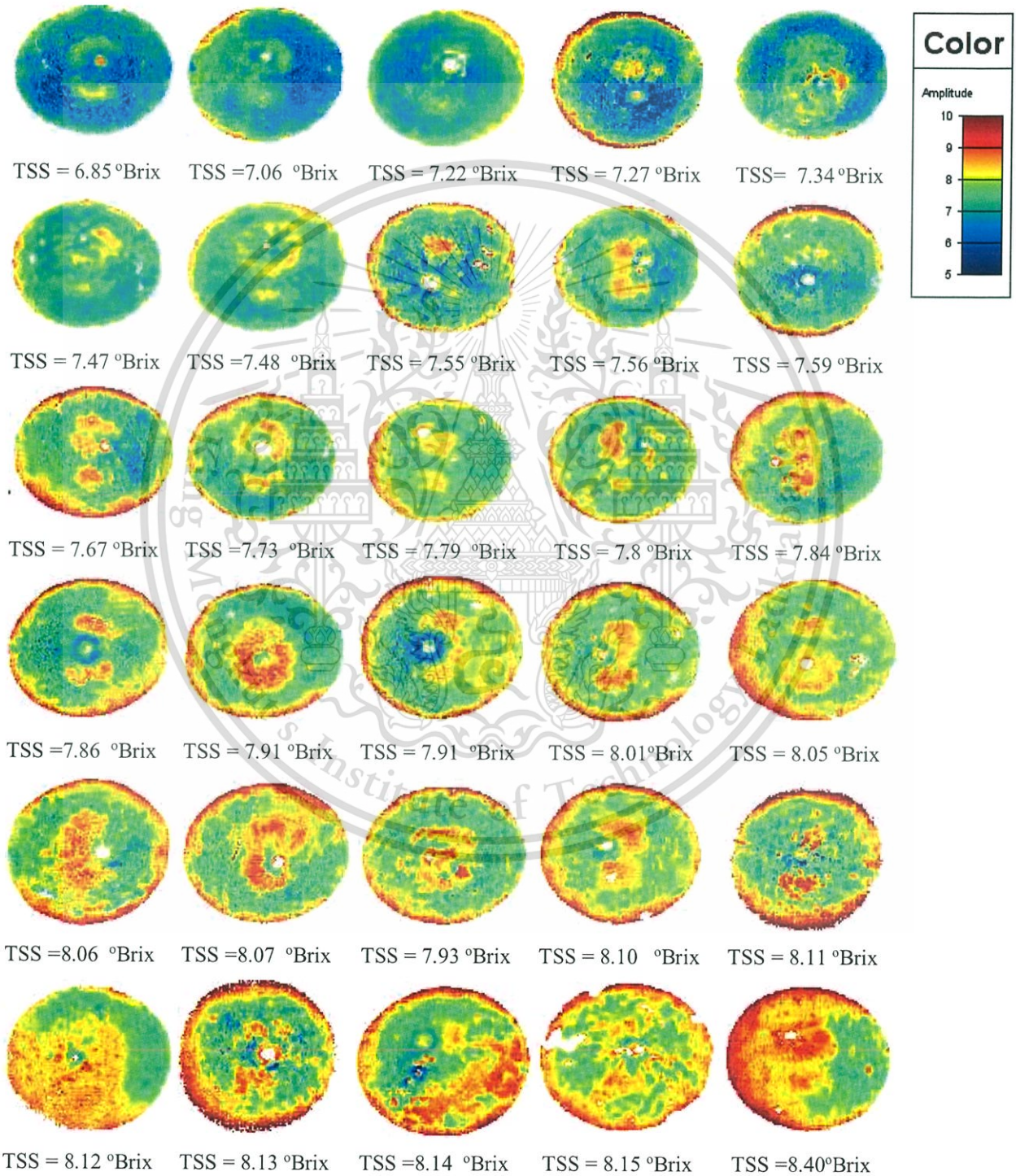

Figure 4.9 Chemical images of TSS in lime samples

In conclusion, based on the obtained results, NIR HSI combined with image processing techniques had the high potential to predict and illustrate the TSS gradient within the lime and among limes.

4.3.3 Nondestructive prediction of citric acid of "Paan" limes in the range of 929-1671nm measured by HSI spectrometer

Table 4.9 showed the summary statistics for all samples selected in calibration set and prediction set. Citric acid values in both data sets were 6.34 – 9.18 and 6.97 – 9.08 (%), respectively. It was observed that citric acid showed a wide spread which would simplify building successful prediction models.

Table 4.9 Statistical analysis of the calibration and prediction for citric acid (%) determination

Characteristic	Item	Calibration	Prediction
Citric Acid (%)	N	70	30
	Range	6.34 -9.18	6.97-9.08
	Mean	7.71	7.94
	SD	0.57	0.62

The effect of pre-processing of spectra (MSC, SNV, smoothing, 1st derivative, 2nd derivative (using SavitzkyGolay method) and combination of MSC and SNV on original spectra were presented in Table 4.10. PLSR was employed with full cross-validation that was used to find the most accurate PLSR model for the prediction of citric acid. The obtained model was used for the prediction of citric acid in the sample. As the results, no pre-processing enhances the performance of the calibration model. Original spectral obtained the best results (R_{CV} =0.89, RMSECV=0.16%) in the calibration model. The results indicated that PLSR models for citric acid displayed low values of RMSECV and high values of R_{CV}, determine good performance of the models for predicting citric acid. The actual citric acid values and the predicted citric values by the PLSR calibration model for lime samples was showed in Figure 4.10a. The predicted citric acid values range from 6.34 to 9.30%, and there was a significant correlation between the measured and predicted values. The calibration model for citric acid obtained R_C = 0.95 and RMSEC= 0.16 % then the model was used to predict the other 30 samples (Figure 4.10b) in order to get distribution map of citric acid in lime samples (Figure 4.11).

Table 4.10 Effect of pre-processing techniques on selected models in the wavelength range of 929 -1671 nm and PLSR technique for prediction of citric acid of lime

No.	Pre-processing techniques	Wavelength (nm)	Factor	Rcv	RMSECV (%)
1	Original	929-1671	8	0.89	0.16
2	Smoothing	929-1671	8	0.79	0.21
3	1st Derivative	929-1671	6	0.81	0.22
4	2nd Derivative	929-1671	6	0.81	0.26
5	MSC	929-1671	7	0.86	0.19
6	SNV	929-1671	8	0.76	0.24
7	Smoothing + MSC	929-1671	6	0.63	0.30

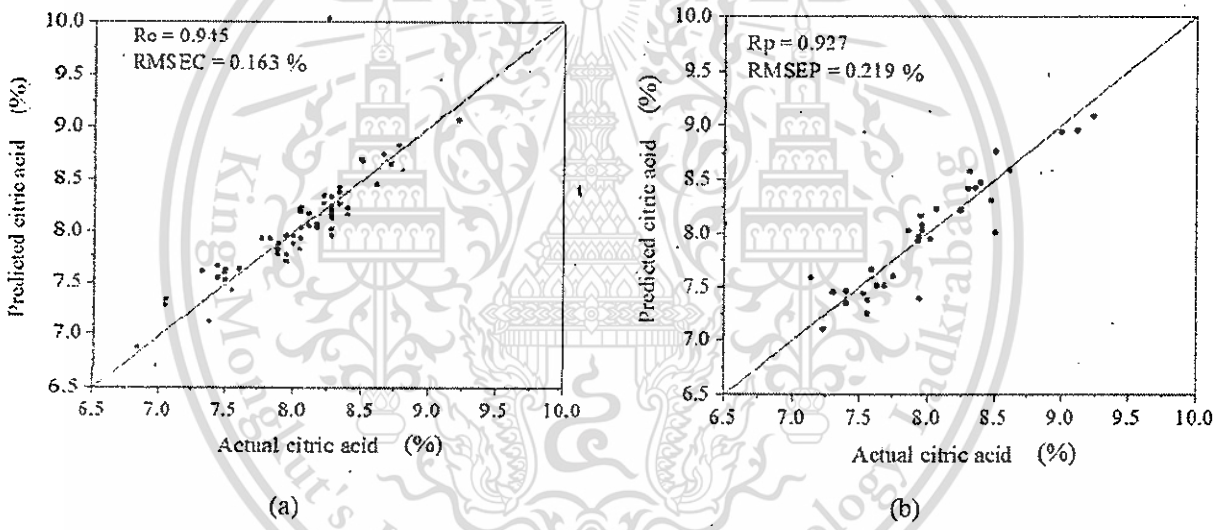

Figure 4.10 The established PLS model (a) in the calibration set and (b) in the prediction set for citric acid (%) of limes

For a better illustration of the model's performance, a scatter plot between the measured citric acid and the predicted citric acid in the prediction set is shown in Figure 4.10b. The plot showed that the model was able to predict the citric acid in lime samples with high accuracy (R_P = 0.93, RMSEP = 0.22%). Therefore, the model which was established from obtained spectral in the range of 929-1671nm using HSI could be used to predict citric acid in limes.

Chemical images of citric acid were achieved by applying the resulting PLSR model in a pixel-wise manner that process pixels in one location at a time by a simple interpolation to constructing new data points within the range of an isolated set of known data points. It

showed the distribution of citric acid and its gradients from point to point in the sample. In the resulting chemical images, pixels having similar spectral features gave the same predicted value of citric acid and were visualized in a similar color. On the other hand, pixels having different spectral patterns displayed different values of citric acid and were visualized in different colors.

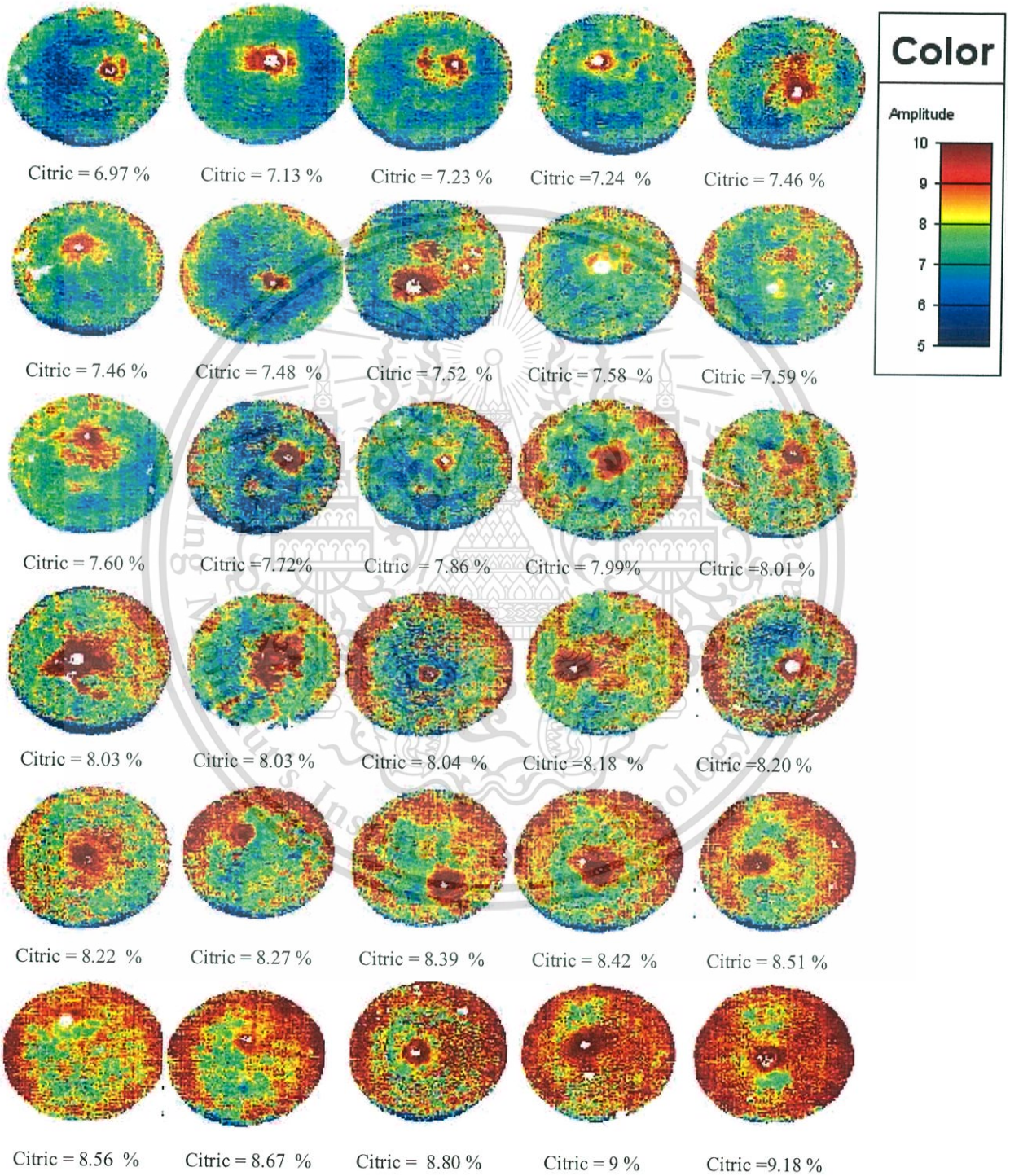

Figure 4.11 Chemical images of Citric acid in lime samples

Figure 4.11 shows the final PLSR images of citric acid of lime samples. The images were constructed by multiplying the obtained regression coefficient from the PLSR model

with the spectra of each pixel in the image. Color scale ranges from 5 (blue) to 10 (red) that meant fruit had high intensity of red color indicated that fruit had high citric acid value. The changes in citric acid were assigned to a linear color scale and the numbers below each sample were the average of predicted citric acid in the whole lime fruit. The highest citric acid (9.18%) and the lowest citric acid (6.97%) were found in prediction set. Therefore, red color increases steadily. Differences in citric acid distribution observed among limes were mainly due to differences amount of organic acids and ascorbic acid of limes in difference of maturation, cultivar, growing condition (Burns and Ciurczak, 1990). The citric acid varied among different parts of the lime fruit that as same as what other studies mentioned about titratable acid differed with fruit position in citrus (Blondel, 1992; Moon *et al.*, 2002). That could be explained by the difference of chemical composition from stem end to blossom end, and from the sun-exposed side, where light intensity and photosynthetic activity would be greatest, to the shade sides of the fruit based on the study of Guthrie and Walsh (1997).

In conclusion, based on the obtained results, NIR-HSI combined with image processing techniques had the high potential to predict and illustrate the citric acid gradient within the lime and among limes.

4.3.4 Nondestructive prediction of juice content of "Paan" limes in the range of 929-1671nm measured by HSI spectrometer

The summary statistics for all samples selected in calibration set and prediction set was shown in Table 4.11. Juice content values of lime in both data sets were 27.70 – 59.65 and 39.17 – 56.72 (%), respectively. It was observed that juice content showed a wide spread which would simplify building successful prediction models.

Table 4.11 Statistical analysis of the calibration and prediction for juice content (%) determination

Characteristic	Item	Calibration	Prediction
Juice content (%)	N	100	30
	Range	27.70-59.65	39.17– 56.72
	Mean	47.41	45.61
	SD	2.03	1.72

The effect of pre-processing of spectra (MSC, SNV, smoothing, 1st derivative, 2nd derivative (using SavitzkyGolay method) and combination of MSC and SNV on original spectra were presented in Table 4.12.

Table 4.12 Effect of pre-processing techniques on selected models in the wavelength range of 929 -1671 nm and PLSR technique for prediction of juice content of lime

No.	Pre-processing techniques	Juice content (%)			
			Factor	Rcv	RMSECV (%)
1	Original	929-1671	8	0.91	2.24
2	Smoothing	929-1671	8	0.89	2.41
3	1st Derivative	929-1671	6	0.72	3.76
4	2nd Derivative	929-1671	3	0.44	4.95
5	MSC	929-1671	7	0.84	2.93
6	SNV	929-1671	7	0.84	2.95
7	Smoothing + MSC	929-1671	11	0.85	2.83

PLSR was employed with full cross-validation that was used to find the most accurate PLSR model for the prediction of juice content. The obtained model was used for the prediction of juice content in the sample. As the results, no pre-processing enhances the performance of the calibration model. Original spectral obtained the best results (R_{CV} = 0.910, RMSECV=2.243%) in the calibration model. The results indicated that PLSR model from original spectra for juice content displayed low values of RMSECV and high values of R_{CV}, obtained good performance of the models for predicting juice content.

The actual juice content values and the predicted juice content values was shown in Figure 4.12a using the PLSR calibration model for lime samples. The predicted juice content values range from 27.71 to 59.65%, and there was a significant correlation between the measured and predicted values. The calibration model for juice content obtained R_C = 0.95 and RMSEC= 1.68% then the model was used to predict the other 30 samples (Figure 4.12b) in order to get distribution map of juice content in lime samples (Figure 4.13).

For a better illustration of the model's performance, a scatter plot between the measured juice content and the predicted juice content in the prediction set is shown in Figure 4.12b. The plot showed that the model was able to predict the juice content in lime samples with high accuracy (R_P =0.93, RMSEP = 1.83%). Therefore, the model which was established from obtained spectral in the range of 929-1671nm using HSI could be used to predict juice content in limes. Chemical images of juice content were achieved by applying the resulting PLSR model in a pixel-wise manner that process pixels in one location at a time by a simple interpolation to constructing new data points within the range of an isolated

pixels in one location at a time by a simple interpolation to constructing new data points within the range of an isolated set of known data points. It showed the distribution of juice content and its gradients from point to point in the sample. In the resulting chemical images, pixels having similar spectral features gave the same predicted value of juice content and would be visualized in a similar color.

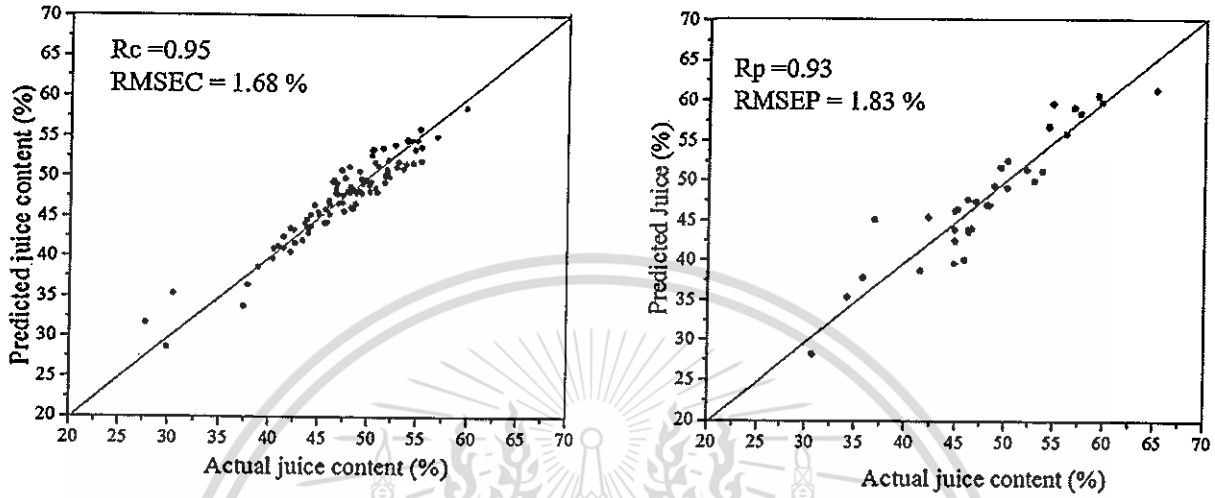

(a) (b)

Figure 4.12 Scatter plot of cross validation result of the established PLSR model (a) in the calibration set and (b) in the prediction set for juice content (%) of limes

On the other hand, pixels having different spectral patterns would display different values of juice content and would be visualized in different colors. Figure 4.13 shows the final PLSR images of juice content of lime samples. The images were constructed by multiplying the obtained regression coefficient from the PLSR model with the spectra of each pixel in the image. Color scale ranges from 35 (blue) to 60 (red) that meant fruit had high intensity of red color indicated that fruit had high juice content value.

The changes in percentage of juice was assigned to a linear color scale and the numbers below each sample were the average of predicted juice content in the whole lime fruit. Differences in juice distribution observed among limes were mainly due to differences of maturation, cultivar, growing condition (Burns and Ciurczak, 1990). The result shows that juice in the central part of fruit was higher than in the outer of the fruit. That can be easily observed when cut lime into peace (Figure 3.2), the juice concentrate in the segment of fruit. The highest juice content (56.72%) and the lowest juice percentage (39.17%) were found in prediction set. Therefore, red color increases steadily.

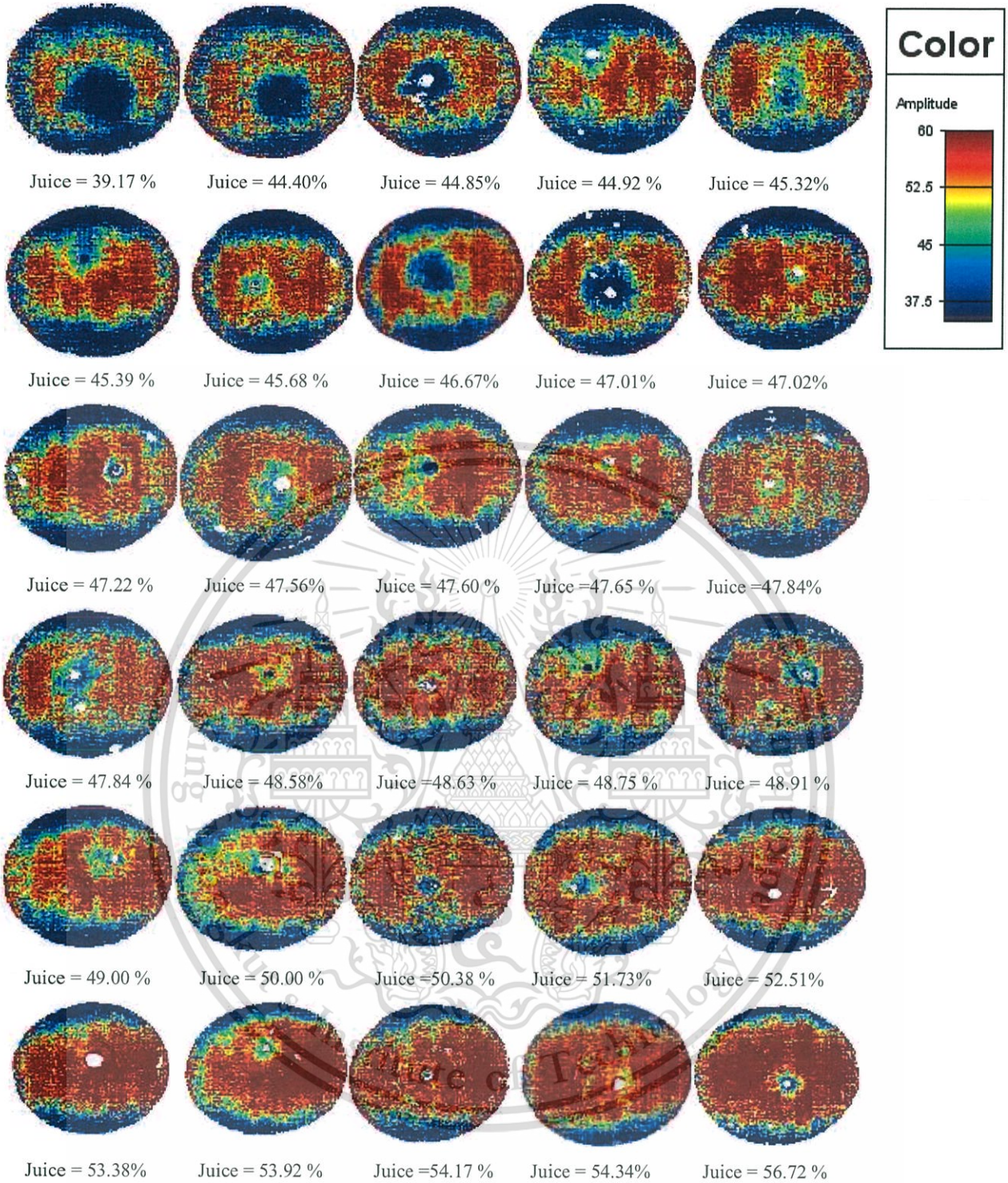

Figure 4.13. Chemical images of Juice content in lime samples

In conclusion, based on the obtained results, NIR-HSI combined with image processing techniques had the high potential to predict and illustrate the juice content gradient within the lime and among limes.

CHAPTER 5 CONCLUSIONS AND SUGGESTIONS

5.1 CONCLUSION

Limes grown from different locations showed significant difference in the physiochemical quality that could be explained by many factors: cultivar, growth region, growing year and mature level of the fruit. In addition, "Paan" limes collected at Khon Kaen, Thailand had the highest quality among other limes selected at other locations. The gained knowledge of the physiochemical characteristic of lime, selected from four different geographies was a helpful reference in developing the new system for determining the quality of lime nondestructively in the market.

Due to the traditional chemical analysis methods with experience labors for determined the internal quality of limes are highly time-consuming, inconsistency and destructive, the nondestructive method based on NIRs has been applied for simultaneous classification and prediction of TSS, citric acid and moisture content in intact limes which selected in different geography vary in growing conditions, handling behaviors etc. Using portable handheld FQA-NIR Gun in classification and prediction of internal quality of lime facilitate sorting and handling lime in the market and on-field which provide a useful technique for both the farmers and the fruit exporters.

In addition, NIR HSI applied on nondestructive prediction of internal qualities of lime fruits results in high accuracy of information from both spectral and spatial data. Moreover, the concentration gradients of TSS, citric acid and juice could be visualized in a pixel-wise manner which showed the distribution and content of chemical constituent within and between samples. Chemical images produced for testing internal quality of lime can be obtained quickly. Therefore, it is possible to implement HSI technique for nondestructively sorting of limes for TSS, citric acid and juice content clearly.

5.2 SUGGESTIONS

Suggestions for further study:

- Increase the range and validate the models to ensure that it is sufficiently robust to accurately measure the quality of internal limes from any cultivar.

- Remove the peel then analysis peel and fruit without peel in order to compare the accuracy with the recent result and ascertain the effect of skin on accuracy that is good for further online application. Although, this method is destructive and cannot be used tracking fruit continuously, the only advantage this type of measurement can offer is an increase of analysis' speed, compared to oven or microwave drying methods.
- Investigate the effect of storage conditions of limes on the robustness of model using conventional NIRs and NIR HSI.
- Apply transmittance mode on identification of seed in limes fruit using NIRs.

REFERENCES

Amolsiri, N and Intira, L. 2016. Effect of nitric oxide on postharvest quality of lime fruit (Citrus auratifoliaSwingle). KKU Research journal. 21(1), 86-96.

Antonucci, F., Pallottino, F., Paglia, G., Palma, A., D'Aquino, S., and Menesatti, P. 2010. Non-destructive estimation of mandarin maturity status through portable Vis/NIR spectrophotometer. Food and Bioprocess Technology, 3.doi:10.1007/s11947-010-0414-5.

AOAC 17th edn. 2000. Official method 942.15 Acidity (titrable) of fruit products.

Ariana, D.P. and Lu, R. 2010. Hyperspectral waveband selection for internal defect detection of pickling cucumbers and whole pickles. Computer and Electronic in Agriculture. 74, 137–144.

Ariana, D.P., Lu, R. and Guyer, D.E. 2006.Near–infrared hyperspectral reflectance imaging for detection of bruises on pickling cucumbers. Computer and Electronic in Agriculture. 53, 60–70.

ASAE Standards. 1994. Moisture Measurement-forages. ASAES358.2 DEM93, 471.American Society of Agricultural Engineering, 2950 Niles Road, Michigan, USA.

Barnes, R.J., Dhanoa, M.S., and Lister, S. J. 1989. Standard Normal Variate Transformation and De-trending of Near-Infrared Diffuse Reflectance Spectra. Applied Spectroscopy. 43 (5). 772-777.

Belton, P.S., Kemsley, E.K., McCann, M.C., Ttofis, S., Wilson, R.H. and Delgadillo, I. 1995. The identification of vegetable and matter using Fourier transform infrared spectroscopy journal of Food Chemistry54:437-441.

Berzaghi, P., and Riovanto, R. 2009. Near infrared spectroscopy in animal science production. Principles and applications. Italian journal of animal science, 8(3), 39-62.

Birth, G. S. 1976. How light interact with foods. In J. J. Gafney (Ed.).Quality detection of foods. 6-11. St Joseph, MI: ASAE.

Blakey, R.J., and van Rooyen, Z. 2011. Non-destructive measurement of moisture content in avocados using handheld near-infrared spectroscopy. Proceedings VII World Avocado Congress, Cairns, Australia, 1–6.

Blanco, R.M., and Alcal. B. M. 2009.Multivariate calibration for quantitative analysis.In D.-W. Sun (Ed.), Infrared spectroscopy for food quality analysis and control. Amsterdam, London: Elsevier/Academic Press. 51-82.

Blondel, L. 1952. Determination of the maturity of citrus fruits. Artificial neural network, Institute of Agriculture, Et Services, Experimental Agriculture Algeric. 7: 1-56.

Broadhurst, D. I and Kell, D.B. 2006. Statistical strategies for avoiding false discoveries in metabolomics and related experiments. Metabolomics, 2: 171-196.

Burns, D. A. and Ciurczak, E. W. (Eds.). 1990. Handbook of near-infrared analysis. Boca Raton: CRC, 529-568.

Chalmers, J.M., and Griffiths, P.R. 2002. Handbook of Vibrational Spectroscopy. Wiley Publication. Online ISBN: 9780470027325. DOI: 10.1002/0470027320.

Chen, Y. R., Chao, K., and Kim, M. 2002. Machine vision technology for agricultural applications. Computers and Electronic in Agricultural, 36(2), 173-191.

Cogdill, R. P., Hurburgh, C. R., and Ripple, G. R. 2004.Single-kernel maize analysis by near-infrared hyperspectral imaging. Transactions of the ASAE, 47(1), 311-320.

Cooper, P. J. 1983. NIR analysis for process control. Cereal Foods World, 28, 241-245.

Da-Wen Sun. 2010.Hyperspectral imaging for food quality analysis and control. Elsevier. UK. ISBN.978-12-374753-2.

Davies, F. S. and Albrigo, L. G. 1994. Citrus. CAB International. Wallingford, UK.

Davies, A. M. C., and Grant, A. 1987.Near infra-red analysis of food. International Journal of Food Science and Technology, 22, 191-207.

De Noord, O. E. 1994. The Influence of Data Preprocessing on the Robustness and Parsimony of Multivariate Calibration Models. Chemometrics and intelligent laboratory systems. 23(1). 65-70.

Echeverria, E. and Ismail, M. 1987. Changes in sugars and acids of citrus fruits during storage. Proceeding of the Florida State Horticulture Society, 100, 50-52.

Elmasry, G., Wang, N. and Vigneault, C. 2009. Detecting chilling injury in red delicious apple using hyperspectral imaging and neural networks. Postharvest Biology Technology. 52, 1–8.

Erickson, L. C. 1968. The general physiology of citrus. In: Reuther, W., Batchelor, L.D. and Webber, H.J. (eds), The citrus industry. University of California Press, Berkeley, California, 86-126.

Fraser, D. G., Jordan, R. B., Kunnemeyer, R., and McClone, V. A. 2003. Light distribution inside mandarin fruit during assessment by NIR spectroscopy. Postharvest Biology and Technology, 27, 185-196.

Fujita, S. and Tono, T. 1985.The relationship between browning due to rind-oil spot of citrus fruit peel and the absorption spectra of its extract. Journal of the Japanese Society for Horticultural Science, 54 (1), 109-115.

Gaffney, J. J. 1973. Reflectance properties of citrus fruit. Transaction of the ASAE, 16 (2), 310-314.

Gamal, M. and Shigeki, N. 2016. Image analysis operations applied to hyperspectral images for non-invasive sensing of food quality – A comprehensive review. Biosystems Engineering, 142, 53-82.

Gao, X., Heinemann, P.H., and Irudayarai, J. 2003. Nondestructive apple bruise on-line test and classification with Raman spectroscopy. Paper No. 033025, ASAE Annual International Meeting, Las Vegas, Nevada, USA.

Gloria, A. M. 2001. Oranges and lemons: clues to the taxonomy of citrus from molecular markers. TRENDS in Genetics, 17.

Gomez. J., Blasco, J., Aleixos, N., Juste, F., and Molto, E. 2006. Hyperspectral computer vision system for early detection of penicilliumdigitatum in citrus fruits. XVIth CIGR World Congress: Agricultural Engineering for the better world, Book of Abstract, Bonn, Germany, 241-242.

Gómez, A. H., He, Y., and Pereira, A. G. 2006.Nondestructive measurement of acidity, soluble solids and firmness of Satsuma mandarin using Vis/NIR spectroscopy techniques. Journal of Food engineering, 77, 313-319.

Gómez-Sanchis, J., Moltó, E., Camps-Valls, G., Gómez-Chova, L., Aleixos, N., and Blasco, J. 2008a.Automatic correction of the effects of the light source on spherical objects. An application to the analysis of hyperspectral images of citrus fruits. J. Food Eng. 85, 191–200.

Gómez-Sanchis, J., Gómez-Chova, L., Aleixos, N., Camps-Valls, G., Montesinos-Herrero, C., Moltó, E. and Blasco, J. 2008b.Hyperspectral system for early detection of rottenness caused by penicilliumdigitatum in mandarins. J. Food Eng. 89, 80–86.

Goodson, D. Z. 2011. Mathematical methods for Physical and Analytical Chemistry. Published by Wiley. ISBN: 978-0-470-47354-2.

Grierson, W., Miller, W. M. and Wardowski, W. F. 1978. Packing line Machenery for Florida Citrus Packinghouses. Bulletin 803, University of Florida.

Guthrie, J., Walsh, K. 1997. Non-invasive assessment of pineapple and mango fruit quality using near infrared spectroscopy. Aust. J. Exp. Agric. 37, 253–263.

Guthrie, J. A., Wedding, B., and Walsh, K. B. 1998.Robustness of NIR calibrations for soluble solids in intact melon and pineapple. Journal of Near Infrared Spectroscopy, 6, 259–265.

Guthrie, J. A., Walsh, K. B., Reid, D. J., and Liebenberg, C. J. 2005a. Assessment of internal quality attributes of mandarin fruit. 1. NIR calibration model development. Australian Journal of Agricultural Research, 56, 405–416.

Guthrie, J. A., Reid, D. J., and Walsh, K. B. 2005b. Assessment of internal quality attributes of mandarin fruit. 2. NIR calibration model robustness. Australian Journal of Agricultural Research, 56, 417–426.

Herold, B., Kawano, S., Sumpf, B., Tillmann, P., and Walsh, K. B. 2009.Vis/NIR spectroscopy.In M. Zude (Ed.), Optical monitoring of fresh and processed agricultural crops.141-249.

Huang, M. and Lu, R. 2010.Apple mealiness detection using hyperspectral scattering technique.Postharv. Biol. Technol. 58, 168–175.

Jamashidi. B., Minaei. S, Mohajerani. E., and Gassemian. H. 2011. Analysis of citrus peel for non-destructive determination of fruit composition by reference Vis/NIR spectroscopy. CIOSTA CIGR V Conference.

Jerome. J. W. 1992. NIR Spectroscopy calibration basics in *Handbook of Near-infrared Analysis*. Vol.13. Donald A. Burn and Emil W. Ciurczak. New York: Marcel dekker, 1992, 247-280.

Joseph, I. and Christoph, R. 2008. Nondestructive testing of food quality. Blackwell Publishing and the institute of Food Technologists.

Juan, F. G. M. 2015. Optical path length and wavelength selection using Vis/NIR spectroscopy for olive oil's free acidity determination. International Journal of Food Science and Technology 2015, 50, 1461–1467.

Kader, A. A. 2002. Opportunities in using biotechnology to maintain postharvest quality and safety on fresh produce. HortScience, 37, 24-25.

Kandpal, L. M., Lee, H., Kim, M. S., Mo, C., and Cho, B. K. 2013. Hyperspectral reflectance imaging technique for visualization of moisture distribution in cooked chicken breast. Sensors. ISSN 1424-8220, 13, 13289-13300

Kawano, S., Fujiwara, T., Iwamoto, M., 1993. Non-destructive determination of sugar content in 'Satsuma' mandarins using NIRS transmittance. J. Japan. Soc. Hort. Sci. 62, 465–470.

Kawano, S. 2002. Sampling and sample presentation. In H. W. Siesler, Y. Ozaki, S. Kawata, & H. M. Heise (Eds.), Near-infrared spectroscopy: Principles, instruments, applications. 115-162.

Kondo, N. 1995.Quality evaluation of orange fruit using neural networks.In food Processing Automation IV, Chicago, USA, 95-101.

Kondo, N., Murase, H., Monta, M., Shibano, Y., and Mohri, K. 1995. Study on evaluation of orange fruit using image processing. In IFA International Federation of Automatic Control Preprints, 93-96.

Kondo, N., Ahmad, U., Monta, M., and Murase, H. 2000. Machine vision based quality evaluation of Iyokan orange fruit using neural networks. Computer and Electronic in Agriculture, 29 (1-2), 135-147.

Kondo, N., Namba, K., Nishiwaki, K., Ling, P., and Monta, M. 2006. Effectiveness of PL Filtering Image with halogen Lamp for Agricultural Products, ASABE 2006 Annual International Meeting Technical Paper, CD-Room, St. Joseph, MI, USA.

Lammertyn, J., Peirs, A., De Baerdemaeker, J., and Nicolai, B. 2000. Light penetration properties of NIR radiation in fruit with respect to non-destructive quality assessment. Postharvest biology and technology, 18(1), 121-132.

Lee, K. A. 2007. On-line analysis in food engineering.In Y. Ozaki, W. F. McClure, and A. A. Christy (Eds.), Near-infrared spectroscopy in food science and technology. Hoboken: John Wiley & Sons. 361-378.

Li, J., Rao, X., and Ying, Y. 2011.Detection of common defects on oranges using hyperspectral reflectance imaging. Comput. Electron. Agric. 78, 38–48.

Liu, Y., Sun, Y., and Ouyang, A. 2010a. Non-destructive measurements of soluble solid content of navel orange fruit by visible-near infrared spectrometric technique with PLS and PCA-BPNN. LWT-Food Science and Technology, 43, 602-607.

Liu, Y., Sun, Y., Zhang, H. and Aiguo, O. 2010b. Nondestructive measurement of internal quality of Nanfeng mandarin fruit by charge coupled device near infrared spectroscopy. Computers and electronic of Agriculture, 71 (S1), S10-S14.

Liu, Y., Sun, Y., Zhang, H. and Ouyang, A. 2009. Nondestructive assessment of quality of Nanfeng mandarin fruit by the portable near infrared spectroscopy. International Journal of Agricultural and Biological Engineering, 2, 65-71.

Liu, Y., Chen, X. and Aiguo, O. 2008. Nondestructive determination of pear internal quality indices by visible and near-infrared spectrometry. Food Science and technology.41 (9).1720-1725.

Liu Yan-de, and Ying Yi-bin. 2004. Measurement of sugar content in Fuji apples by FT-NIR spectroscopy. Journal of Zhejiang University SCIENCE ISSN 1009-3095.

Lu, R. 2003. Imaging spectroscopy for assessing internal quality of apple fruit.Paper No. 036012, ASAE Annual international meeting, Las Vegas, Nevada, USA.

Lu, R. 2004. Multi spectral imaging for predicting firmness and soluble solids content of apple fruit.Postharvest biology and technology, 31(2), 147-157.

Magwaza, L. S., Opara, U. L., Nieuwoudt, H., Cronje, P. J. R., Saeys, W., and Nicolaï, B. 2012.NIR spectroscopy applications for internal and external quality analysis of citrus fruit - a review. Food and Bioprocess Technology, 5, 425 - 444.

Mark, H. 2008. Data Analysis: multilinear regression and principal component analysis. In D. A. Burns, and E. W. Ciurczak (Eds.), Handbook of near-infrared analysis.151-188.

Martens, H., and Næs, T. 1989.Multivariate calibration.Chichester, New York: John Wiley and Sons.

McClure, W. F., and Hamid, A. 1994.Near-Infrared Spectroscopy. Am. Lab. 12, 57-59.

McGlone, V.A., Kawano, S., 1998. Firmness, dry-matter and soluble solids assessment of postharvest kiwifruit by NIR spectroscopy. Postharvest and Biology Technology. 13, 131–141.

McGlone, V. A., Fraser, D. G., Jordan, R. B., and Kunnemeyer, R. 2003.Internal quality assessment of mandarin fruit by Vis/NIR spectroscopy. Journal of Near Infrared Spectroscopy, 11, 323–332.

Mehl, P. M., Chen, Y. R., Kim, M. S., and Chan, D. E. 2004.Development of Hyperspectral imaging technique for the detection of apple surface defects and contaminations. Journal of Food Engineering, 61, 67-81.

Mendoza, F., Lu, R., Ariana, D., Cen, H. and Bailey, B. 2011. Integrated spectral and image analysis of hyperspectral scattering data for prediction of apple fruit firmness and soluble solids content. Postharv. Biol. Technol. 62, 149–160.

Milind. A. 2008. Citrus fruit: Biology, Technology and Evaluation. 1st edition. Elsevier Inc. London, UK. ISBN: 978-0-12-374130-1.

Moon, D.G., Mizutani, F., 2002. Soluble solids and titratable acid content in different portions of maturing Satsuma mandarin fruit as affected by water stress. Journal of Japan. Society Horticultural Science. 71, 1-7.

Nagy, S. and Attaway, J. A (eds). 1980. Citrus nutrition and quality. American Chemical Society, Washinton, D.C.

Næs, T., Isaksson, T., Fearn, T., and Davies, T. 2002.A user-friendly guide to multivariate calibration and classification.Chichester: NIR Publications.

Naoshi, K., 2011. Image Acquisition: Plant Materials. Encyclopedia of Agricultural. Food, and Biological engineering, Second Edition DOI: 10.1081/E-EAFE2-120042383. Copyright © 2011 by Taylor & Francis.

NIR Flex N-500 Solid Technical Data Sheet. Retrieved by http://www.donserv.pl/imagesdb_nirflexn500dsa4ena-technical-data-sheet-140708-0.pdf.

Nicolaï, B. M., verlinden, B. E., Desmet, M., Saevels, S., Saeys, S., W. Theron, K. 2008. Time-resolved and continuous wave NIR reflectance spectroscopy to predict soluble solids content and firmness of pear. Postharvest Biology and Technology, 47, 68-74.

Osborne, B. G. 2000. Near infrared spectroscopy in food analysis. Australia: BRI Australia Ltd. 1–14.

Palmer, K.F., Williams, D., 1974. Optical properties of water in the near infrared. Journal of the optical society of American. 64, 1107–1110.

Pantastico, Er. B. (Editor). 1975. Postharvest Physiology, Handling and Utilisation of Tropical and Sub Tropical Fruits and Vegetables. AVI Publishing, Westport, CT.

Park, B., Abbott, A.J., Lee, K.J.Choi, C.H., and Choi, K.H. 2002.Near-infrared spectroscopy to predict soluble solids and firmness of apple. Pare number 023066, ASAE/CIGR Annual International Meeting, Chicago, Illinois, USA.

Peng, Y. and Lu, R. 2008. Analysis of spatially resolved hyperspectral scattering images for assessing apple fruit firmness and soluble solids content. Postharvest Biology and Technology. 48, 52–62.

Peirs, A., Scheerlinck, N., Touchant, K., Nicolai, B.M. 2002. Comparison of Fourier transform and dispersive near-infrared reflectance spectroscopy for apple quality measurements. Biosystems Engineering, 81(3), 305-311.

Pranmornkith, T., Mawson, A. J. and Heyes, J. A. 2005.Effect of CA and alternative postharvest treatments on quality of lime (Citrus latifolia Tanaka) fruit. In: Proceedings of 9th International Controlled Atmosphere Research Conference, Michigan State University, ISHS, 5–10 July, 21–27.

Qin, J. and Lu, R. 2008. Measurement of the optical properties of fruits and vegetables using spatially resolved hyperspectral diffuse reflectance imaging technique. Postharvest Biology and Technology. 49, 355–365.

Qin, J. Burks, T.F. Ritenour, M.A. and Bonn, W.G. 2009. Detection of citrus canker using hyperspectral reflectance imaging with spectral information divergence. Journal of Food Engineering. 93, 183–191.

Reginald. H. W (Editor). 1994. Spectroscopic Techniques for Food Analysis. ISBN 1-56081-037-8 VCH Publishers.

Robert J. Band Zelda. V. R. 2011. Nondestructive measurement of moisture content using handheld NIR. South African Avocado growers' association yearbook 34, 2011.

Rodriguez-Saona, L. E., Fry, F. S., McLaughlin, M. A. and Calvey, E. M. 2001. Rapid analysis of sugars in fruit juices by FT-NIR spectroscopy. Carbohydr. Res. 336, 63–74.

Schulz, H., and Baranska, M. 2009. Fruits and vegetables.In D.-W. Sun (Ed.), Infrared spectroscopy for food quality analysis and control. Amsterdam, London: Elsevier/Academic Press. 321-353.

Shao, Y., He, Y., Gómez, A. H. and Zhang Y. 2007. Visible/near infrared spectrometric technique for nondestructive assessment of tomato 'Heatwave' (Lycopersicum esculentum) quality characteristics. Journal of Food Engineering, 81(4), 672–678.

Shaw, G. and Manolakis, D. 2002. Signal processing for hyperspectral image exploitation. IEEE Signal Processing Magazine, 19(1), 12-16.

Sisu CHEMA Chemical Imaging Analyzer. Retrieved by http://www.spectralcameras.com/files/SisuCHEMA_brochure.pdf.

Specification for FQA-NIR Gun. Retrieved http://www.nirsresearch.com/NP-15967-fqa_nir_gun.html.

Technical Specification for XDS Rapid Content TM Analyzer. Retrieved by file:///C:/Users/lib/Downloads/XDS_Analyser_Solution_Brochure_GB%20pdf.pdf.

Thompson, A. K., Magzoub, Y. and Silvis, H. 1974. Preliminary investigations into desiccation and de-greening of limes for export.Sudan journal Food science technology 6, 1-6.

Umezuruike, L. O., Hèléne, H. N., Wouter, S. and Bart, N. 2011. NIR spectroscopy quality analysis of citrus fruit – A review. Food Bioprocess Technology. 5. 425-444.

Varmuza, K., Filzmoser, P. 2009. Introduction to multivariate statistical analysis in chemometrics, CRC Press: Boca Raton, FL. USA.

Vidal, M., and Amigo, J. M. 2012. Pre-processing of hyperspectral images. Essential steps before image analysis. Chemometrics and Intelligent Laboratory Systems, 117, 138-148.

Wang, H., Peng, J., Xie, C., Bao, Y. and He, Y. 2015. Fruit Quality Evaluation Using Spectroscopy Technology: A Review. Sensors 2015, 15, 11889-11927.

Williams, P. C., and Norris, K. H. 1987. Qualitative applications of near-infrared reflectance spectroscopy. In: Williams, P.C., Norris, K.H. (eds), Near-Infrared Technology in the Agricultural and Food Industries, 241–246. American Association of Cereal Chemistry, St Paul, MNL.

Williams, P. C. and Norris, K. H., 2001. Variables affecting near infrared spectroscopic analysis. In: Williams, P., Norris, K.H. (Eds). Near Infrared Technology in the Agriculture and Food Industries, 2nd ed. The American Association of Cereal Chemists, St. Paul, MNL, 171–185.

Williams, P.C. 2007. Grains and seeds. In Y. Ozaki, W. F. McClure, and A. A. Christy (Eds.), Near-infrared spectroscopy in food science and technology.163-217.

Williams, P.C. 2008. Sampling, sample preparation, and sample selection. In D. A. Burns, & E. W. Ciurczak (Eds.), Handbook of near-infrared analysis.268-295.

Williams, P., Geladi, P., Fox, G. and Manley, M. 2009. Maize kernel hardness classification by near infrared (NIR) hyperspectral imaging and multivariate data analysis. A 653, 121–130.

Wilson, R. H. 1994. Spectroscopic techniques for food analysis. New York: VCH publishers.

Wold, J. P., Johansen, I.-R., Haugholt, K. H., Tschudi, J., Thielemann, J., Segtnan, V.H., Narum, B. and Wold, E., 2006. Non-destructive transflectance near infrared imaging for

representative on-line sampling of dried salted coalfish (bacalao). Journal of Near Infrared Spectroscopy 14, 59–66

Workman, J. Jr. and Weyer. L. 2008. Practical Guide to Interpretive Near Infrared Spectroscopy.Taylor and Francis Group.ISBN 1-57444-784-X.

Xing, J., Bravo, C., Jancsó, P. T., Ramon, H., and De Baerdemaeker, J. 2005. Detecting bruises on 'Golden Delicious' apples using hyperspectral imaging with multiple wavebands. Biosystems Engineering, 90, 27–36.

Young, R. H. 1977. The effect of rootstocks on citrus cold hardiness. International Citrus Congress (2nd: 1977: Orlando, Florida), International Society of Citriculture. 2: 518-522.

Zude, M., Pflanz, M., Kaprielian, C., Aivazian, B., 2008. NIRS as a tool for precision horticulture in citrus industry. Biosystem of Engineering. 99, 455–459.

APPENDIX

The process of building the chemical images of Lime using Evince Program are described in the order steps that involved three main steps: (1) Cut background; (2) Exclude outliers, such as black-spot or stem of fruit; and (3) Predict the interior qualities of lime (TSS, Citric acid and Juice content) using the obtained models, individually.

Table A1 Hyperspectral imaging analysis results and Chemical images of limes

1.1	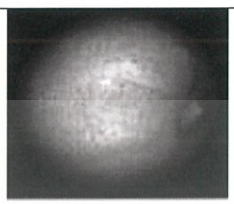	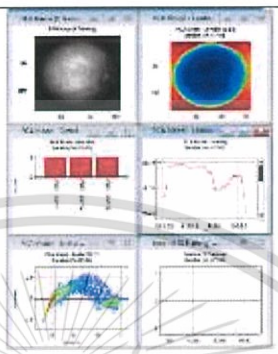	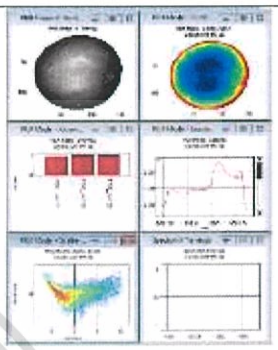
	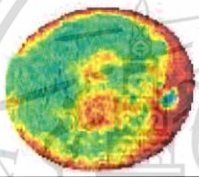	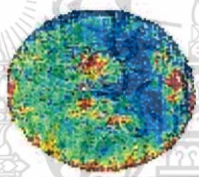	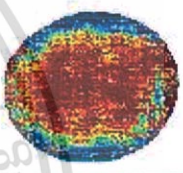
	TSS = 8.13	Citric = 7.16%	Juice = 49.36%
1.2		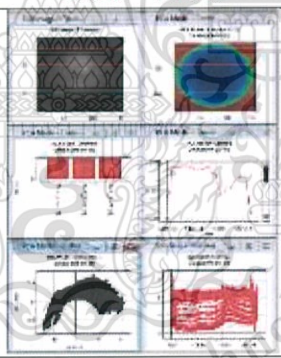	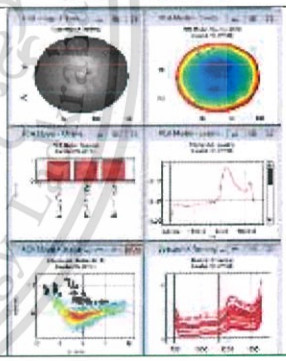
	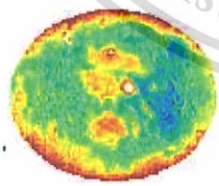	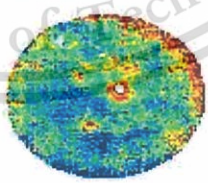	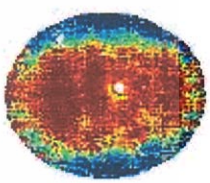
	TSS= 7.34°Brix	Citric = 7.86 %	Juice = 47.02%
2.1	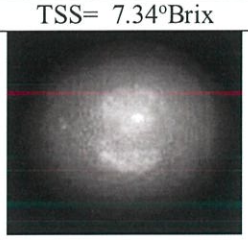	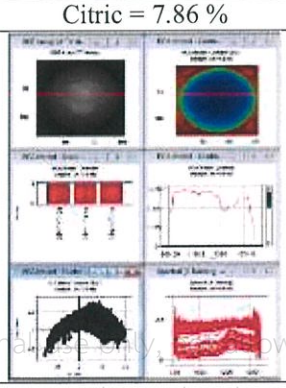	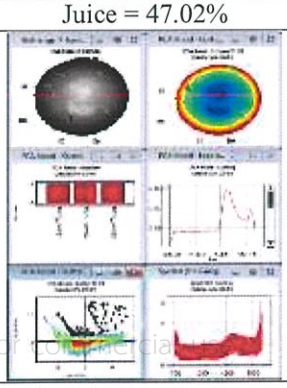

	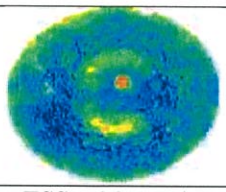	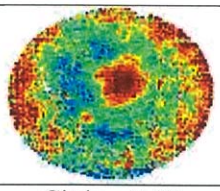	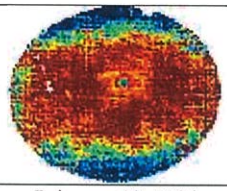
	TSS= 6.85° Brix	Citric = 7.99	Juice = 48.58%
2.2	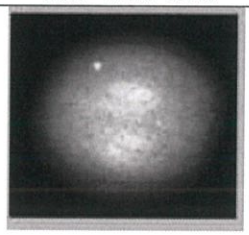	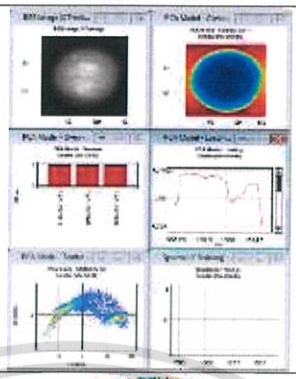	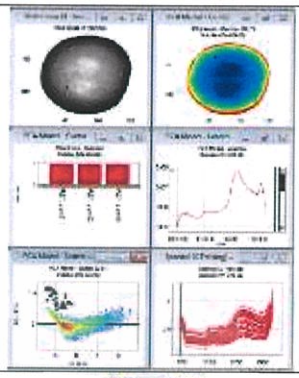
	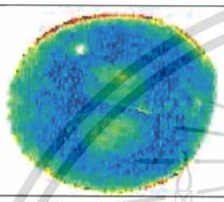	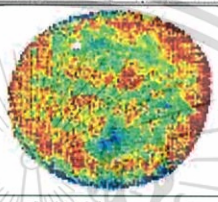	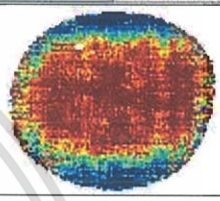
	TSS = 6.84 °Brix	Citric =8.17 %	Juice = 48.41%
3.1	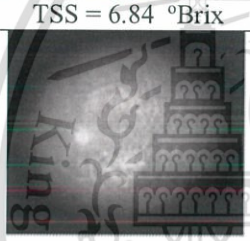	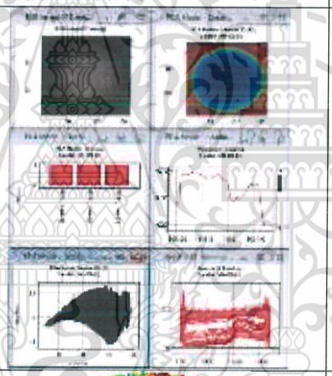	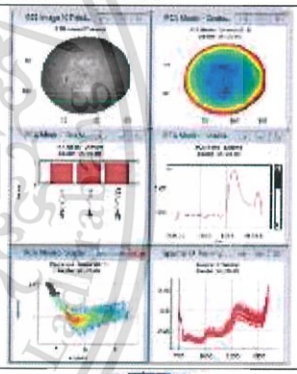
	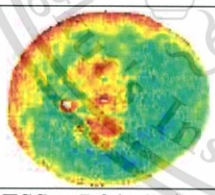	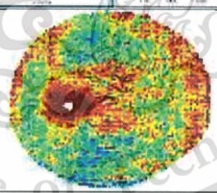	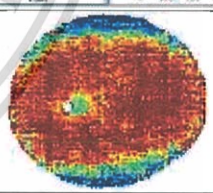
	TSS = 7.84 °Brix	Citric =8.18 %	Juice = 51.73%
3.2	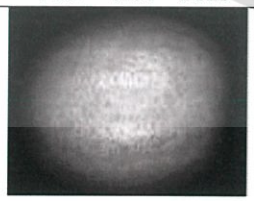	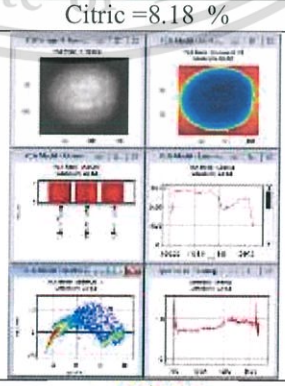	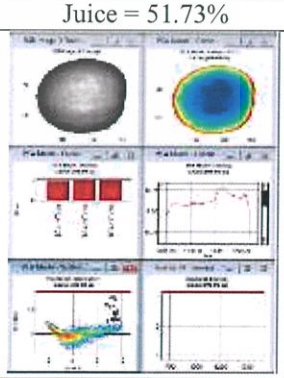
	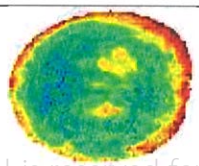	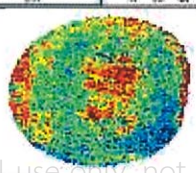	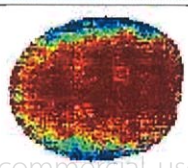
	TSS =7.72 °Brix	Citric = 7.72 %	Juice = 55%

4.1	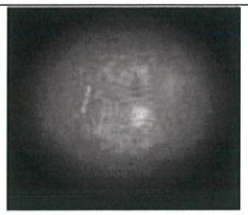	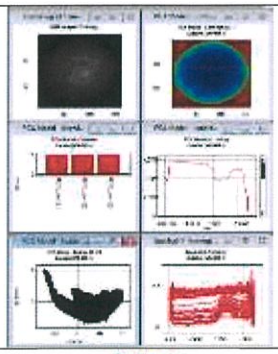	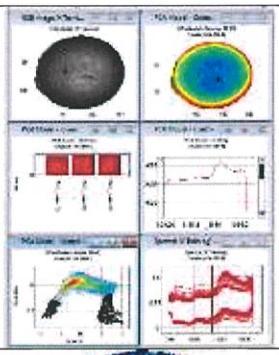
	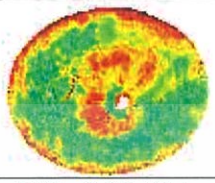	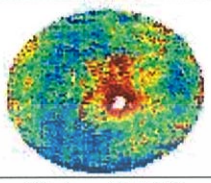	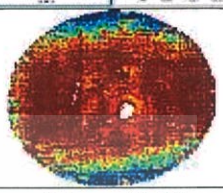
	TSS =8.07 °Brix	Citric = 7.46 %	Juice = 54.34
4.2	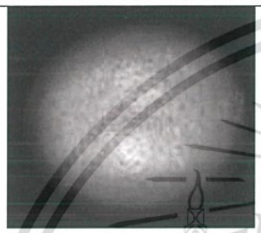	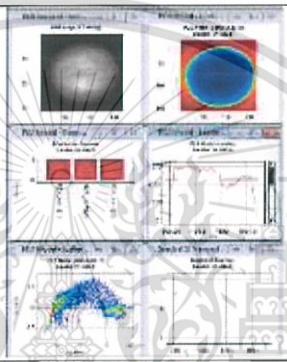	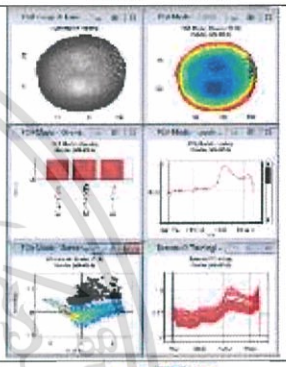
	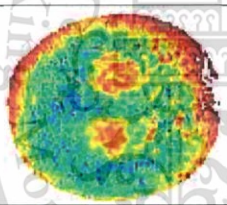	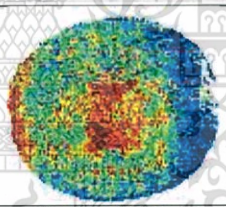	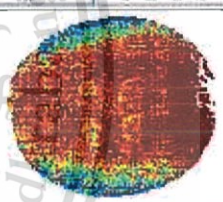
	TSS = 7.87 °Brix	Citric = 7.53 %	Juice = 54.69
5.1	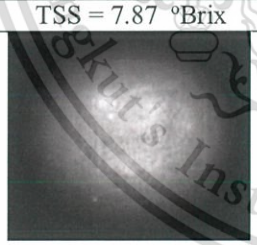	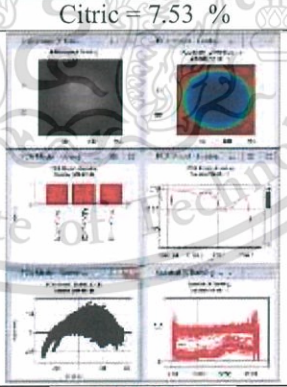	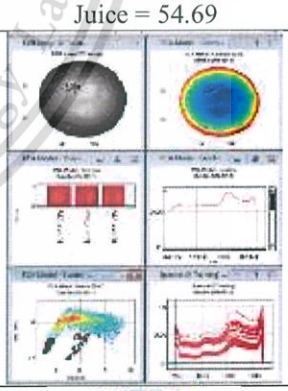
	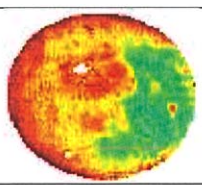	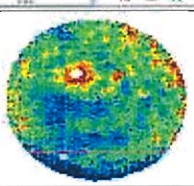	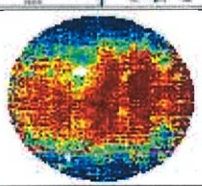
	TSS =8.40 °Brix	Citric =7.24 %	Juice = 44.92 %

5.2	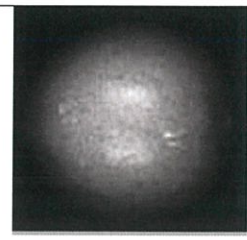	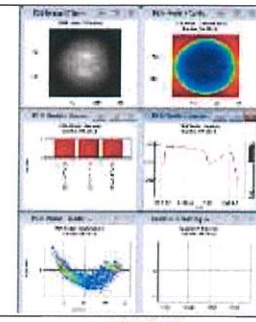	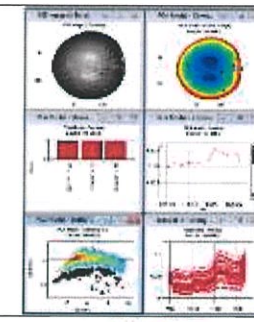
	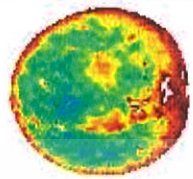	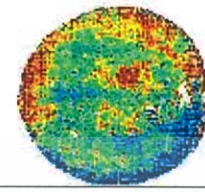	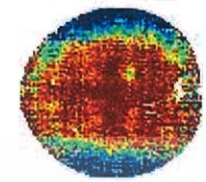
	TSS =7.64°Brix	Citric = 8.03 %	Juice = 47.57%
6.1	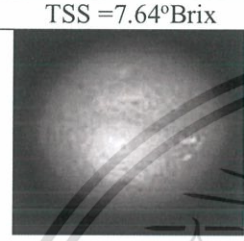	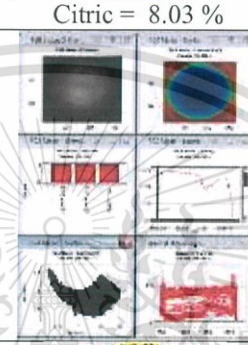	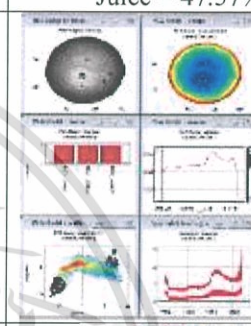
	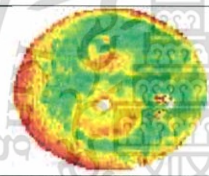	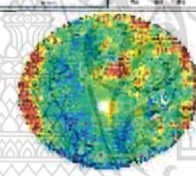	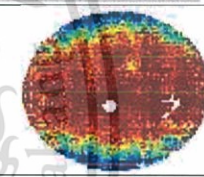
	TSS = 8.05 °Brix	Citric =7.59 %	Juice = 52.51%
6.2		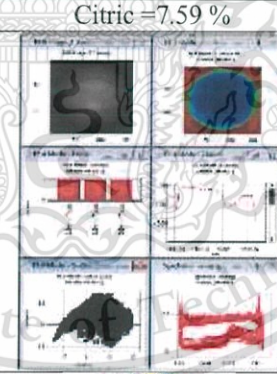	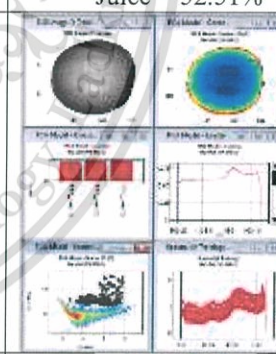
	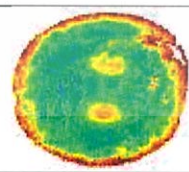	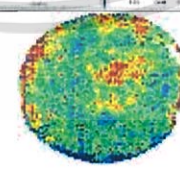	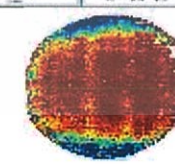
	TSS = 7.82 °Brix	Citric =7.58 %	Juice = 53.30%

7.1	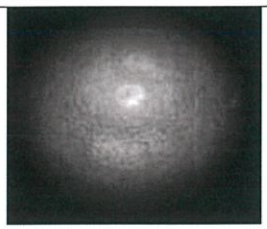	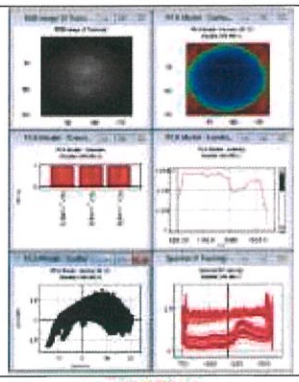	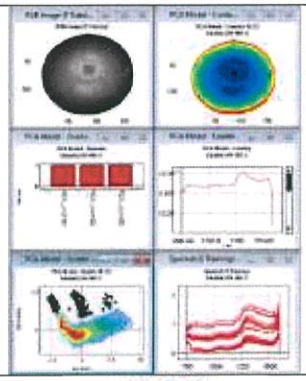
	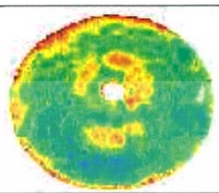	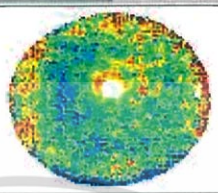	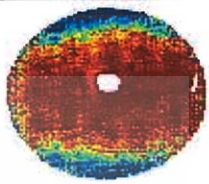
	TSS = 7.73 °Brix	Citric = 7.58 %	Juice = 53.38%
7.2	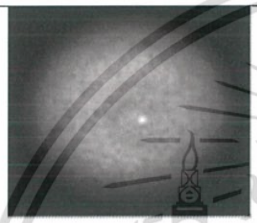	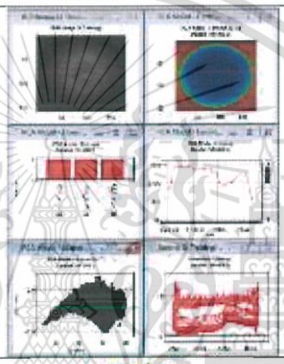	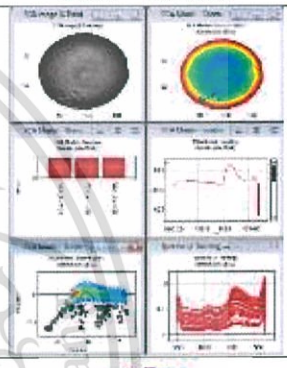
	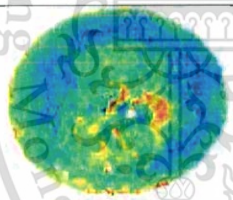	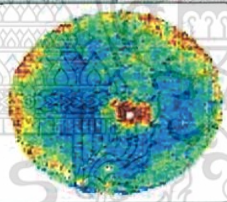	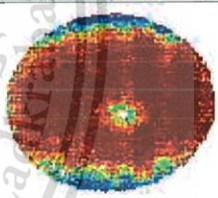
	TSS = 7.48 °Brix	Citric =7.17 %	Juice = 56.72 %
8.1	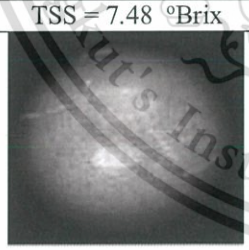	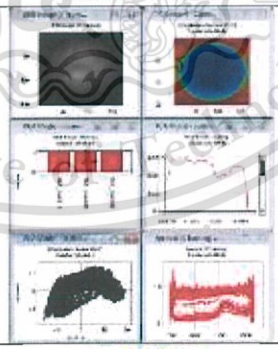	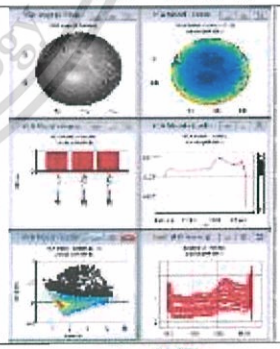
	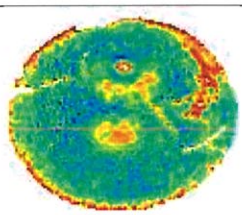	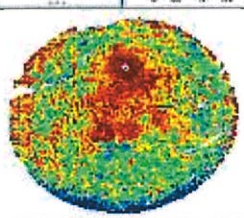	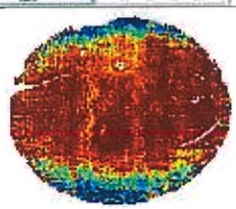
	TSS = 7.47 °Brix	Citric = 8.09 %	Juice = 54.45 %

8.2	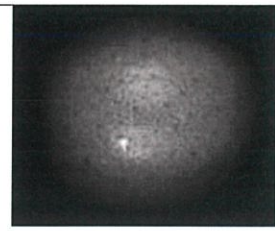	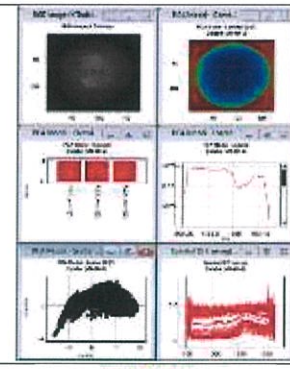	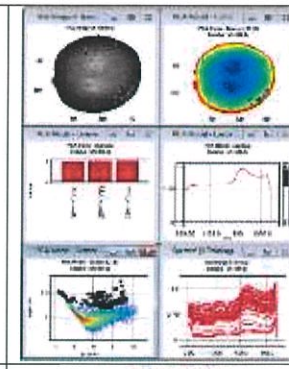
	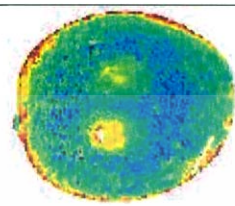	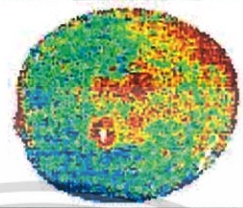	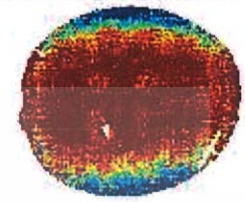
	TSS = 7.25 °Brix	Citric =7.78 %	Juice = 55.33 %
9.1		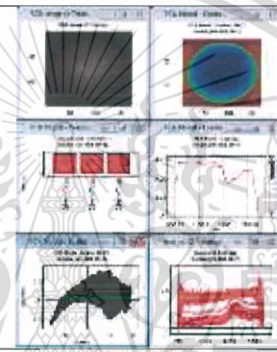	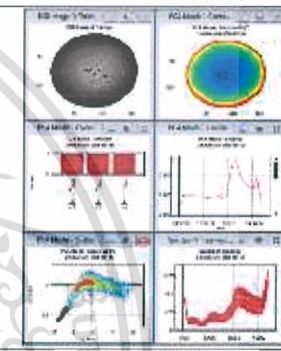
	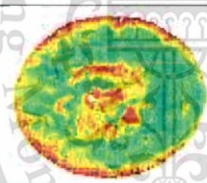	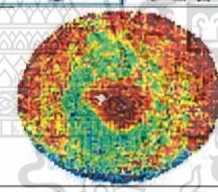	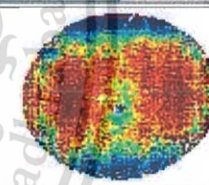
	TSS = 7.93 °Brix	Citric = 8.42 %	Juice = 45.32%
9.2	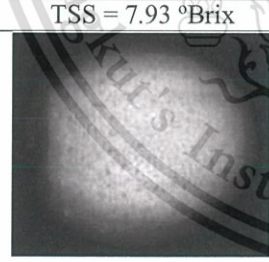	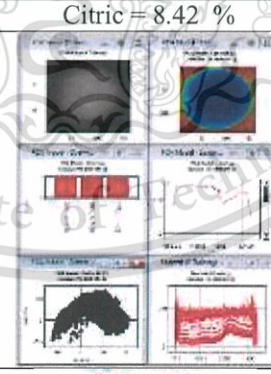	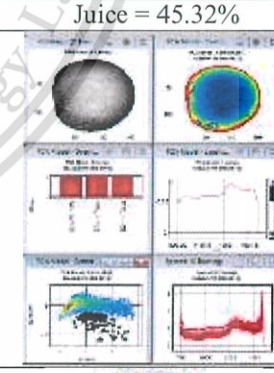
	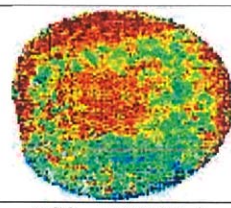	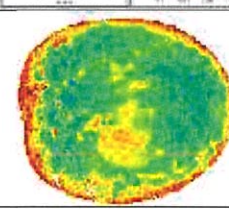	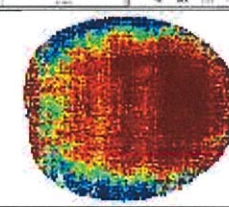
	TSS = 7.89 °Brix	Citric = 8.20 %	Juice = 52.32 %

10.1	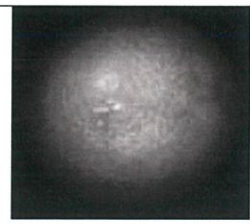	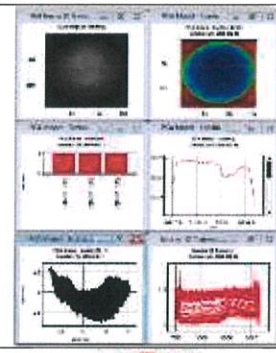	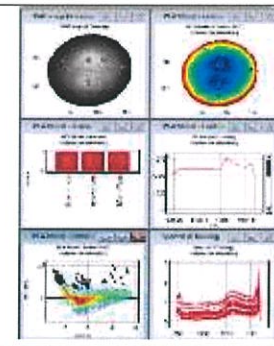
	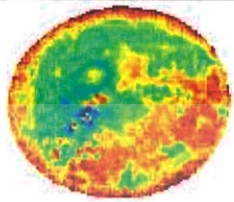	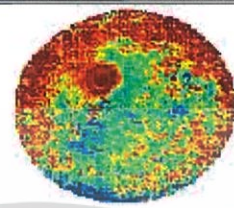	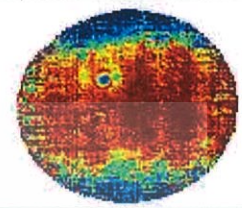
	TSS =8.14 °Brix	Citric = 8.27 %	Juice = 48.75 %
10.2	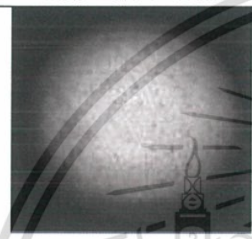	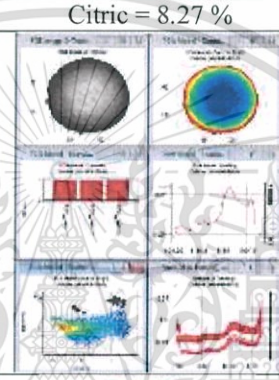	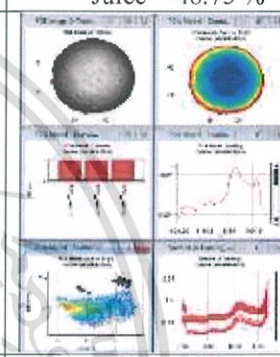
	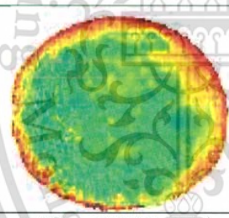	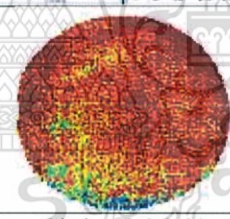	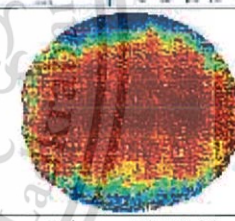
	TSS = 7.891 °Brix	Citric =9.26 %	Juice = 50.75 %
11.1	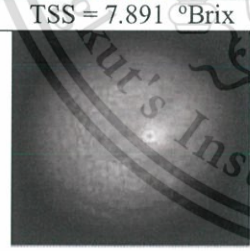	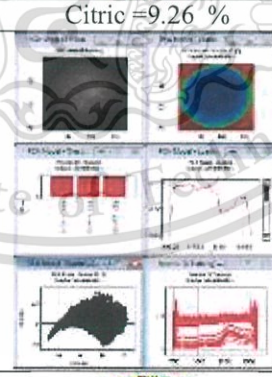	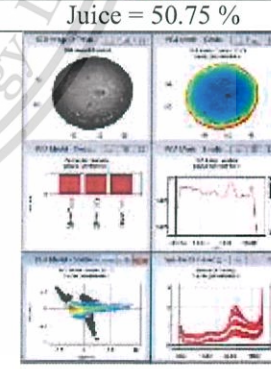
	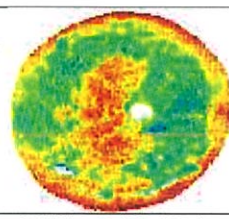	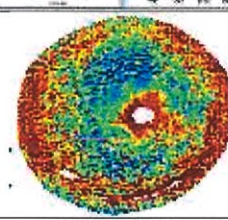	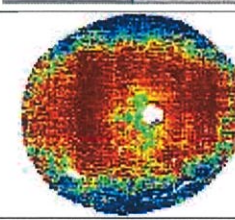
	TSS = 8.06 °Brix	Citric =8.20 %	Juice = 47.56%

11.2	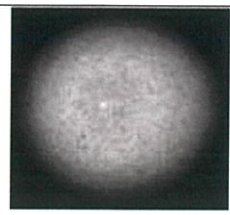	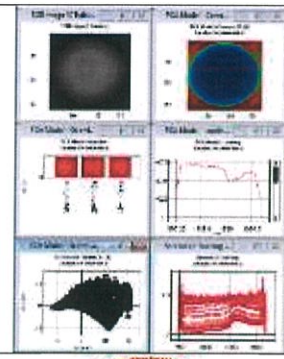	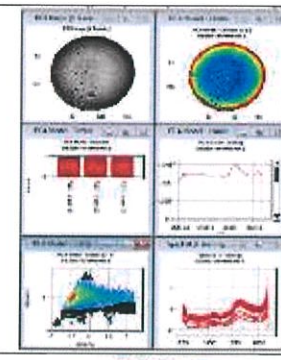
	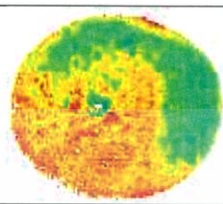	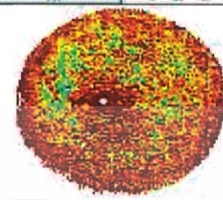	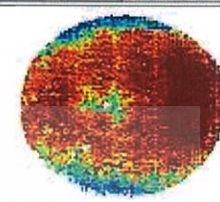
	TSS = 8.12 °Brix	Citric = 8.96 %	Juice =53.81%
12.1	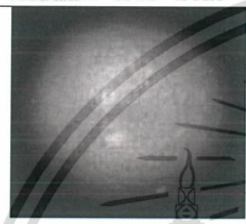	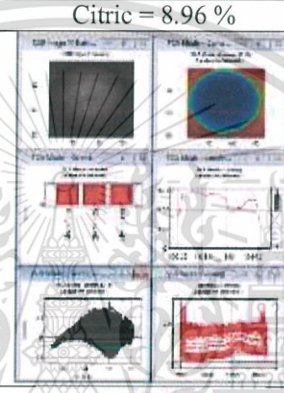	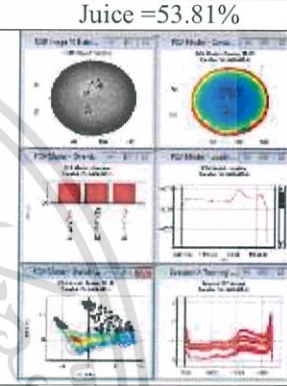
	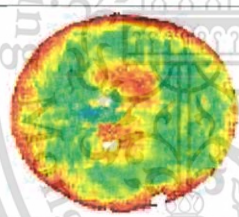	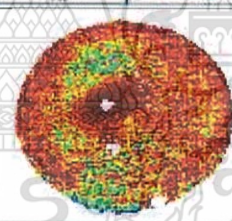	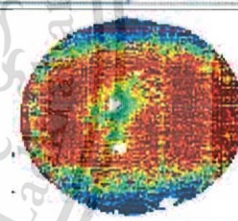
	TSS = 8.10 °Brix	Citric = 9 %	Juice =47.84%
12.2	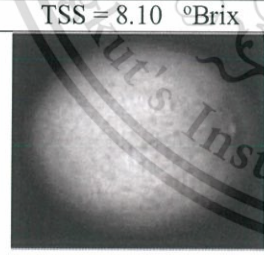	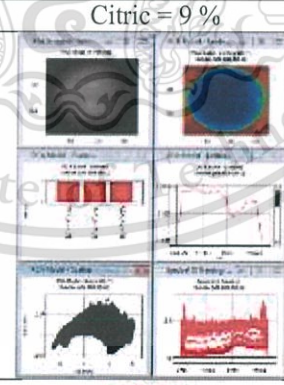	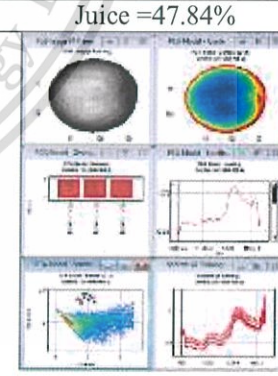
	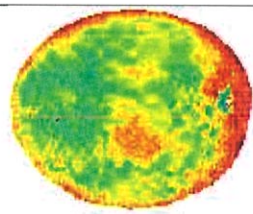	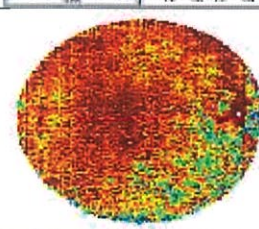	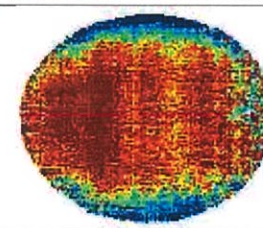
	TSS = 8.10 °Brix	Citric = 8.89 %	Juice =49.54 %

13.2	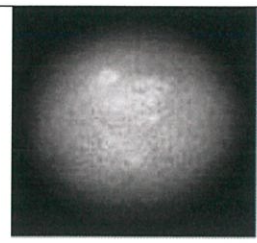	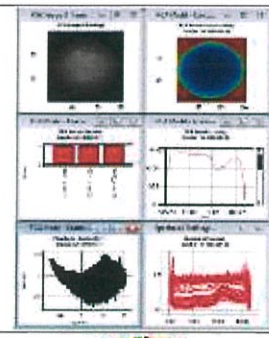	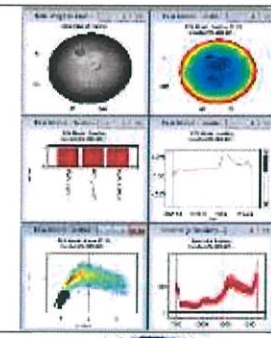
	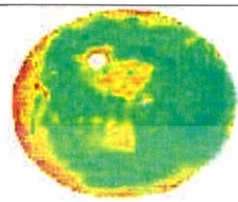	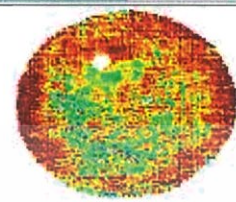	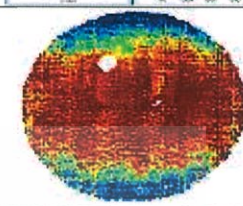
	TSS = 7.79 °Brix	Citric = 8.56 %	Juice =50.30 %
14.1	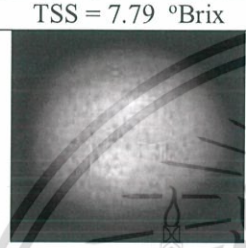	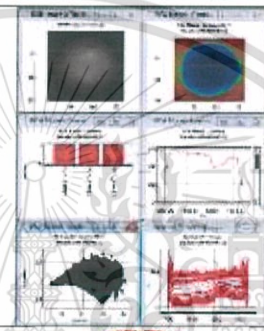	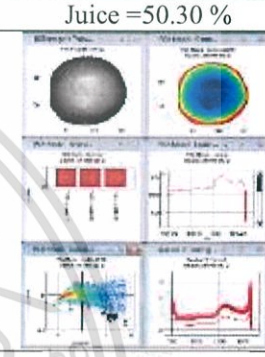
	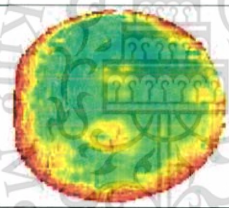	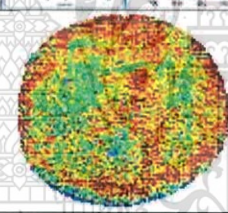	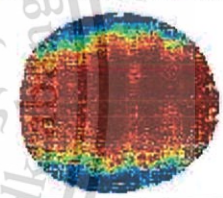
	TSS = 7.94 °Brix	Citric = 8.29 %	Juice =50.30 %
14.2	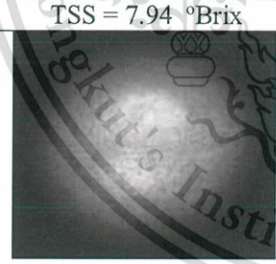	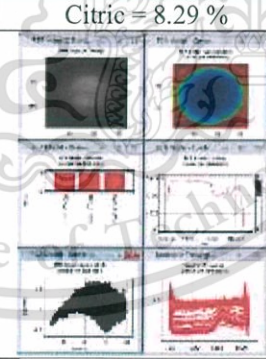	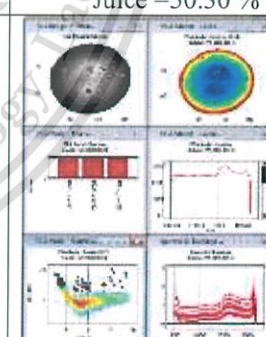
	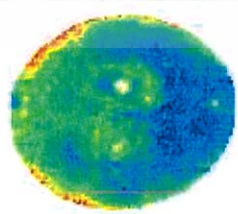	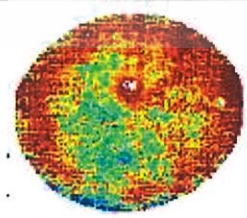	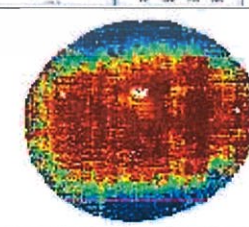
	TSS = 7.06 °Brix	Citric = 8.67 %	Juice =47.65 %

15.1	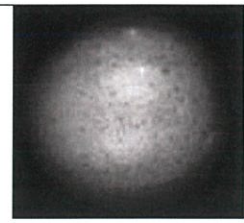	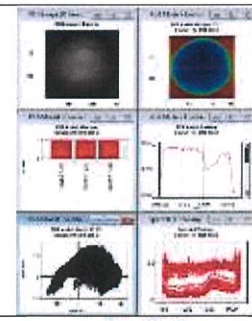	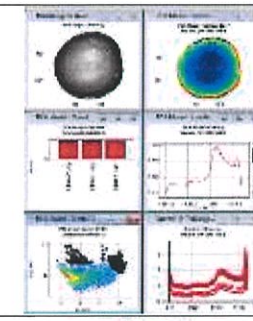
	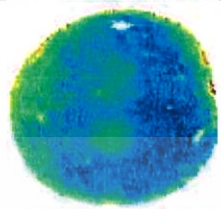	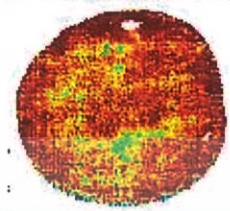	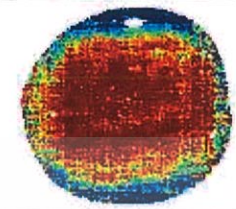
	TSS = 6.71 °Brix	Citric =9.16 %	Juice =49.26 %
16.1	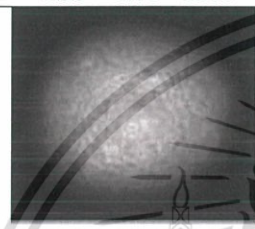	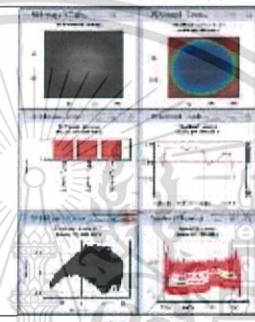	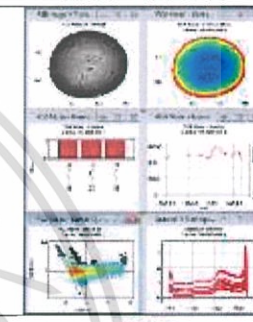
	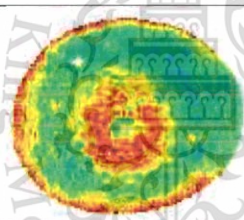	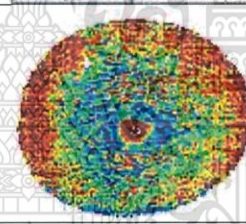	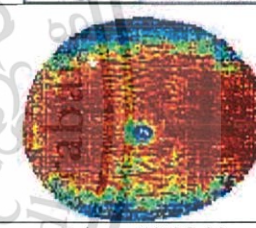
	TSS = 7.91 °Brix	Citric = 8.04 %	Juice =50.38 %
16.2	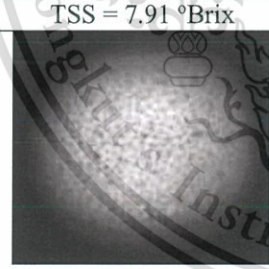	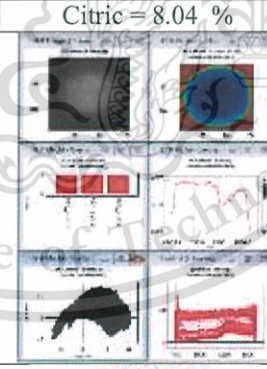	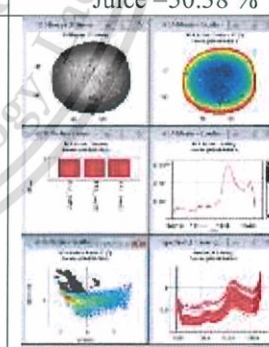
	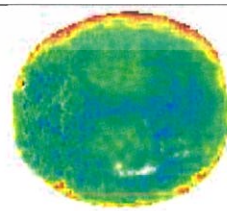	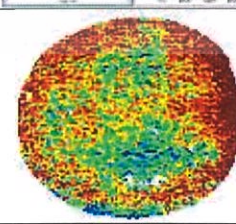	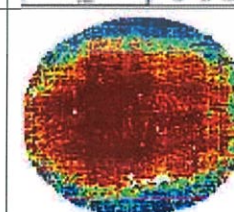
	TSS = 7.37 °Brix	Citric = 8.40 %	Juice =51.29 %

17.1	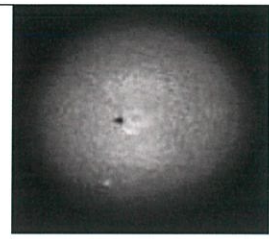	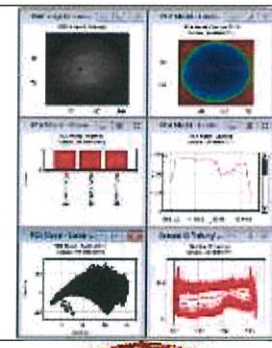	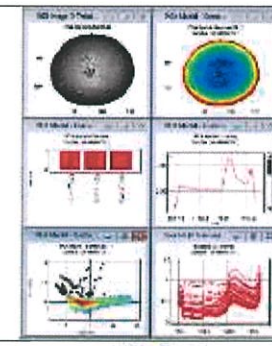
	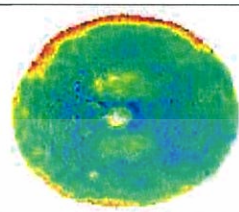	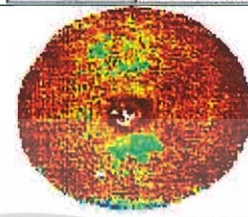	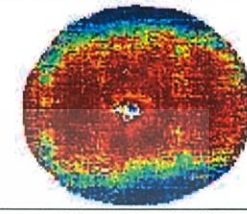
	TSS = 7.34 °Brix	Citric =9.18 %	Juice =48.63 %
17.2	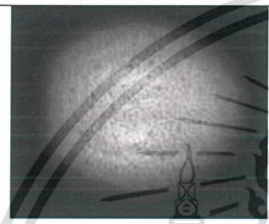	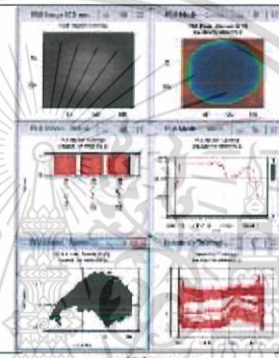	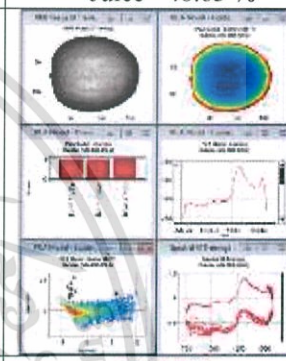
	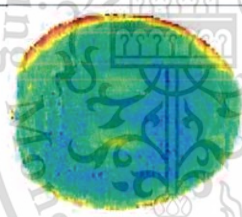	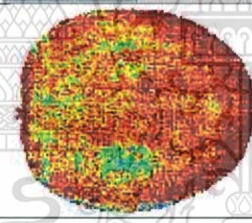	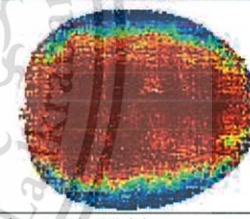
	TSS = 7.19 °Brix	Citric = 9.18 %	Juice =52.55 %
18.1	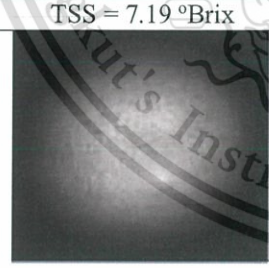	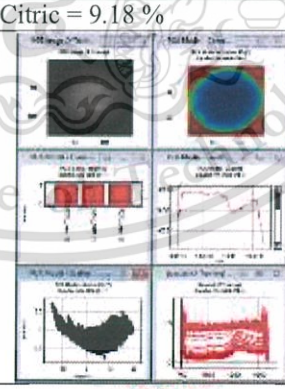	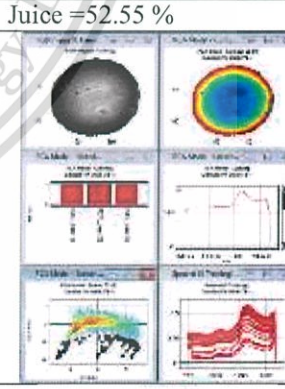
	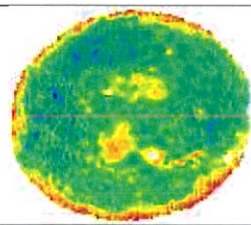	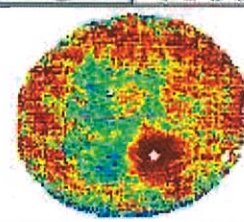	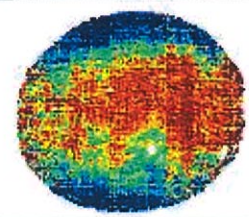
	TSS =7.63 °Brix	Citric = 8.39 %	Juice = 42.32 %

18.2	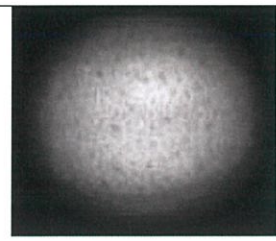	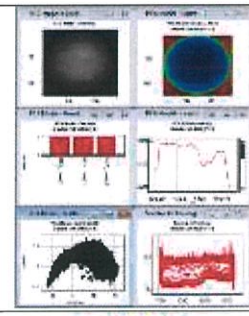	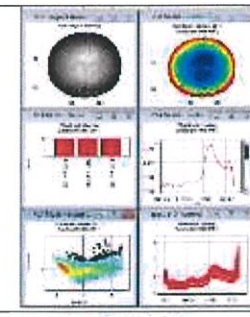
	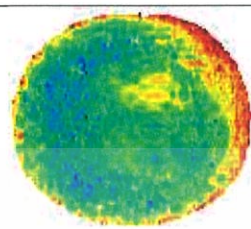	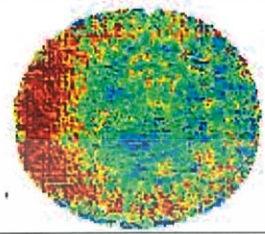	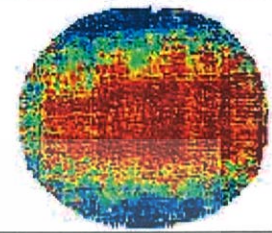
	TSS = 7.59 °Brix	Citric = 7.94 %	Juice = 45.58 %
19.1	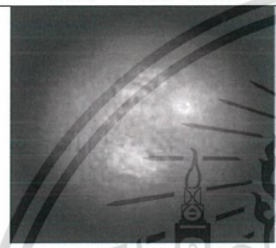	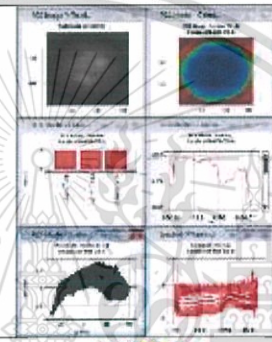	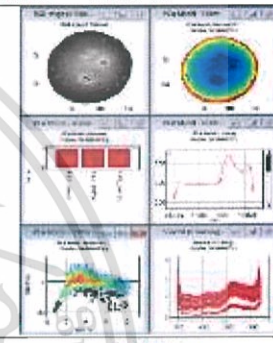
	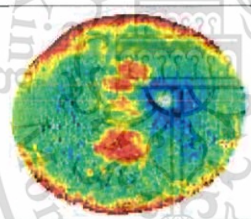	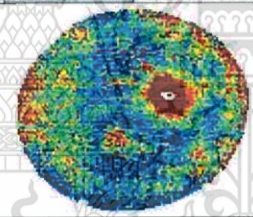	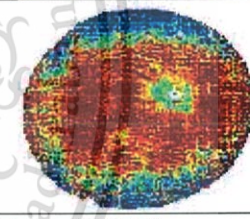
	TSS = 7.22 °Brix	Citric =7.72 %	Juice = 48.91 %
19.2	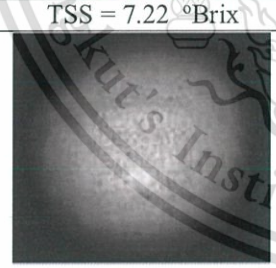	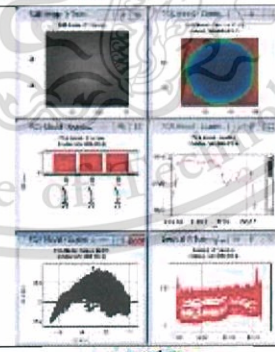	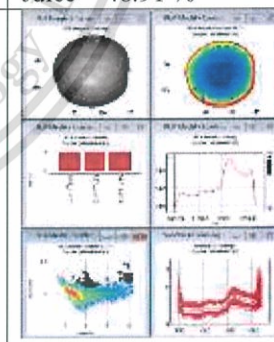
	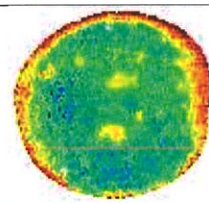	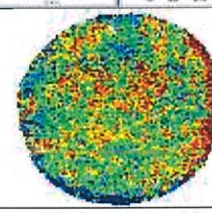	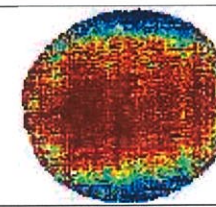
	TSS = 7.70°Brix	Citric = 7.80 %	Juice = 50.99 %

20.1	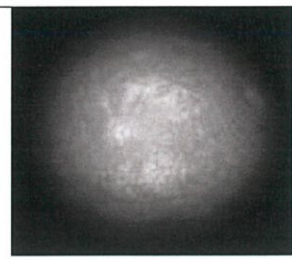	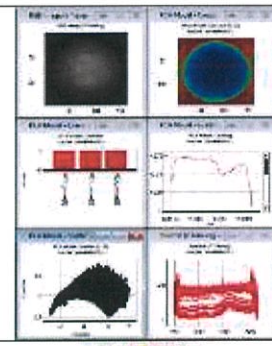	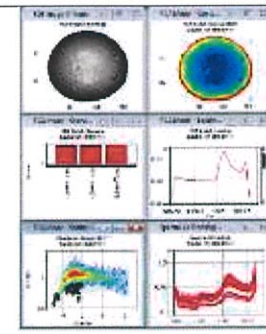
	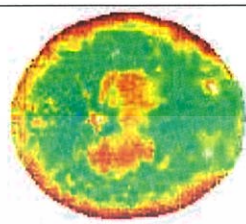	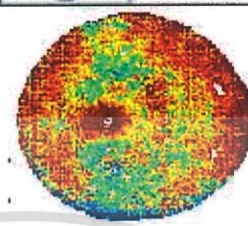	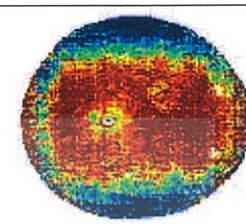
	TSS = 8.01°Brix	Citric = 8.51 %	Juice = 45.68 %
20.2	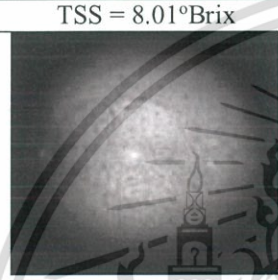	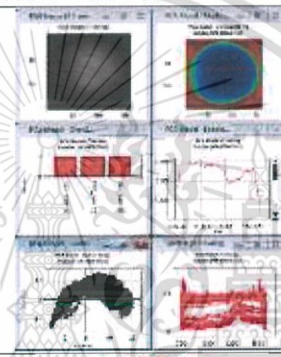	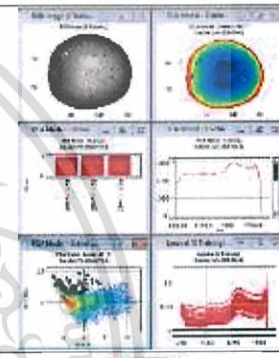
	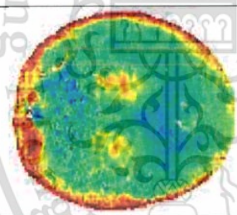	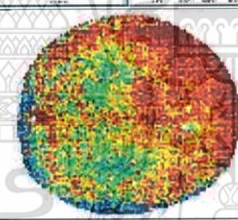	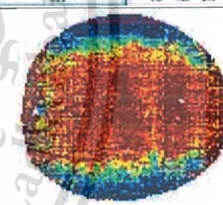
	TSS = 7.65 °Brix	Citric = 8.44 %	Juice = 47.94 %
21.1	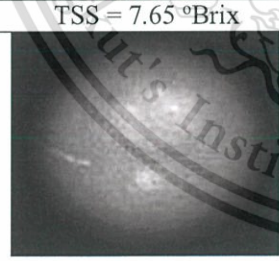	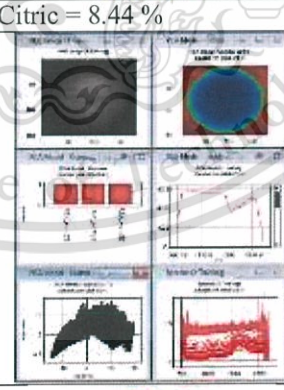	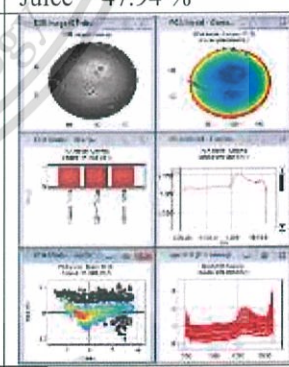
	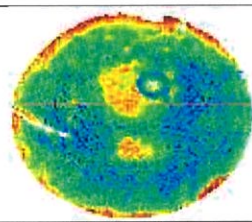	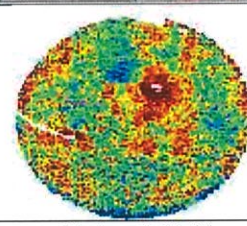	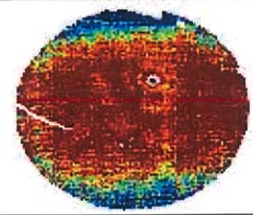
	TSS = 7.36 °Brix	Citric =8.01 %	Juice = 54.77 %

21.2	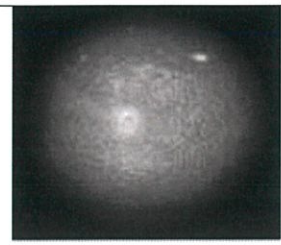	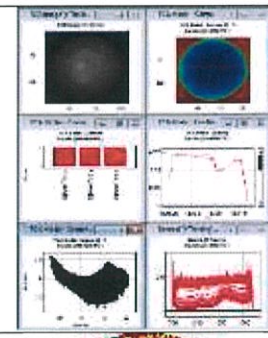	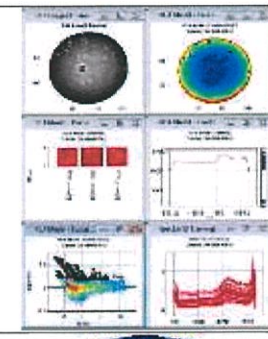
	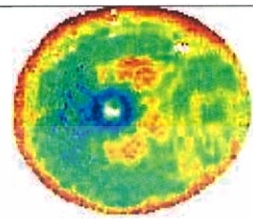	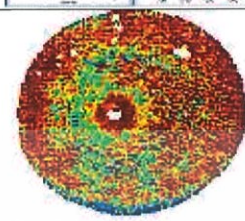	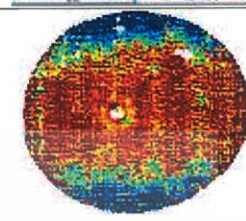
	TSS = 7.91 °Brix	Citric = 8.80 %	Juice = 47.84 %
22.1	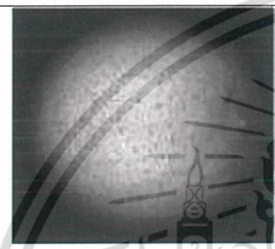	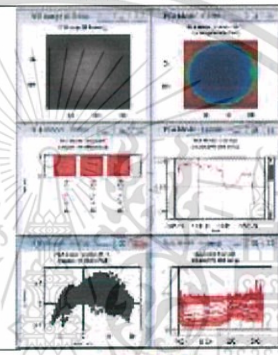	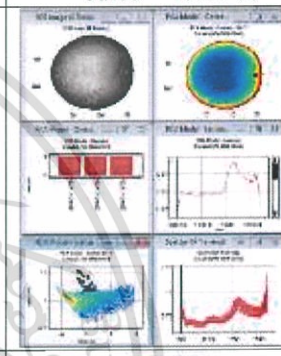
	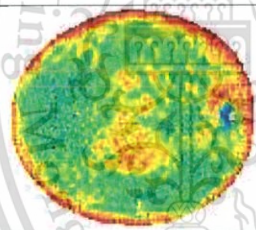	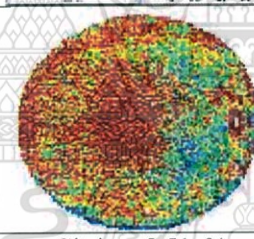	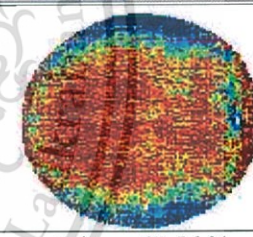
	TSS = 7.96 °Brix	Citric = 8.51 %	Juice = 47.56 %
22.2	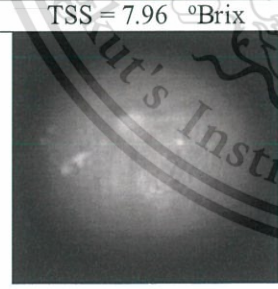	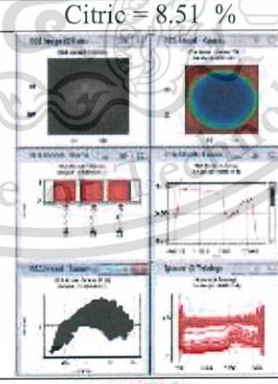	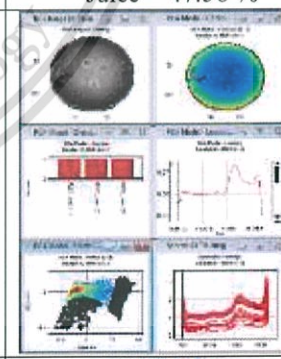
	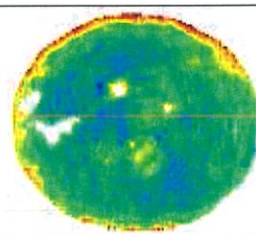	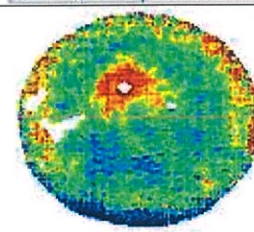	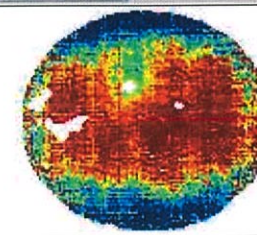
	TSS = 7.36 °Brix	Citric = 7.46 %	Juice = 45.39 %

23.1	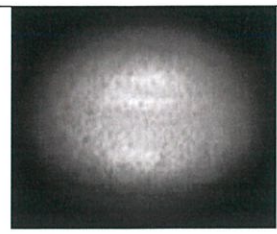	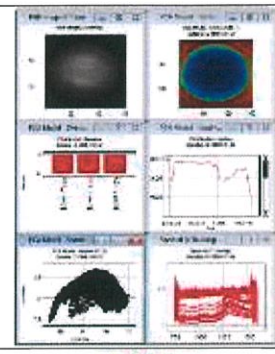	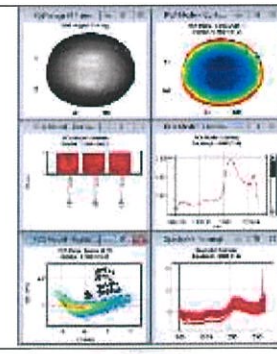
	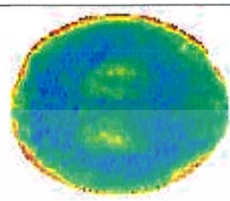	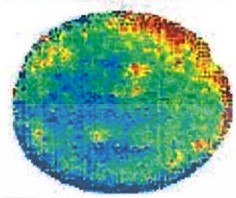	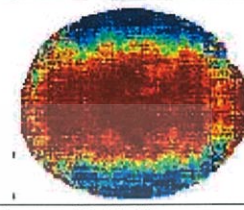
	TSS = 7.13 °Brix	Citric = 7.24 %	Juice = 48.50 %
24.1	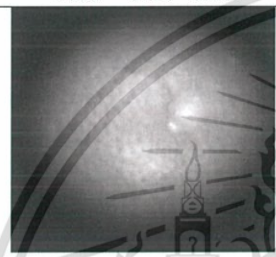	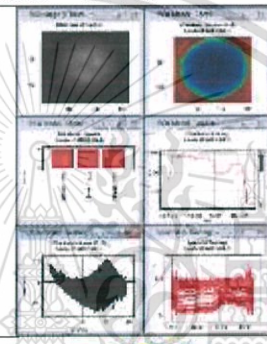	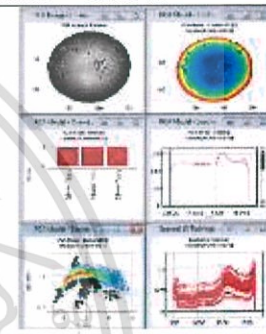
	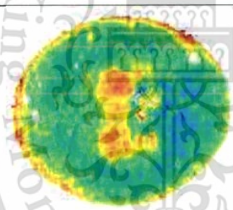	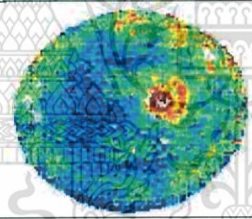	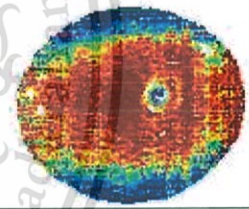
	TSS = 7.59 °Brix	Citric = 6.97 %	Juice = 47.22 %
24.2		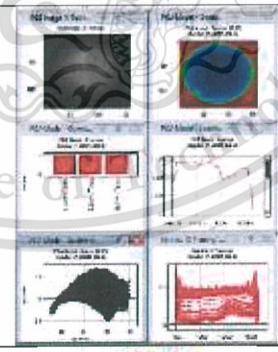	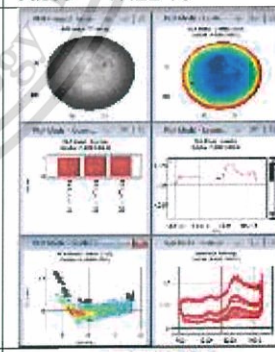
	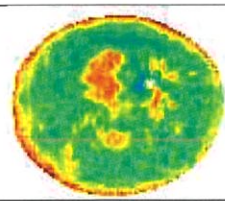	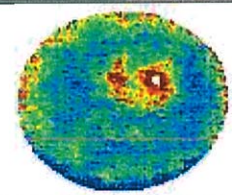	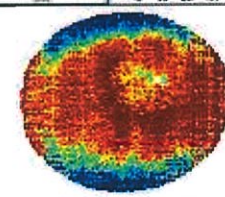
	TSS = 7.8 °Brix	Citric = 7.23 %	Juice = 49.00 %

25.1	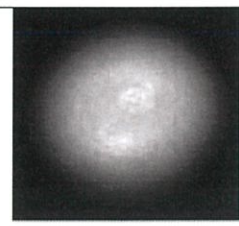	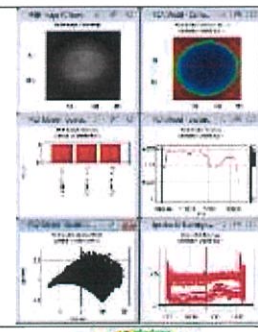	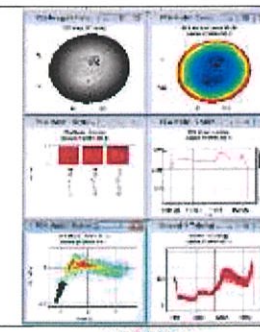
	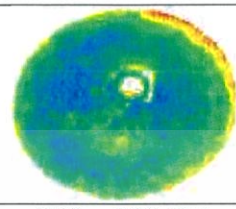	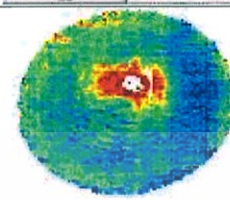	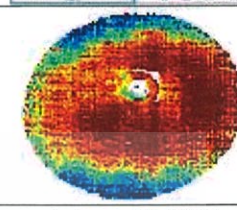
	TSS = 7.22 °Brix	Citric = 7.13 %	Juice = 50.00 %
25.2	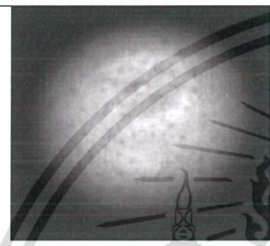	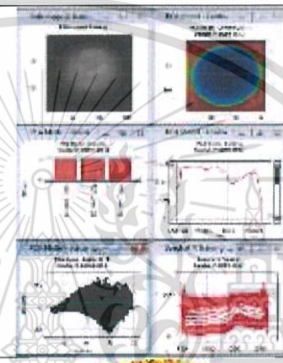	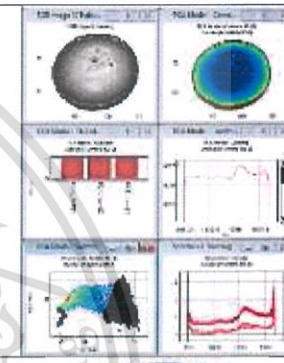
	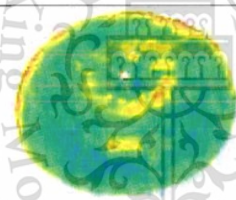	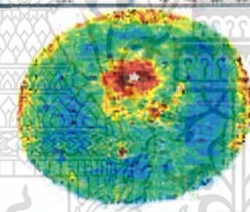	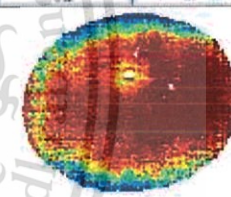
	TSS = 7.55 °Brix	Citric = 7.13 %	Juice = 53.92 %
26.1	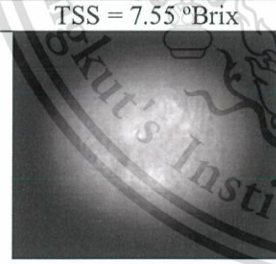	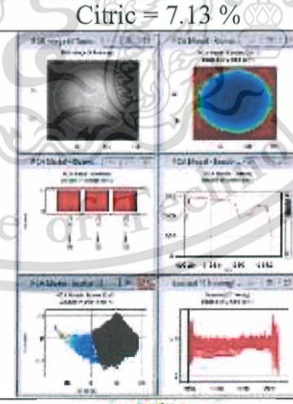	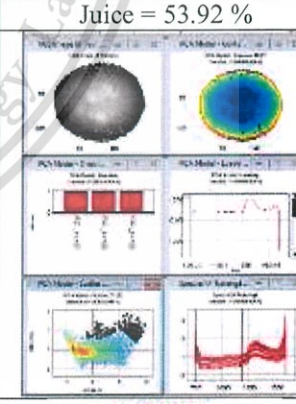
	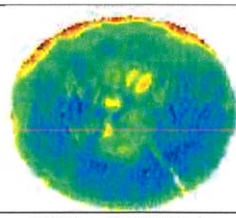	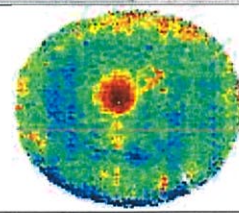	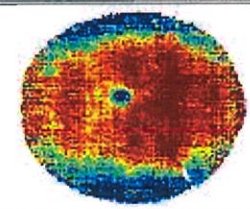
	TSS = 7.17 °Brix	Citric = 7.42 %	Juice = 47.60 %

26.2	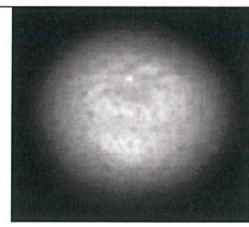	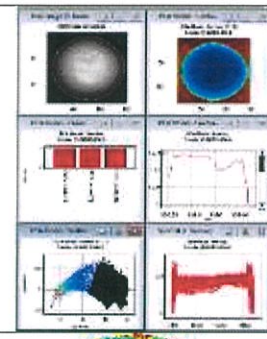	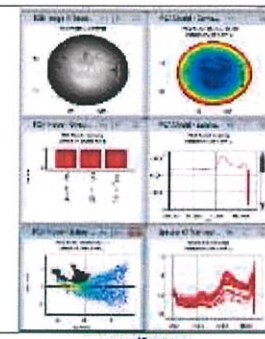
	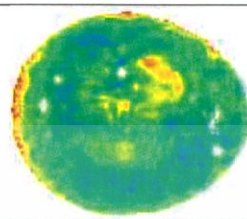	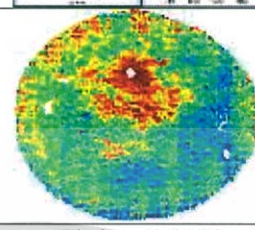	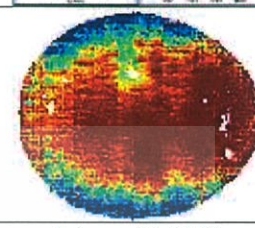
	TSS = 7.47 °Brix	Citric = 7.60 %	Juice = 51.51 %
27.1	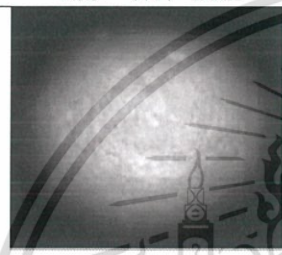	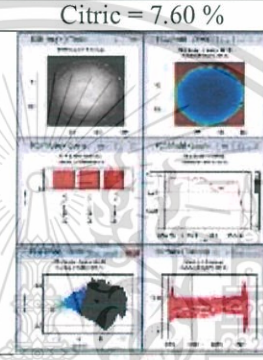	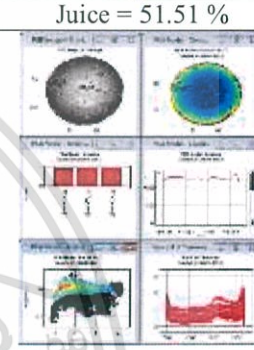
	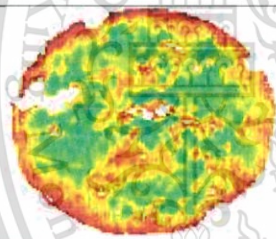	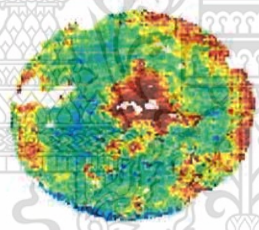	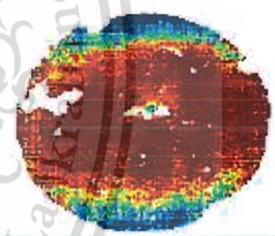
	TSS = 8.15 °Brix	Citric = 7.89 %	Juice = 55 %
27.2	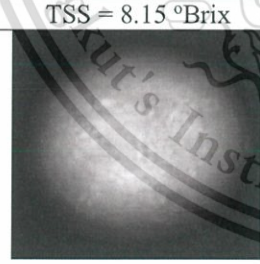	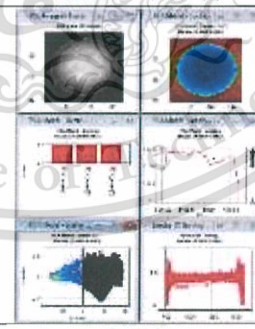	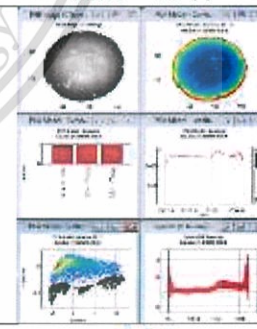
	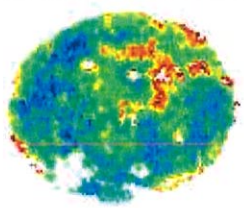	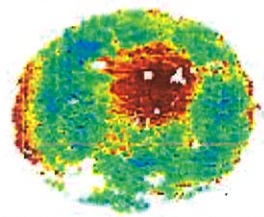	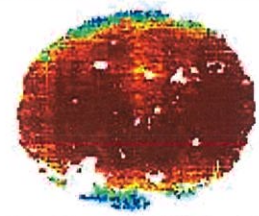
	TSS = 8.15 °Brix	Citric = 7.95 %	Juice = 59.63 %

28.1	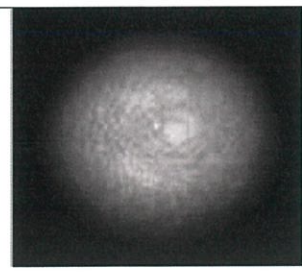	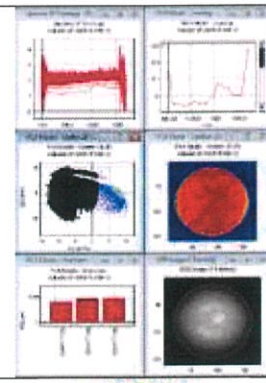	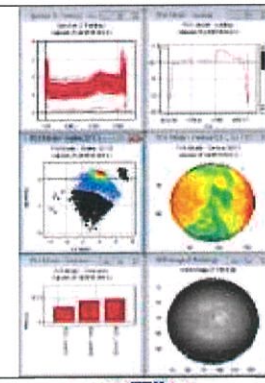
	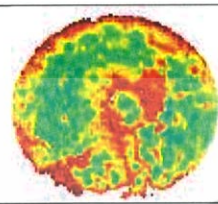	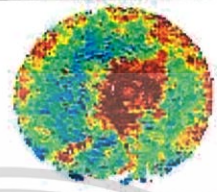	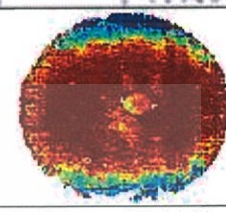
	TSS = 8.15 °Brix	Citric = 8.03 %	Juice = 55.64 %
28.2		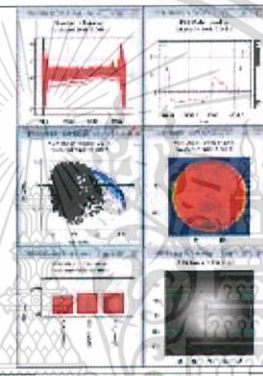	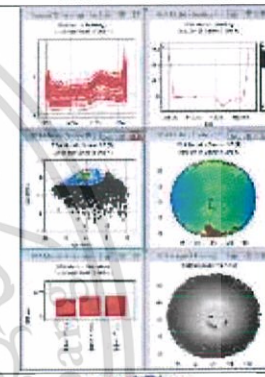
	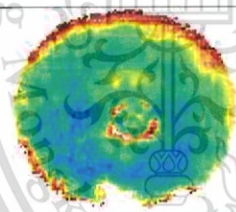	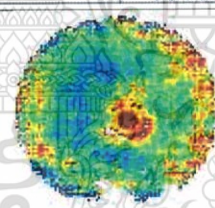	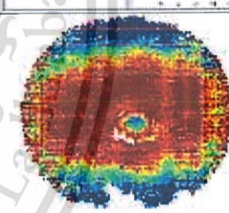
	TSS = 7.48 °Brix	Citric = 7.60 %	Juice = 47.56 %
29.1	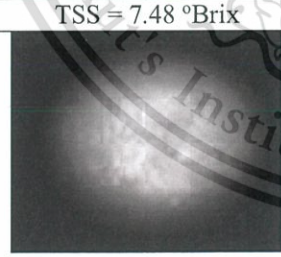	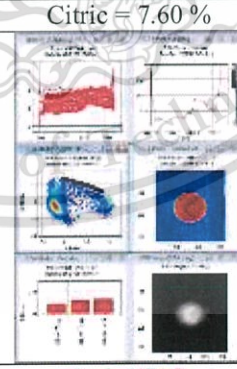	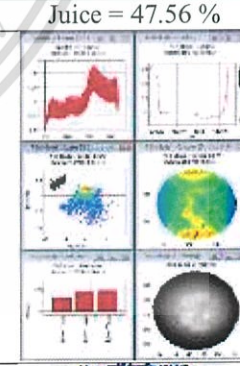
	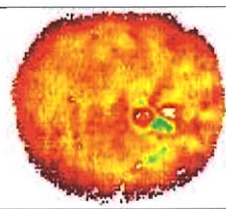	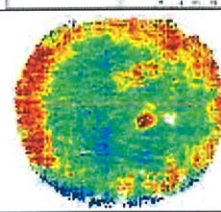	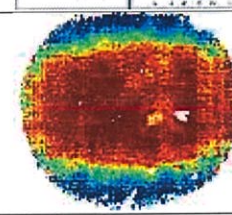
	TSS = 8.84 °Brix	Citric = 7.83 %	Juice = 49.31 %

29.2	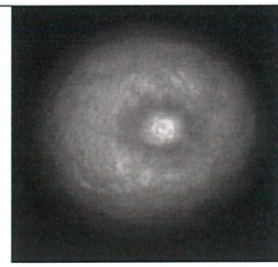	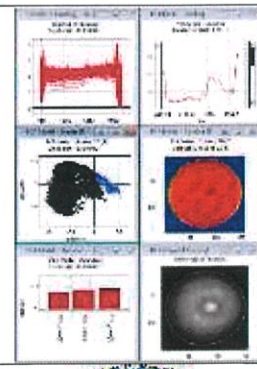	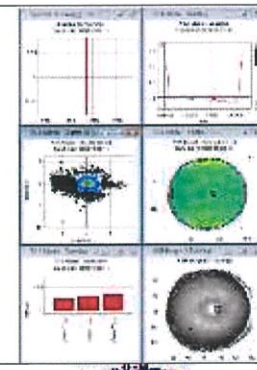
	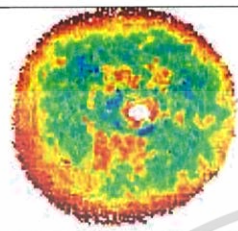	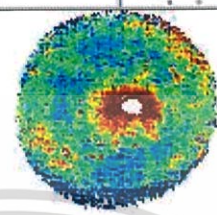	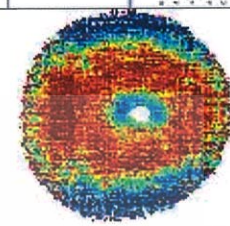
	TSS = 8.13 °Brix	Citric = 7.39 %	Juice = 45.08%
30.1	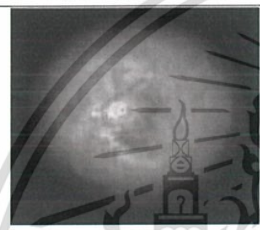	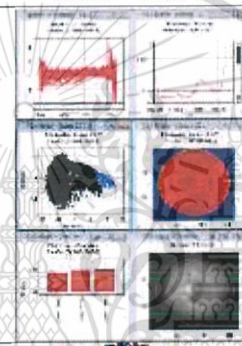	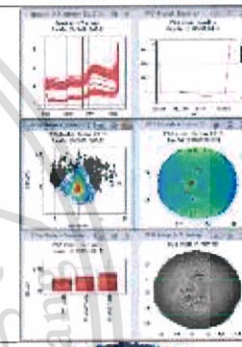
	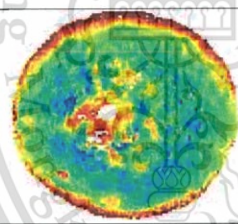	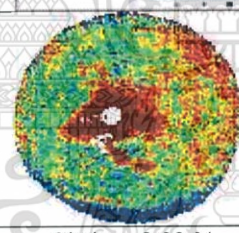	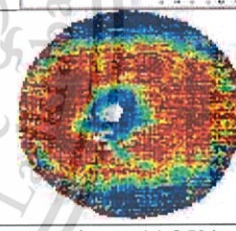
	TSS = 7.71 °Brix	Citric = 8.03 %	Juice = 44.85%
30.2	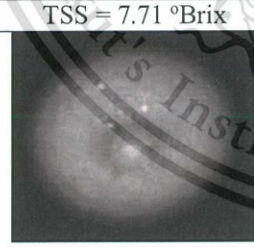	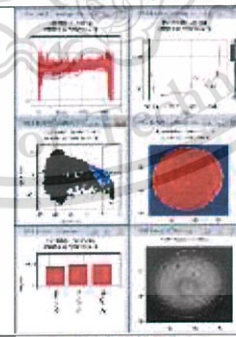	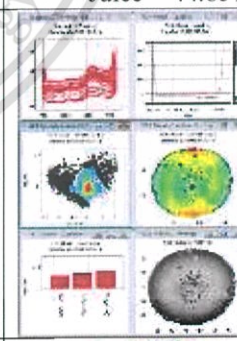
	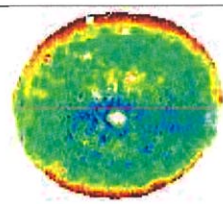	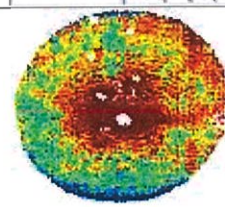	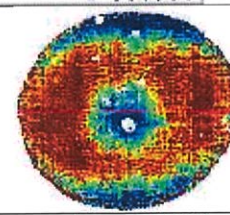
	TSS = 7.67 °Brix	Citric = 8.42 %	Juice = 47.01%